Power-Split Strategies for Hybrid Marine Propulsion Plants in Transient Loading Conditions for Optimal Energy Management and Emissions Reduction

Thesis submitted to the

School of Naval Architecture and Marine Engineering

for the degree of

Doctor of Philosophy

at

NATIONAL TECHNICAL UNIVERSITY OF ATHENS

by

Nikolaos P. Planakis

Thesis Supervisor:
Assist. Professor G. Papalambrou

April 2021

Laboratory of Marine Engineering
School of Naval Architecture and Marine Engineering
National Technical University of Athens
Zografos, Athens, Greece

Power-Split Strategies for Hybrid Marine Propulsion Plants in Transient Loading Conditions for Optimal Energy Management and Emissions Reduction

Abstract

The need to increase vessels' efficiency, reduce their environmental footprint and adapt quickly to new regulations, makes it as urgent as possible to develop and use novel control technologies on ship energy management systems. Marine hybrid propulsion plants are complex multivariable systems, in terms of the underlying technology, principles of operation, size, and physical limitations. System performance specifications strive for competitive objective satisfaction to ensure efficiency and safety.

This Thesis investigates power-split strategies for hybrid marine propulsion plants for optimal energy management and emissions, during the operation in transient loading conditions. In this context, two predictive control schemes were developed, implemented, and experimentally evaluated. At first, a NMPC-based control scheme was proposed to deal with the load-split between the power sources during transient loading conditions, ensuring the dynamic torque delivery with respect to the powertrain physical and operating limits. In the next step, the optimal control problem is reformulated and extended to develop an energy management and emissions minimization strategy. The energy management planning is performed according to the trade-off criteria between fuel consumption and NOx emissions minimization.

For the development of the Energy Management and Emissions Minimization System (EMEMS), the following procedure was followed. Initially, first principle and data-based models were fitted to powertrain measurement data to derive models that approximated accurately the dynamical system behavior during transient operation, as well as the patterns that were observed within the measured data. Secondly, to evaluate the interaction of the system "power plant-propulsion system-environment", a parametric propulsion plant model that matches the experimental facility was employed, to apply propeller loading considering several vessel operating scenarios and irregular wave disturbance. Also, a propeller observer is designed and implemented to quantify the propeller load characteristics, without knowledge of the uncertain propulsion plant parameters. The approach is based on the propeller law principle to produce accurate estimates, in both steady-state and transient loading conditions. Thirdly, using machine learning techniques and data from actual ship operation, identification and prediction of the operator's reference input during ship maneuvering are performed. Profiles that contain rich information about the transient operation were identified and utilized for control system development. A neural network model is designed to predict future speed reference input based on historic data. The online information generated by the prediction model is used along with the propeller observer by the controller to calculate the future propeller load disturbance. EMEMS is tuned to perform similarly to the benchmark optimization problem and the trade-off performance between fuel consumption and NOx emissions is investigated in simulation.

HIPPO-2 experimental facility at LME/NTUA is used for the experimental implementation and evaluation of the developed power-split control schemes. The EMEMS are experimentally tested in real-time operation, where their capabilities for robustness to disturbance load characteristics are investigated. Offset-free reference tracking independently of the propulsion plant size, the uncertainty of the propeller and ship characteristics, as well as the modeling errors between the powertrain components and the internal model of the controller is achieved. In parallel, with the EMEMS design, the power-split control can be performed according to the energy management and emission minimization targets. For the considered scenario, where the aim was to have a charge sustaining strategy at the end of the load cycle, fuel consumption and NOx emissions reduction up to 6.5% and 8%, respectively, were achieved.

Στρατηγικές Κατανομής Ισχύος σε Ναυτικές Υβριδικές Εγκαταστάσεις Πρόωσης κατά την Διάρκεια Μεταβατικής Φόρτισης για Βέλτιστη Διαχείριση Ενέργειας και Ελαχιστοποίηση Αέριων Ρύπων

Περίληψη

Η ανάγκη αύξησης της ενεργειακής αποδοτικότητας των πλοίων και της ταυτόχρονης μείωσης των εκπομπών αέριων ρύπων από τα συστήματα πρόωσης των πλοίων, καθιστούν επείγουσα την ανάπτυξη και την χρησιμοποίηση νέων τεχνολογιών που θα επιτύχουν την άμεση εναρμόνιση στους νέους κανονισμούς.Οι υβριδικές εγκαταστάσεις πρόωσης αποτελούν πολυμεταβλητά συστήματα και εμφανίζουν αυξημένη πολυπλοκότητα, όσον αφορά την υποκείμενη τεχνολογία, τις αρχές λειτουργίας, το μέγεθος και τους φυσικούς περιορισμούς. Οι προδιαγραφές απόδοσης του συστήματος διαχείρισης ενέργειας ορίζουν την ικανοποίηση ανταγωνιστικών στόχων για την επίτευξη αυξημένης αποδοτικότητας και ασφαλούς λειτουργίας του συστήματος.

Η παρούσα Διδακτορική Διατριβή διερευνά στρατηγικές κατανομής ισχύος σε ναυτικές υβριδικές εγκαταστάσεις πρόωσης πλοίων για βέλτιστη διαχείριση ενέργειας και εκπομπές αέριων ρύπων, κατά την διάρκεια επιβολής μεταβατικού φορτίου. Σε αυτό το πλαίσιο, αναπτύχθηκαν στρατηγικές ελέγχου βασισμένες σε μη-γραμμικό προβλεπτικό έλεγχο (MPC). Σε πρώτο επίπεδο, προτείνεται μια στρατηγική για τον υπολογισμό της κατανομής φορτίου μεταξύ των πηγών ισχύος κατά τη διάρκεια μεταβατικής φόρτισης, η οποία εξασφαλίζει τη δυναμική παραγωγή και απόδοση ροπής στον άξονα της προπέλας, σε συμμόρφωση με τα φυσικά και λειτουργικά όρια του συστήματος πρόωσης. Στο επόμενο βήμα, το πρόβλημα βελτιστοποίησης αναδιατυπώνεται και επεκτείνεται για να αναπτυχθεί μια στρατηγική διαχείρισης ενέργειας και ελαχιστοποίησης εκπομπών αέριων ρύπων. Ο σχεδιασμός διαχείρισης ενέργειας πραγματοποιείται σύμφωνα με έναν συντελεστή που καθορίζει την στάθμιση μεταξύ κατανάλωσης καυσίμου και ελαχιστοποίησης εκπομπών οξειδίων του αζώτου NOx.

Για την ανάπτυξη του Συστήματος Διαχείρισης Ενέργειας και Ελαχιστοποίησης Εκπομπών (EMEMS), ακολουθήθηκε η διαδικασία που περιγράφεται παρακάτω. Σε πρώτο επίπεδο, αναπτύχθηκαν μοντέλα βασισμένα τόσο σε βασικές αρχές μηχανικής όσο και σε δεδομένα, τα οποία βασίστηκαν σε πειραματικά δεδομένα, στοχεύοντας στην προσέγγιση της δυναμικής συμπεριφοράς του συστήματος κατά τη διάρκεια μεταβατικής λειτουργίας, καθώς και στην αναγνώριση μοτίβων που παρατηρήθηκαν στα πειραματικά δεδομένα. Κατά δεύτερον, για την αξιολόγηση της αλληλεπίδρασης του συζευγμένου συστήματος ¨κινητήρες - σύστημα πρόωσης - περιβάλλον¨, χρησιμοποιήθηκε ένα μοντέλο πρόωσης πλοίου όμοιου μεγέθους με την πειραματική εγκατάσταση, για προσομοίωση φορτίου έλικας, λαμβάνοντας υπόψη διάφορες καταστάσεις λειτουργίας του πλοίου και την διαταραχή μη-αρμονικών κυματισμών. Επιπλέον, σχεδιάστηκε και υλοποιήθηκε ένας παρατηρητής έλικας, προκειμένου να ποσοτικοποιούνται, κατά την λειτουργία του συστήματος σε πραγματικό χρόνο, τα χαρακτηριστικά του φορτίου της έλικας, χωρίς γνώση των παραμέτρων του συστήματος πρόωσης πλοίου, οι οποίες περιλαμβάνουν αβεβαιότητα. Η προσέγγιση βασίζεται στην αρχή του νόμου της προπέλας για την εκτίμηση του φορτίου, τόσο σε συνθήκες σταθερής πλεύσης όσο και σε κατάσταση μεταβατικής φόρτισης. Σε τρίτο επίπεδο, χρησιμοποιώντας τεχνικές μηχανικής μάθησης και δεδομένα από πραγματική λειτουργία πλοίου, πραγματοποιήθηκε αναγνώριση και πρόβλεψη της εισόδου αναφοράς στο σύστημα από τον χειριστή, κατά τη διάρκεια πραγματοποίησης ελιγμών πλοίου. Αναγνωρίστηκαν μοτίβα που περιέχουν πληροφορίες σχετικά με την μεταβατική λειτουργία, τα οποία χρησιμοποιήθηκαν για την ανάπτυξη συστήματος ελέγχου. Τέλος, σχεδιάστηκε ένα μοντέλο βασισμένο σε νευρωνικό δίκτυο για την πρόβλεψη μελλοντικής εισόδου αναφοράς βάσει ιστορικών δεδομένων. Οι πληροφορίες που παράγονται κατά την λειτουργία από το μοντέλο πρόβλεψης, χρησιμοποιούνται, μαζί με τον παρατηρητή έλικας, από τον ελεγκτή για την εκτίμηση της μελλοντικής ζήτησης του φορτίου της έλικας. Τέλος, έγινε ρύθμιση έτσι ώστε το EMEMS να αποδίδει παρόμοια με το πρόβλημα βελτιστοποίησης αναφοράς, το οποίο επιλύεται με εκ των προτέρων γνώση του κύκλου φόρτισης. Διερευνήθηκε η αντιστάθμιση μεταξύ της κατανάλωσης καυσίμου και των εκπομπών αέριων ρύπων NOx κατά την λειτουργία του υβριδικού συστήματος πρόωσης.

Για την πειραματική επιβεβαίωση και αξιολόγηση των στρατηγικών ελέγχου κατανομής ισχύος

που αναπτύχθηκαν, χρησιμοποιήθηκε η πειραματική εγκατάσταση HIPPO-2 στο ΕΝΜ / ΕΜΠ. Το EMEMS δοκιμάστηκε σε λειτουργία σε πραγματικό χρόνο, όπου διερευνήθηκε η ευρωστία έναντι διαταραχών του φορτίου της προπέλας.Με βάση τα πειραματικά αποτελέσματα, επιτυγχάνεται παρακολούθηση της τιμής αναφοράς χωρίς σφάλμα, ανεξάρτητα από το μέγεθος του συστήματος πρόωσης, την αβεβαιότητα των παραμέτρων της έλικας και του πλοίου, καθώς και τα σφάλματα μοντελοποίησης μεταξύ της συμπεριφοράς του συστήματος παραγωγής ισχύος και του εσωτερικού μοντέλου του ελεγκτή. Παράλληλα, με τον σχεδιασμό του EMEMS, η στρατηγική κατανομής ισχύος μπορεί να ικανοποιήσει ταυτόχρονα τους στόχους διαχείρισης ενέργειας και ελαχιστοποίησης εκπομπών αέριων ρύπων. Για το σενάριο το οποίο εξετάστηκε, με ζητούμενο την διατήρηση του επιπέδου φόρτισης της μπαταρίας στο τέλος του κύκλου φόρτισης, επιτεύχθηκε μείωση κατανάλωσης καυσίμου έως 6.5% και εκπομπών αερίων ρύπων NOx έως 8%.

Acknowledgments

Firstly, I owe my sincere gratitude to my advisor, As. Professor George Papalambrou for his continuous support during my PhD studies. He provided me with tireless advice, guidance, and encouragement at each and every phase of the related research work. His passion for novel methodologies and concepts motivated me to always deepen my scientific and academic background.

I would like to express my special thanks to Professor Nikolaos Kyrtatos, member of my Thesis Committee and Director of the Laboratory. He was a real mentor for me. His advice helped me in all the time of research with his knowledge and entrusted me to use the experimental facility for all the required results.

I would like also to thank Prof. K. Kyriakopoulos, member of my Thesis Committee, for his insightful comments and guidance.

My sincere thanks goes to Dr.-Ing. N. Alexandrakis for his constructive guidance on the experimental facility and for our inspirational conversations.

I would also like to thank the Laboratory technicians and administrative staff for their support through all the phases of my work, the students that cooperated fruitfully with me during their final-semester diploma thesis, contributed to gain insight and realize various methods and concepts. My special thanks goes to my colleagues Michalis Foteinos and Zoe Lygizou for the great times together. Especially, I would like to thank Vasilis Karystinos, for his full commitment and dedication to our project. I wish him all the best in his PhD studies.

I would like to thank Eugenides Foundation for the partial financial support of my doctoral studies. This work was partially supported by EC/DG RTD H2020/HERCULES-2 project. My thanks goes also to MarineTraffic for providing us data from ship operation.

Finally, I would like to thank my parents Petros and Artemis, my brother Konstantinos and my close people, family and friends, for supporting me in any conventional and unconventional way throughout my studies and my life in general. Last but not least, I would like to thank Evi, as I feel extremely grateful for having her beside me, supporting me and sharing together all joyful and difficult moments during all this time and in my life. Thank you!

Athens, February 2021 Nikolaos Planakis

Contents

THIS PAGE INTENTIONALLY LEFT BLANK

List of Figures

List of Tables

THIS PAGE INTENTIONALLY LEFT BLANK

Preface

Thesis Objective

Hybrid propulsion is an attractive technology for ships with multivariable operation profile and vessels that operate in coastal areas and within ports where strict emission regulations are applied. Hybrid powertrains can provide increased operational efficiency of the vessel and compliance with strict environmental legislation. However, marine hybrid propulsion plants are complex multivariable systems, as the installed power-sources diversify in terms of the underlying technology, principles of operation, size, and physical limitations. On the other hand, system performance specifications strive for competitive objective satisfaction, such as immediate power availability at the propeller shaft, maximized engine energy efficiency, and minimized emissions.

In this context, the control strategy has to explicitly tackle the non-linear system behavior, system physical and operating limits, and ensure optimal energy management and minimized environmental burden during ship operation. This Thesis focuses on integrated Energy Management and Emissions Minimization Strategies (EMEMS) in the operation of parallel marine hybrid propulsion plants in transient loading conditions. It addresses the development of energy management strategies for the transient and fluctuating propeller load sharing for optimal energy management and minimized emissions.

Thesis Contributions

The core contribution of the present work is the development and implementation of an integrated, real-time capable, predictive control scheme for the power-split control of parallel hybrid diesel-electric propulsion plants, able to satisfy the current and predicted propeller load and minimize both fuel consumption and NOx emissions efficiency of the system according to the selected criteria.

The tasks of the control scheme are to perform the power-split calculation for minimized consumption and emissions, propeller load estimation, and operator demand prediction within a future time window. Consequently, an optimal energy management plan can be drawn. Furthermore, a framework for energy management system development for hybrid ship propulsion

with the implementation of data-driven models and machine learning techniques in the development loop is proposed. Marine loading profiles are developed using measured data that resemble typical operator input in marine applications.

For proof of concept, the validation of the control concept is performed using a propeller load emulation model and one of the created marine loading cycles, in simulation, where the performance of the energy management system is compared to benchmark problem results as well as in experiments, where the control scheme is experimentally implemented and tested for different fuel consumption to NOx emissions weighting parameters. In this framework, the overall behavior of the EMEMS is optimized and evaluated.

The research performed in the context of this Thesis yielded the following scientific publications

[1] N. Planakis, G. Papalambrou and N. Kyrtatos, "Predictive power-split system of hybrid ship propulsion for energy management and emissions reduction", Control Engineering Practice, Volume 111, 2021, 104795.

[2] N. Planakis, G. Papalambrou, N. Kyrtatos, P. Dimitrakopoulos, "Recurrent and Time-Delay Neural Networks as Virtual Sensors for NOx Emissions in Marine Diesel Powertrains," SAE Technical Paper 2021-01-5042, 2021.

[3] N. Planakis, G. Papalambrou and N. Kyrtatos (October 21, 2020). "Integrated Load-Split Scheme for Hybrid Ship Propulsion Considering Transient Propeller Load and Environmental Disturbance." ASME. J. Dyn. Sys., Meas., Control. March 2021; 143(3): 031004

[4] N. Planakis, G. Papalambrou and N. Kyrtatos, (2020) "A real-time power-split strategy for a hybrid marine power plant using MPC", Int. J. Modelling, Identification and Control, Vol. 34, No. 2, pp.147-157.

[5] N. Planakis, V. Karystinos, G. Papalambrou and N. Kyrtatos "Transient Energy Management Controller for Hybrid Diesel-Electric Marine Propulsion Plants using Nonlinear MPC", 21st IFAC World Congress, Berlin, Germany, 2020.

[6] N. Planakis, V. Karystinos, G. Papalambrou and N. Kyrtatos, "Nonlinear Model Predictive Control for the Transient Load Share Management of a Hybrid Diesel-Electric Marine Propulsion Plant," 2020 American Control Conference (ACC), Denver, CO, USA, 2020.

[7] N. Planakis, V. Karystinos, G. Papalambrou and N. Kyrtatos, "A Predictive Energy Management System for a Hybrid Diesel-Electric Marine Propulsion Plant," 2020 European Control Conference (ECC), Saint Petersburg, Russia, 2020.

[8] N. Planakis, G. Papalambrou and N. Kyrtatos, "Power-Split Strategies for Hybrid Diesel Electric Marine Power Plant Using Predictive Control and Transient Load Preview", 29th CIMAC World Congress, Vancouver, June 2019.

[9] N. Planakis, G. Papalambrou and N. Kyrtatos, "Predictive Control for a Marine Hybrid Diesel-Electric Plant During Transient Operation," 2018 5th International Conference on Control, Decision and Information Technologies (CoDIT), Thessaloniki, 2018. (received Best Paper Award).

Publications currently under review:

R1. N. Planakis, G. Papalambrou and N. Kyrtatos, "Ship energy management system development and experimental evaluation utilizing marine loading cycles based on machine learning techniques", in revision for Applied Energy, 3/2021.

R2. G. Papalambrou, N. Planakis and N. Kyrtatos,, "Transient and disturbed propeller load compensation in hybrid propulsion using propeller estimator and predictive control", submitted to the Proceedings of the Institution of Mechanical Engineers, minor revision submitted to Part M: Journal of Engineering for the Maritime Environment, 3/2021.

R3. N. Planakis, G. Papalambrou and N. Kyrtatos, "A Predictive Strategy for Consumption and Emissions Minimization for Marine Hybrid Propulsion Powertrains", submitted to IEEE Transactions on Control Systems Technology, 9/2020.

Thesis Outline

The Thesis is divided in the following chapters:

Introduction The introductory chapter provides a survey on the current state-of-the-art research and applications on the control of hybrid powertrains, as well as a description of the problem and the operation principles of the marine hybrid powertrain used for this Thesis.

Experimental Facility and Virtual Sensor Design In this chapter, the experimental setup of the hybrid powertrain used for this Thesis, as well as the design of virtual sensors, are described.

Powertrain Modeling This chapter introduces the powertrain modeling to derive models for control system design and powertrain behavior simulation.

Load Emulation and Observer Design for Propeller In this chapter, emulation, and estimation of the propeller load characteristics are investigated, to simulate and observe the interaction of the system controller-powertrain-propulsion plant-environment.

Transient Operational Profile Identification and Prediction This chapter deals with the operating profile of a marine propulsion plant in transient operating conditions. Based on data

from ship operations, typical marine loading cycles are identified and a prediction model for the operator's future input is developed.

Transient Power-Split Controller In this chapter the framework of designing and implementing a fast real-time non-linear predictive controller is presented. A predictive control scheme is designed to perform the power-split control during transient and disturbed loading conditions, which is experimentally implemented and evaluated.

Energy Management and Emissions Minimization Strategy This chapter introduces a reformulation of the predictive control scheme to incorporate energy management and NOx emissions minimization. The trade-off between fuel economy and emissions reduction is investigated. Simulation results and experiments on the hybrid testbed are presented.

Conclusions and Future Work This is the closing chapter of this Thesis, where the main results are summarized and research for future work is proposed.

Chapter 1

Introduction

1.1 Motivation

The growing global environmental concern results in the implementation of ever tightening legislation regarding the emission limits during ship operation. This effort to reduce pollutant emissions has rapidly changed the operating conditions of ships. The need for vessels to increase their efficiency and adapt quickly to new regulations makes it as urgent as possible to research and use novel control technologies on ship energy management systems. As such, the interest in alternative powertrain technologies for marine propulsion plants that are capable to increase the overall efficiency of the vessel energy generation system is increasing. Hybrid propulsion is used mainly in ships with multivariable operation profiles and vessels that operate in coastal areas and within ports where strict emission regulations are applied, such as offshore supply vessels, naval vessels, tugboats, and passenger ships. Marine powerplant installations are designed based on each specific application.

Hybrid propulsion is defined as the combination of more than one power-sources that delivers propulsion power to assure ship operational capability, by providing at each moment the required amount of power and torque to the propeller. Several marine applications have been developed and many hybrid topologies have been considered so far, [10]. Usually, the hybrid powertrain includes one or more internal combustion engines, which consume a high energy density fuel that can provide the required operational range. Additionally, a PTI/PTO unit, that can either contribute to propulsion power take up or buffer energy at a high efficiency, which is consumed by other shipboard systems (e.g. electric loads) or utilized at moments when a conventional system would under-perform, e.g. at low speed cruising.

The configuration is justified by the connection between ship power sources and the propeller shaft. In a series hybrid configuration, the power sources are electrically connected to the propulsion motor. On the other hand, the parallel configuration includes mechanical connections, where the system components are connected on a common shaft. The mechanical

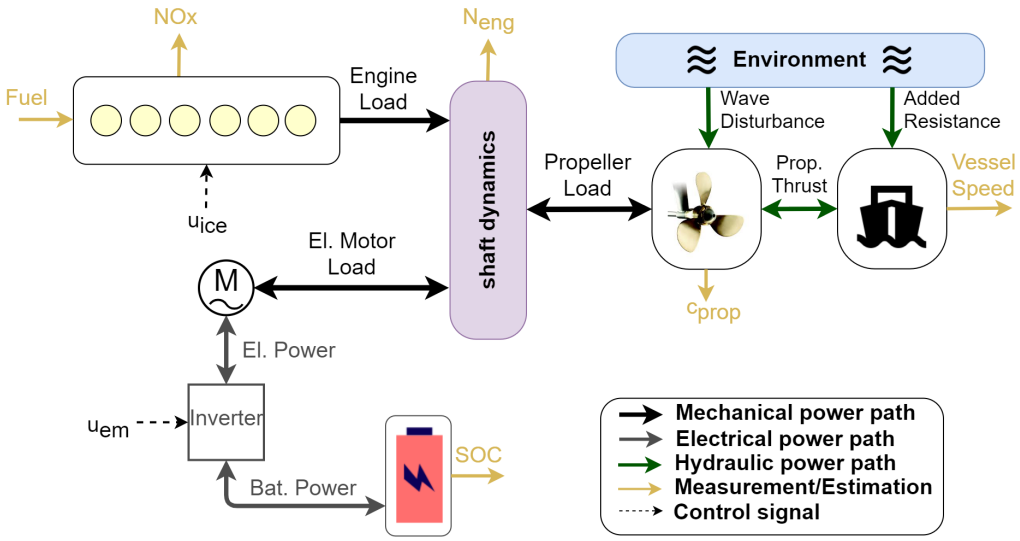

Figure 1-1: Schematic representation of the parallel hybrid diesel electric powertrain.

connection implies a constraint on the system rotational speeds, but the electrical power transmission losses of the series configuration are avoided. Furthermore, series-parallel configurations can benefit from the advantages of both series and parallel systems. The special characteristic in marine hybrid applications, as compared with the automotive sector, is that there does not exist braking where a considerable amount of the system energy can be regenerated. As such, energy storage is not always considered or it can buffer energy from renewable energy sources, e.g. solar or wind-powered. A parallel hybrid ship propulsion system is depicted in Fig. 1-1. The physical connections, as well as the interaction between the power sources, the energy storage, the propulsion plant, the vessel, and the environment, are also shown in the schematic diagram. As it can be noted, it is a multi-variable system with increased complexity as compared to a conventional propulsion plant. Each subsystem is physically constrained or should be operationally limited, e.g maximum brake torque of internal combustion engine and the range of battery charge which can be utilized.

The power management problem in hybrid marine powertrains, which is assessed in this Thesis, remains a challenging issue. It decides how much power shall be produced by the internal combustion engine and how much should be supplied by the electric motor to achieve the total power demand at the driving shaft of the propeller. High system complexity and the extra degrees of freedom that are introduced by the new subsystems, as well as the numerous system limitations, increase the need for sophisticated controls for the Energy Management System (EMS) that lead to the optimal operation of the plant, [11]. Moreover, as compared to conventional propulsion plants, with the proper control system design, it can deal with issues that affect the propulsion plant operation, such as the transient propeller load during ship acceleration and engine power fluctuations that are caused by environmental conditions and

particularly irregular wave disturbance. The interaction of the system engine-propeller-ship-environment, shown in Fig. 1-1, has to be taken into consideration, as it could lead to additional system limitations or introduce further performance specifications to the control system design [12, 13, 14].

As such, energy management control systems of hybrid marine propulsion plants in novel applications must perform multiple tasks; reference tracking, disturbance load estimation, and energy management according to the selected criteria, assist the engine during transient loading by engaging the EM to take up propeller load and finally ensure that the physical and operating constraints, such as the engine overloading, of the hybrid system are not violated. Also, the control system has to deal with the different nature of the underlying dynamics of the propulsion plant, as the various subsystems have multi-scale time constants. On top of that, the energy management system should meet the performance and applicability requirements of the end-user.

1.2 Literature Review

Methodological approaches

The various novel control concepts and methodologies that are applied to marine hybrid propulsion power-split problems are derived mainly from the automotive sector, where several strategies for the optimal power management of hybrid powertrains have been developed and implemented with success, such as dynamic programming (DP), stochastic dynamic programming (SDP), Pontryagin's minimization principle (PMP), equivalent fuel consumption minimization strategies (ECMS), and model predictive control (MPC). In [15], the power management of a hybrid electric vehicle (HEV) is optimized along with the engine thermal management and cabin heating to achieve minimized fuel consumption. In [16] DP and PMP are compared for off-line and real-time integrated management of the diesel engine and the after-treatment unit of a heavy-duty powertrain is performed, to optimize the total costs of fuel and additive NOx abatement fluid.

ECMS is a formulation that considers the energy consumption of all the available power sources, scaled with a factor that represents the equivalence fuel consumption cost, and is widely used for online implementation of optimal power-split control in HEVs, [17, 18]. Reference [19] performs a comparative analysis between DP, PMP and ECMS. Moreover, [20] deals with the transient behavior of the engine while following the ECMS control commands, by using transient power smoothing ECMS strategies to avoid additional fuel consumption or increased emissions respectively.

Among the advanced control design methodologies, MPC seems the most promising, as it can optimize a performance index by generating a sequence of appropriate control actions over a future prediction window, within which the available information can serve the optimization

problem. It is capable to handle at the same time multivariable processes, satisfy constraints, deal with long-time delays and utilize knowledge for plant disturbance response. It has been widely considered for HEV applications. Furthermore, linear MPC has been used in a broad range of applications in automotive and engine control and has been integrated into mass production, [21].

The current research and development focus is the application of nonlinear MPC (NMPC) in real-time applications. So far NMPC has been applied to numerous problems such as energy management of HEV, [22, 23] and engine control, [24, 25, 26, 27, 28]. In [22], the nonlinear equations which describe the plant dynamics, as well as the nonlinear equations of the weighting factors and the constraints are integrated into the controller, which performs the power-split objective, which is to operate the engine on its optimal operation line and track the desirable battery state of charge.

Optimal transient load sharing for the minimization of fuel consumption and emissions in hybrid electric vehicles has not been investigated widely in the literature. In [29], the problem of fuel and time-optimal path of diesel engine transient loading is investigated in a hybrid diesel-electric powerplant. In [30], the effect of the powertrain dynamics has been considered in the power split optimization problem, while [31] considers the effects of turbo lag phenomenon on the engine efficiency during load application to the hybrid powerplant, to achieve better fuel economy. In [32], the effect of sudden engine loading, on transient NOx and soot emissions is considered. An objective function is proposed, which takes into consideration the weighted fuel consumption and engine emissions of a HEV, and Pareto graphs are designed to identify the most satisfying trade-off solution. It is shown that although using a quasi-static NOx model does not affect the cumulative emissions, the solution diversifies when a transient particle matter model is used; however, from a practical point of view, in both cases, the legislation limits could be satisfied. Moreover, [20] and [33] deal with the transient behavior of the engine while following the ECMS control commands, by using transient power smoothing strategies to avoid additional fuel consumption or increased emissions respectively.

In most recent applications, also emissions efficiency has gained importance and its equivalent production has been integrated into the optimization problem to be minimized as well. However, fuel consumption and pollutant emissions production goals cannot be minimized simultaneously and the trade-off between them has to be justified. According to this, in [32], the effect of sudden engine loading, on transient NOx and soot emissions is considered. An objective function is proposed, which takes into consideration the weighted fuel consumption and engine emissions of a HEV, and Pareto graphs are designed to identify the most satisfying trade-off solution. It is shown that although using a quasi-static NOx model does not affect the cumulative emissions, the solution diversifies when a transient particle matter model is used; however, from a practical point of view, in both cases, the legislation limits could be satisfied. In [34], authors propose

a multi-linear MPC control scheme that considers the averaged emissions over the prediction window, so that the engine behavior does not lack in instant performance, but also comply with the required average emissions constraints over a time window.

Today's state-of-the-art applications, strategies including Machine Learning (ML) are implemented, either in an effort to address the issue of computational effort of optimization algorithms online or to provide information to the optimization algorithm. Machine-learning techniques are utilized to complement the system energy optimization problem. Data-driven models are trained using machine learning algorithms to simulate, reproduce or predict the behavior of various subsystems such as the operator demand (system input), environmental conditions (disturbance), control actions, or the behavior of powerplant (system output). In [35, 36] the optimal control problem is solved offline and neural networks are trained to apply the optimal solution online. On the other hand, in [37, 38] authors use a neural network which is trained using measured vehicle and trip data, to predict the future vehicle speed, while in [23] a Markov chain model is trained online to represent the driver behavior. In both works, these models are used to perform future vehicle velocity predictions, which are provided to the optimization algorithm as future reference or disturbance values. With this technique, the control system performance can get closer to the solution of optimization with full knowledge of the operational profile.

Hybrid marine applications

Hybrid propulsion can be reviewed in accordance with the implemented configuration. In applications with series hybrid electric power plants, the propulsive and auxiliary power demand are satisfied by a number of generator sets. As such, the optimal number of generators that operate in order to achieve minimum fuel consumption. However, in series topologies, a trade-off exists between the achieved power plant adaptability and the electric transmission losses at higher loads, which lower the overall power plant efficiency. On the other hand, in parallel hybrid applications where the propeller is driven by a main propulsive system, such as a diesel engine, the electric motor is connected to the main shaft line. The underlying idea is that an internal combustion engine provides propulsive power at higher speeds and loads, where the engine efficiency is increased. Additionally, an electric motor, which is mechanically connected to the propeller shaft, is used to produce power in generation mode which can be stored to the battery or supplied to the electric grid of the vessel, and provides propulsive power in operation points or during load transients and when the diesel engine efficiency is significantly lower.

In the marine sector, several contributions have been made regarding hybrid propulsion and electric power distribution, which either refer to battery-aided power plants or regard the control of multiple power sources to achieve optimal energy management. The control objective diversifies according to the selected topology. In series applications, the engines operate at a constant speed, where voltage or frequency control is performed by regulating the delivered

power of the generator engines. Fuel consumption and emission curves of the engine are used to find the optimal operating points. In parallel topologies, the power plant is operated such as to meet either the desired propeller rotational speed or the reference torque demand at the propeller shaft. As such, fuel and emissions performance mapping of the engine, as well as more intensive search, are required in order to find the optimal operation path and achieve minimum usage of energy, fuel consumption, and emissions.

The operational profile of each ship as well as its power consumption demands is unique and change over the life-time of the vessel. Besides, marine propulsion plants have slow dynamics, due to their size; as a result, transients last longer compared to automotive engines. Rapid load acceptance of diesel engines leads to higher fuel consumption, and consequently to the production of more CO_2 as well as higher NOx concentration and smoke formation, and usually happen in emissions regulated areas. In such cases, the ship-specific needs are considered as criteria for the system design. Therefore rule-based power management strategy, such as the one proposed in [39], which is the common-place in current applications, in combination with the operator's experience has shown to achieve remarkable fuel savings, that is comparable to these of advanced control strategies.

On the contrary, off-line optimization for component sizing and system control using specific operational scenarios is still the main focus in many applications. In [40], the energy storage capacity based on various EMS and operational profiles is optimized. The battery load follows the power fluctuations, while the generator engines are loaded according to the average power demand, avoiding power fluctuations. In [41], a strategic loading strategy is developed and the various operation points of the power sources for maximized efficiency are determined. Optimization over a known profile to minimize the total fuel consumption for a series hybrid application is studied in [42].

Dynamic optimization generally provides the optimal solution for a problem over a certain driving cycle; as such the solution can only be utilized as a benchmark problem. However, in the marine environment, the operation profile for vessels cannot be known a priori and there is no driving cycle for testing such power plants. As a consequence, the optimization should be short-termed, depending on the knowledge of the present state of the power plant.

Implementable sub-optimal control schemes were developed in the last decade. In [43], a control system architecture is proposed in order to satisfy the power demand during crane operations. In [44, 45, 46] for series hybrid power-trains, where greater fuel savings have been achieved, however with lower final state of charge in the battery. In [14], the shaft motor/generator is used to mitigate speed and power fluctuations during the operation of the propulsion plants in waves. However, optimal power management is not guaranteed. ECMS has been studied widely, as it is a sub-optimal method that can be implemented online. [44] proposes an ECMS strategy for series hybrid tugs, where the equivalence factor depends on the efficiencies of the genera-

tor engine and the battery. In [47], an ECMS controller is developed for a parallel hybrid tug with shore charging capability, where the equivalence factor is adapted based on probabilistic operating load estimation.

Most recent and advanced works use predictive control for the power-split problem and the power-plant performance. In [45], a predictive ECMS over a future time window. For each subsequent window, the operating load estimation is performed based on the percentage of time on low- medium- and high- power demand of the vessel. [48] also follows a predictive strategy, where the objective function includes fuel consumption, engine emissions, and powertrain efficiency. On top of that, the load prediction is made by a neural network with wavelet excitation functions. The implementation of MPC problem in real-time and sample time-critical applications has been considered in [49, 50, 51, 52], where Sequential Quadratic Programming (SQP) methods are utilized to solve the optimization problem online. The power sources and the energy storage device are operated optimally, to minimize the power losses of the system and ensure the high quality of the electric power in means of frequency or voltage regulation during power demand fluctuations and transient loading.

In some cases, the power-split control is performed taking into account also the satisfaction of the vessel dynamics. In [53] a multilevel predictive control approach is used for the energy calculation and optimal power split control of a series hybrid OSV during maneuvering under the presence of environmental disturbance. The first level employs robust tube-based MPC to predict the power within the prediction horizon, while the second, linear MPC, performs the power-split control with minimum fuel consumption and power demand tracking error. Furthermore, in [54] the optimal power sources management of an autonomous tug is calculated using trip information. Here, the propulsion power demand is predicted using the input-output feedback linearization formulation, and the power-split is conducted to achieve minimum specific fuel oil consumption of the diesel generator sets.

Further research areas

The core research topic of this Thesis is energy management systems for hybrid marine propulsion plants. To achieve this, several interrelated problems had to be addressed, regarding the research and development framework ad well as the implementation of the control system. They are further discussed below.

The development of new technologies includes a loop of continuous testing, evaluation of the test results, and improvement. It is of crucial importance that the testing environment resembles as close as possible the conditions of real-world applications. The same applies also to marine propulsion plants, where one factor is the load profile that will be used in simulation or the experimental facility. Moreover, a detailed and accurate simulation of the plant is a prerequisite for the design of an optimal control system and performance evaluation during

experimental testing. Hence, the modeling of the propulsion system of the ship as well as the external environmental disturbances, such as sea waves, should be well defined to implement realistic information including the transient effects of system operation.

Further to a relative discussion, evaluation of energy management strategies should be made using a number of widely accepted loading profiles, like the driving cycles that are used in the automotive industry, where extensive literature material exists, [55, 56, 57]. Another approach in [58] compared the existing standard driving cycles with objective methods, including correlation analysis or automatic clustering, and chooses a combination of driving cycles that can be representative. However, comparison of driving cycles regarding ship operation is still difficult to perform and the lack of a definition of representative driving cycles enables subjective judgments.

Hence, the creation of representative loading cycles of vessels, will contribute to the optimization of marine powertrain operation and will assist in pattern identification and categorization in the maritime environment. A group of realistic general loading cycles that resemble these situations would be a useful tool to test and benchmark different engine control strategies.

A substantial number of neural network permutations have been validated as virtual sensors in the automotive, railway, and aerospace industry, [59, 60, 61, 62]. RNN is the corresponding representation of a state-space model, that can be used for dynamic systems modeling, [63]. A dynamic neural network approach has been validated successfully in [64], with recurrent neural networks (RNN) models for predicting the NOx emissions of CI engines. In [65], the previous work was supplemented with online model adaptation. As a result, neural network models, especially RNN, have been widely validated in simulating the dynamic behavior of diesel engines successfully.

1.3 Research Questions and Problem Approach

The objective of this Thesis is to investigate real-time Energy Management and Emissions Minimization Strategies, with optimal transient and steady-state performance in regards to energy consumption and emissions production, as well as robust behavior against external disturbances. In this context, the following research questions are addressed:

1. Which are the dynamic characteristics of the load applied to marine propulsion plants, from a control-oriented perspective?

2. How can the dynamic and steady-state characteristics of the propeller load be estimated by utilizing only basic powertrain measurements, and how can the load disturbance be anticipated in order to achieve offset-free power-split control?

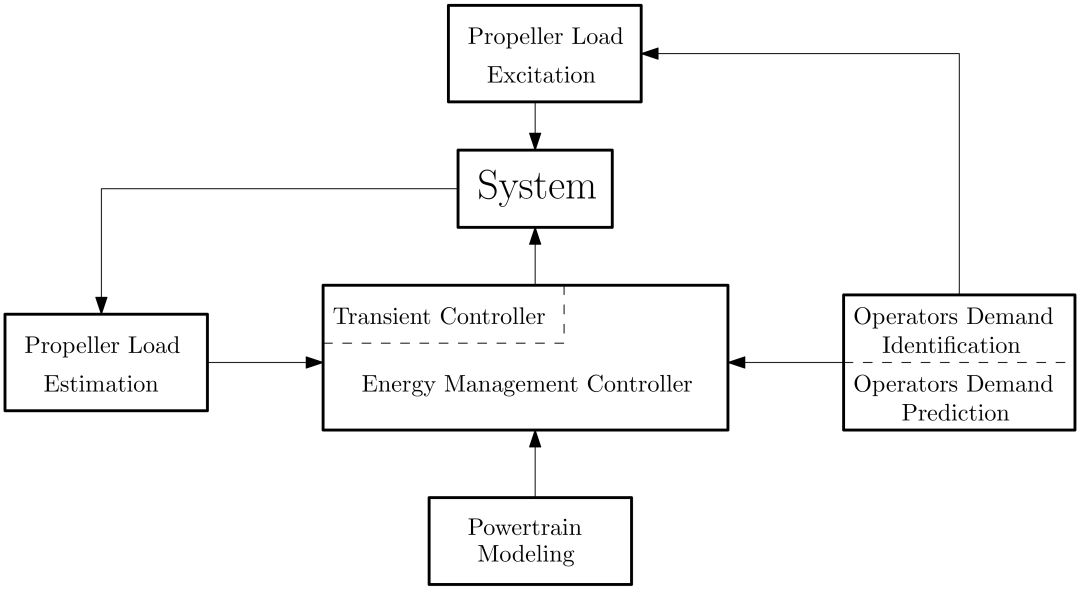

Figure 1-2: Interrelated subproblems addressed in the context of this Thesis.

3. Which is the typical operational profile of a marine propulsion plant during transient operation and how can the future operator demand be predicted?

4. How can the transient and fluctuating behavior of the diesel engine be mitigated with the use of the hybrid power plant, without any lack in power-availability performance?

5. How can the ship power plant be optimally operated to achieve minimum energy consumption and emissions production in transient loading conditions?

The main research areas as well as their interconnection in the overall system design were defined with respect to the above research questions. The interrelated sub-problems that were identified and independently addressed in the context of this Thesis, are presented graphically in Fig. 1-2.

THIS PAGE INTENTIONALLY LEFT BLANK

Chapter 2

Experimental Facility and Virtual Sensor Design

In this chapter, the Hybrid Integrated Propulsion POwertrain (HIPPO-2) experimental facility at LME/NTUA, which was modified and operated in the context of this work, is presented. The testbed represents a full-scale integrated parallel hybrid diesel-electric ship propulsion plant. To complement the physical sensor system that is installed by the engine manufacturer, virtual sensors for engine-out emissions are developed. In addition, on this experimental facility, several power-split and energy management strategies were implemented and evaluated in real-time operation.

2.1 HIPPO-2 Testbed

The experimental facility, seen in Fig. 2-1, is composed of three major components: the Internal Combustion Engine (ICE), the Electric Motor/Generator (EM) and the Electric Brake (EB), all connected on a common shaft. In this configuration, the rotational speed of the ICE and the EM are identical and the supplied torques add together to maintain the total torque demand applied by the electric brake (EB). From a systems point of view, it is noted here that, an Energy Storage component was also considered in modeling; It was considered to be connected at the EM inverter system and was emulated in series configuration during EM operation.

The ICE is a turbocharged CATERPILLAR model C9.3, 6-cylinder, 9.3-liter, 4-stroke industrial diesel engine, rated at 261 kW at 1800-2200 rpm and maximum torque 1596 Nm at 1400 rpm. The EM is a standard AC induction 3-phase, 4-pole motor, with a rated power of 90 kW at 1483 rpm. The speed and torque output of the electric motor is individually controlled by a frequency inverter, based on the direct torque control scheme, [66]. The EM is operated both as a motor and generator by the power-split algorithms that were developed in this work.

The ICE is electronically controlled either in speed control mode or by demanding the desir-

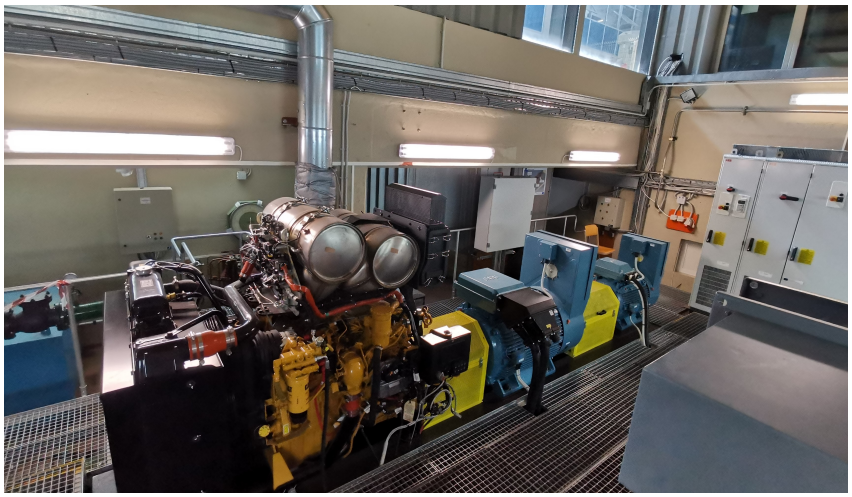

(a) Experimental facility in the Laboratory.

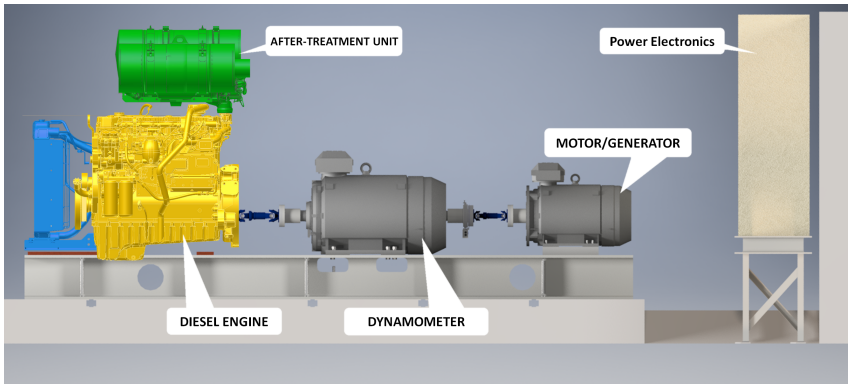

(b) Layout of the experimental testbed.

Figure 2-1: HIPPO-2 experimental testbed at LME/NTUA.

able indicated torque output which leads to injection of a certain amount of fuel by the engine ECU using an internal mapping and is considered as an electronic fuel index. The engine is designed to meet U.S. EPA Tier 4 Final, EU Stage IV emission standards. The HIPPO-2 engine is fitted with Exhaust Gas Recirculation (EGR) and Selective Catalytic Reduction (SCR) systems for NOx reduction, along with a Diesel Particulate Filter (DPF) for soot particles trapping.

The powertrain components are connected in a parallel configuration, thus the operating speed range of HIPPO-2 is from 600 to 2200 rpm, with a maximum load of 351 kW (ICE and EM combined power). The principal concept for component sizing was the need that EM assists the ICE in low speed and load (1200 rpm and 30% of nominal load), where the fuel and emissions efficiency of the ICE are lower. As such, the EM was selected to account for the $\frac{1}{3}$ of ICE nominal load. In addition, as ICE transient response is poor, primarily due to the turbocharger lag phenomenon, the EM dynamics allow for immediate torque availability. With proper control, EM can be used in motoring or generating mode to deal with the fast powertrain dynamics and let the diesel engine follow in a quasi-static way and following the most efficient power path within its operating envelope. The torque curves of HIPPO-2 components are

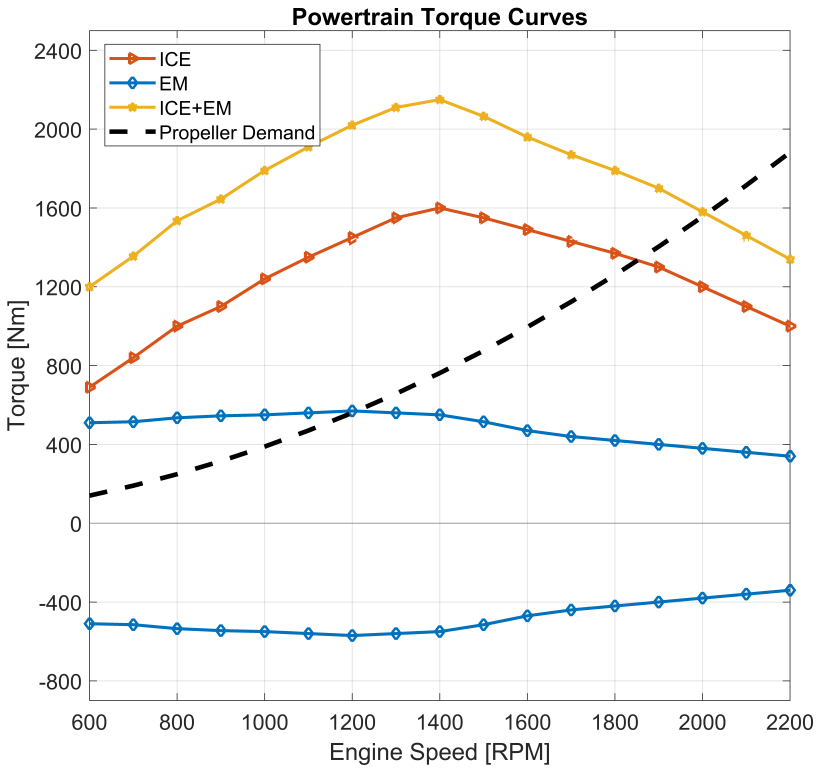

Figure 2-2: HIPPO-2 powertrain torque curves.

presented in Fig. 2-2, where the sizing as well as the behavior of the various power sources can be identified.

2.2 HIPPO-2 Sensors and Prototyping Platform

The control and data acquisition system of the testbed is based on the sensors that are installed by the manufacturer on the ICE and the Electric motors and CAN bus communication protocol, [67]. Also, analog sensors for the torque and two coriolis mass-flow meters were installed during the modifications at LME/NTUA. The flow meters measure the diesel fuel mass flow and density on the feed and return pipes of the engine. They were used to calibrate engine fuel consumption maps and measure the fuel consumption during experimental testing, allowing to evaluate the performance of the power-split algorithms in terms of fuel efficiency.

The torque meter, installed between EM and EB, was used for the mapping of the supplied command to brake torque output of the EB and EM and estimate the rotating friction of the testbed components. In closed-loop control, the speed measurement was used as a feedback signal to the control scheme, while with the torque flange, the actual dynamic behavior of the EM during power-split control was measured and evaluated. Finally, with the use of the torque flange, shaft rotational vibration issues were identified that led to the modification of the testbed

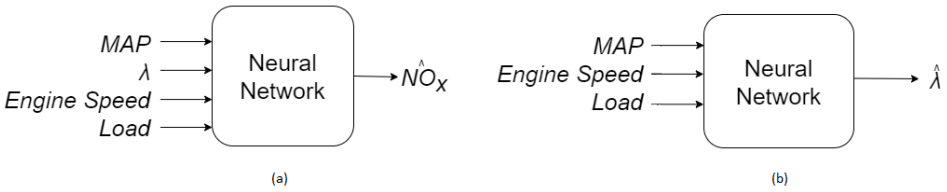

Figure 2-3: Inputs and outputs for NO_x and λ NN models.

shafting configuration.

The control and data acquisition system of the powertrain is based on the dSpace MicroAutoBox II (MAB 2) DS1401/1511 platform, with rapid control prototyping capability, programmed under the MATLAB/Simulink environment and MATLAB Code Generation Toolbox. Taking into account the system dynamics as well as the refresh rate of CAN messages, the fundamental sampling time for data acquisition and testbed control was specified at 100 Hz.

2.3 Engine virtual sensors

To complement the physical sensor system that is installed by the engine manufacturer, virtual sensors for engine-out emissions were developed and used for engine monitoring and powertrain control purposes. Several architectures have been used in the bibliography to capture the steady-state and dynamic response of a system output such as principle and data-based models. From the possible candidates, neural network models were used that can capture dynamic instantaneous phenomena in both transient and static operation of the marine diesel engine and that can be utilized as virtual sensors online. For more details about design and implementation in the testbed in the experimental rig at LME/NTUA, see [2].

Network development The model inputs were chosen based on which signals represent the specific operating point of the engine. For, NO_x emissions, the intake manifold pressure (MAP), the engine shaft speed, load demand ($Load$) and λ value, which expresses the Air Fuel Ratio (AFR) to the stoichiometric AFR, are used as representative quantities of the injection parameters, which are not measured in the experimental setup. The same principles apply to the λ model; MAP, rotational speed, and $Load$ were selected, as shown in Fig. 2-3. This approach is preferred not only because it adheres to the lack of sophisticated measurements, but also satisfies the portability and re-usability purposes. Also, most of the engine operating parameters are correlated with these basic variables that explicitly determine the operating point of the engine and the neural network structure can be used to make all the input-output relations and produce accurate predictions.

Time-delay neural network (TDNN) with input history and recurrent neural networks (RNN) with input and output history, shown in Fig. 2-4 are used to model the engine NO_x emissions

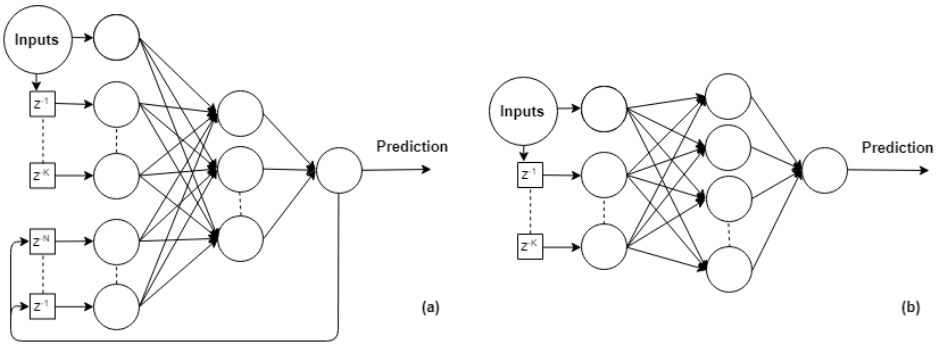

Figure 2-4: (a) Recurrent NN and (b) Time delay NN.

Table 2.1: Internal architecture of the neural network models.

Parameter	NOx RNN	NOx TDNN	λ RNN	λ TDNN
Hidden layers	1	1	1	1
Nodes of hidden layer	2	10	6	7
Input size	8	48	17	18
Input delay	1	12	4	6
Output feedback delay	4	-	5	-

and λ value. For each engine output, the RNN and TDNN models are using the same inputs and their main difference is only the external feedback loop that characterizes RNN models. This enables a direct comparison between models with and without a prediction feedback loop. Both TDNN and RNN models have a tanh function as input and hidden layers activation function and a linear output layer activation function, which helps to capture the non-linear behavior of the process. The structure of the final models for NO_x and λ prediction is summarized in Table 2.1.

Real-time NN validation The models were implemented in the testbed and validated in real-time as virtual sensors in scenarios within their training range but in different patterns than the training data and were also tested near the limits of the training range to evaluate their performance. Fig. 2-5 shows the validation test points and loading patterns that were applied. Some scenarios included load steps with constant ICE shaft speed (Steady Speed -Step Torque) and cases with alternating load and speed (Alt. Speed Torque 1 & 2).

NO_x TDNN and RNN models are evaluated against an engine map and λ models against a physics-based λ observer; both were developed in previous works for control purposes using the same training datasets. The criteria for the neural network models validation are the following as compared to the engine sensors measurements

1. Their average R^2 accuracy over each of the validation experiments.

2. Their ability to predict the steady-state value without oscillating behavior or instability,

especially at high engine loads.

3. Their accuracy to predict the transient dynamics of the NO_x and λ traces.

In Table 2.2, the accuracy of the neural network virtual sensors during the validation experiments is summarized. Although in validation experiments λ TDNN model achieves borderline better R^2 score, in visual evaluation, it lacks in transient performance and is more sensitive to noisy inputs. Also, particularly for validation experiments with alternating speed and torque, where a mediocre R^2 accuracy is scored by the λ models, it refers to a steady-state error at low engine load (and higher λ values), which is not important according to validation criterium 2, which is smaller than the prediction error of the physics-based observer.

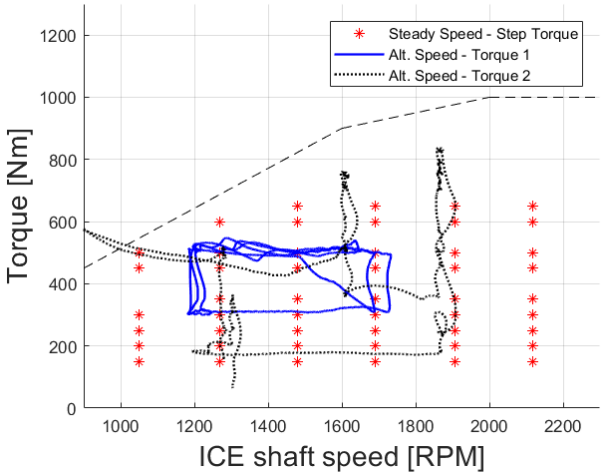

Figure 2-5: Validation area and patterns for the NO_x and λ models.

In Fig. 2-6, the results of the experimental testing by applying unknown loading and speed patterns are presented. It is noted that RNN virtual sensors reproduce well the transient dynamics, even at the speed change time instances, and approach the steady-state values with a small offset at some operating points. λ RNN has offset in predicting values > 4, which is not of great concern. A comparison between the NO_x and λ TDNNs shows that the λ models produce more accurate results than the NO_x models, as compared to their respective RNN counterparts, indeed both are more accurate and stable than the first principles observer. Overall, the validation proves that the RNN models can generalize in patterns similar but different than their

Table 2.2: Average R^2 accuracy score of the NN models during validation experiments.

Dataset	NOx RNN	NOx TDNN	λ RNN	λ TDNN
Training data	0.987	0.983	0.981	0.950
Steady Speed - Step Torque	0.977	0.782	0.858	0.865
Alt. Speed Torque 1	0.918	0.340	0.708	0.733
Alt. Speed Torque 2	0.947	0.021	0.589	0.602

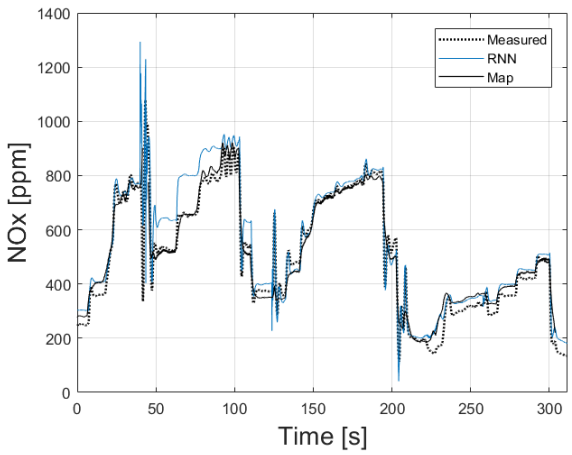

(a) Validation results for the NO_x RNN virtual sensor at alternating engine speed and torque test 1, compared against the actual measurement and an engine map.

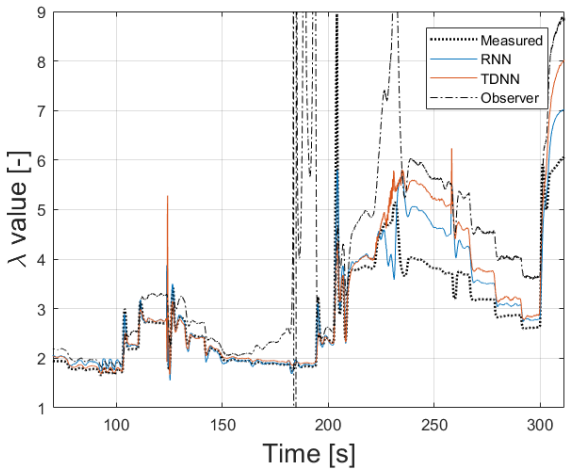

(b) Validation results for the λ TDNN and RNN virtual sensors at alternating engine speed and torque test 2, compared against the actual measurement and a physics based virtual sensor.

Figure 2-6: Validation results for NO_x and λ virtual sensors.

training dataset. Moreover, the RNN models have significantly higher accuracy during transient loading, as compared to TDNN models, static maps, and first principle observers.

2.4 Conclusion

In this chapter, the hybrid diesel-electric experimental facility HIPPO-2 at LME/NTUA was presented. To complement the physical sensor system that is installed by the engine manufacturer, data-based virtual sensors for engine-out emissions were developed and experimentally evaluated. The testbed configuration, component selection, and constraints regarding control system implementation, such as the unavailability of sophisticated measurements, are very close to a commercial application. As a result, the experience of experimental testing resembles working on an actual, full-scale marine hybrid propulsion plant onboard a vessel. Based on the particular configuration and specifications of the experimental system, the next chapters present the modeling methodology as well as control systems development and implementation in the HIPPO-2 experimental powertrain.

THIS PAGE INTENTIONALLY LEFT BLANK

Chapter 3

Powertrain Modeling

In this thesis, predictive control schemes are designed for the optimal power-split calculation for marine hybrid diesel-electric power plants in transient operation. In this context, this chapter is dedicated to control-oriented system modeling. The powertrain model is then utilized as the internal model of the controller.

3.1 Methodology

The model of the powertrain that will be used for controller design, must capture system behavior in a precise manner and be simple enough, so that the optimization problem can be solved online within the time period of a sampling interval, [68]. As predictive control is to a large extent a feedforward approach, it depends strongly on the internal model quality. Besides, many system variables cannot be measured onboard in marine applications; neither are they available as model inputs.

First-principle models have been the main choice of modeling and simulation engineers, as they allow physical insight into the system's design changes; however, sometimes they tend to be too simple to describe the real system behavior to the necessary degree of precision to meet the increasing controller performance requirements, [69]. The alternative to first principle models are data-based models, which typically refer to a parameterized candidate model without any reference to the physics of the real plant. In this case, the choice of the excitation signal during the system identification procedure is critical, [70]. However, for some cases, such as emissions, the candidate model structure will in general not contain the true model, therefore system identification becomes essentially an approximation tool, [71].

Against this background, there is a rationale for combining both approaches so to get simple and high-performing models. Gray-box models use physical understanding to describe explicitly aspects of the models that can be described analytically and combines them with data-based models, [72]. In this context, an efficient approach is to observe global patterns in the data

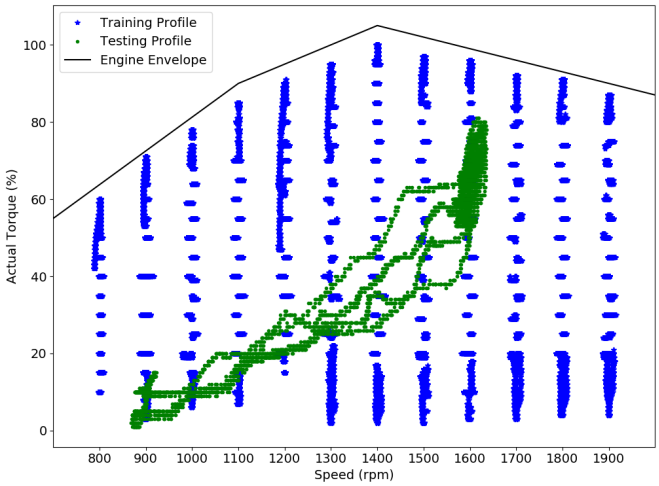

Figure 3-1: Identification and validation engine data points.

which can be expressed analytically with few parameters and thus infer not only the parameters of a given model but also its structure from the data, [73].

3.1.1 Data, Model structure and Input selection

For the system identification procedure, data acquired from HIPPO-2 testbed operation were utilized. These datasets capture ICE operation in step changes of the ICE's electronic fuel index at constant rotational speeds and cover the whole engine operating area, as it can be seen in Fig. 3-1.

For building up data-based models, at first input quantities have to be defined. Here, all available ECU values have been considered as possible inputs. However, priority was given to manipulated variables, such as engine speed and torque, which define the powertrain operating points, and as a consequence, all other quantities change indirectly, according to these manipulated variables. As such, the selection of the model structure was mainly based on black- and gray-box models that yield from some physical knowledge that is included in the structure of f and other terms have to be identified from patterns that were observed in the output quantities according to the selected inputs.

The parametric equations that are derived, describe the ICE and EM quantities directly, and not via their derivatives, by fitting steady-state engine maps to polynomial equations. The advantage of these models is that they are simple, and computationally efficient since no integration is needed. Therefore, this quasi-static approach is popular in hybrid marine and automotive applications, [23].

3.1.2 Data-based model identification

In the data-based model identification, the parameters of each model which relate the input quantities u (here the available powertrain measurements) to the output quantities y, are fitted to measurement data. The relationship is defined by a linear or nonlinear function f which contains parameters that are given in a vector of regressors θ and the prediction error ε as follows

$$y = f(u, \theta) + \varepsilon \tag{3.1}$$

Parametric model identification methods are utilized to find the optimal value of θ, given a criterion J so that the model error $\varepsilon = y - f(u, \theta)$ becomes minimal for the data set Z of length n that is used for this optimization procedure. For each model, the optimization criterion for parameter fitting is the sum of the squared residuals over all n samples as follows

$$J_n(\theta, Z^n) = \frac{1}{n} \sum_{i=1}^{n} \frac{1}{2} \varepsilon_i^2(\theta, Z^n) \tag{3.2}$$

To solve the above minimization, standard solution methods are used for both cases of linear and nonlinear parameter estimation problems, where linear and nonlinear least squares and the Levenberg-Marquardt algorithm are employed respectively.

3.2 Control-Oriented Modeling

The parallel marine hybrid propulsion plant which is investigated in this thesis is presented in Fig. 3-2. It consists of an internal combustion engine (ICE) connected on the same shaft with an electric machine (EM) The EM is connected, through an inverter device to the energy storage. The mechanical and electrical power flow, the input signals, as well as the system outputs (measurements) of interest are also shown in the schematic diagram.

For the design purposes of the energy management system, a MIMO model of the parallel hybrid powertrain is developed to be integrated into the controller. It consists of the following components: the engine, the EM, the battery, and the mechanical shafting. The system dynamics include battery and shaft dynamics, as the engine and EM response time constants are much smaller than the controller's computational interval and it can be assumed that they have a quasi-static behavior.

As system inputs, the commands to the ICE (u_{ice}) and EM (u_{em}) for torque production are selected, and the external load that acts as disturbance (Q_{load}). System outputs are selected the engine rotational speed (ω_{eng}) and the battery state of charge (SOC). System outputs are the state variables and, in addition, engine fuel consumption ($\dot{m}_f$) and NOx emissions ($\dot{m}_N$) of the ICE.

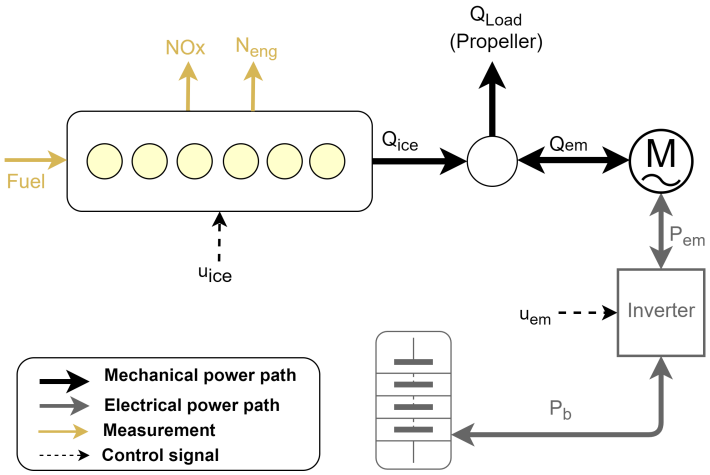

Figure 3-2: Schematic representation of a parallel hybrid diesel electric powertrain.

The control-oriented model consists of four sub-models that are described below. In total, the system state $\mathbf{x}$, input $\mathbf{u}$, disturbance input $\mathbf{u_d}$, and output $\mathbf{y}$ vectors are the following

$$\begin{aligned} &\text{state variables:} && \mathbf{x} = \begin{bmatrix} \omega_{eng} & SOC \end{bmatrix}^T \\ &\text{input variables:} && \mathbf{u} = \begin{bmatrix} u_{ice} & u_{em} \end{bmatrix}^T \\ &\text{disturbance input variable:} && \mathbf{u_d} = Q_{load} \\ &\text{output variables:} && \mathbf{y} = \begin{bmatrix} \omega_{eng} & SOC & \dot{m}_f & \dot{m}_N \end{bmatrix}^T \end{aligned} \tag{3.3}$$

Measurements that are utilized for system modeling and control are the ICE rotational speed, fuel consumption and NOx emissions, ICE and EM torque production, electric power consumption, and battery state of charge. For closed-loop control, only ICE speed and battery state of charge are used. Also, any disturbance characteristics are unknown and should be estimated.

3.2.1 Rotational shaft dynamics

The rotational dynamic behavior of the power plant is derived from

$$\frac{d\omega_{eng}}{dt} = \frac{1}{J_{system}}(Q_{ice} + Q_{em} - Q_{load}) \tag{3.4}$$

where ω_{eng} is the engine shaft rotational speed, J_{system} is the powertrain moment of inertia at the engine side, Q_{ice} is the brake torque of the engine delivered at the shaft, Q_{em} is the output torque of the electric motor/generator (positive if the EM is motoring), and Q_{load} is the torque load which is applied to the powertrain at the engine side of the gearbox.

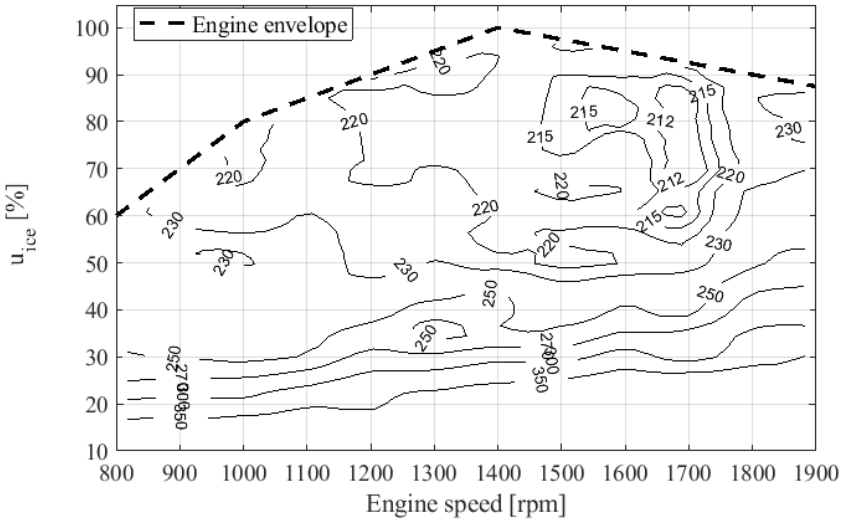

(a) Diesel-engine BSFC map [gr/kWh].

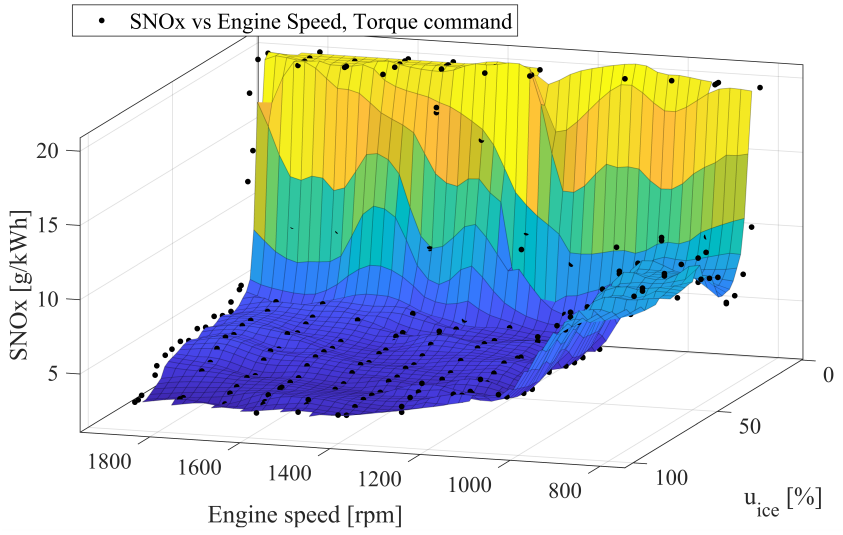

(b) Diesel-engine BSNE map.

Figure 3-3: Measured diesel-engine brake fuel and NOx efficiency maps.

3.2.2 Diesel engine control-oriented model

The ICE considered in this Thesis is a 4-stroke diesel engine with a high-pressure Exhaust Gas Recirculation (EGR) system. The main particulars of the ICE are presented in section **??**, and in Fig.3-3 the measured brake engine performance in terms of fuel efficiency and NOx emissions can be seen. Although the main processes of a diesel engine are theoretically well understood, first-principle models describing these processes, are either not able to provide control-oriented models with sufficient accuracy, as most information is not available or is complicated and cannot serve fast real-time predictive control. Therefore, the main challenge in powertrain modeling consists in finding models that represent the highly non-linear process, such as engine-out NOx emissions with sufficient accuracy, but still can be parameterized using only information available on a typical commercial setup.

The brake torque of the ICE, fuel consumption, and NOx emissions were modeled according to the manipulated input u_{ice} of the diesel engine and the controlled speed output N_{eng}, which also determine the operating point within the ICE loading envelope. The measured brake specific fuel consumption (BSFC) and NOx emissions (BSNE) maps of the diesel engine are shown in Fig. 3-3. Engine brake torque output Q_{ice} and fuel consumption $\dot{m}_f$ were modeled as polynomial functions of these inputs as follows

$$Q_{ice} = \theta_Q^T [1 \; u_{ice} \; N_{eng} \; N_{eng}^2]^T \tag{3.5}$$

$$\dot{m}_f = \rho_f(f, T_f)\theta_f^T [1 \; u_{ice} \; N_{eng} \; N_{eng} u_{ice} \; u_{ice}^2 \; N_{eng}^2]^T \tag{3.6}$$

where u_{ice} is the electronic fuel index which is fed to engine ECU, N_{eng} is the rotational shaft speed in rpm, (i.e. $N_{eng} = \frac{\omega_{eng} \cdot 60}{2\pi}$) , θ_i are matrices of regressors which are fitted to the equations above, using experimental data. In Eq. (3.5), the terms related with rotational speed refer to torque losses due to shaft frictions, etc, [74]. Finally, ρ_f is the measured fuel density, which depends on the fuel quality f and temperature T_f. The fitting accuracy of Eq. (3.5) and Eq. (3.6) are presented in Fig. 3-4 and Fig. 3-5.

As far as the NOx emissions of the diesel engine are concerned, the modeling problem becomes more complicated. The NOx production depends not only on the engine operating point but also on the operation of a high-pressure Exhaust Gas Recirculation (EGR) system. However, in the HIPPO-2 testbed, the EGR actuator is controlled by the engine Electronic Control Unit (ECU) and it cannot be regulated with an external input signal. Besides, the control law of the EGR system cannot be approximated due to the lack of specific measurements such as the intake manifold air mass flow rate which is not available. As such, it was decided to be excluded from the NOx model.

To develop the NOx model, typical model structures have been considered and tested, such

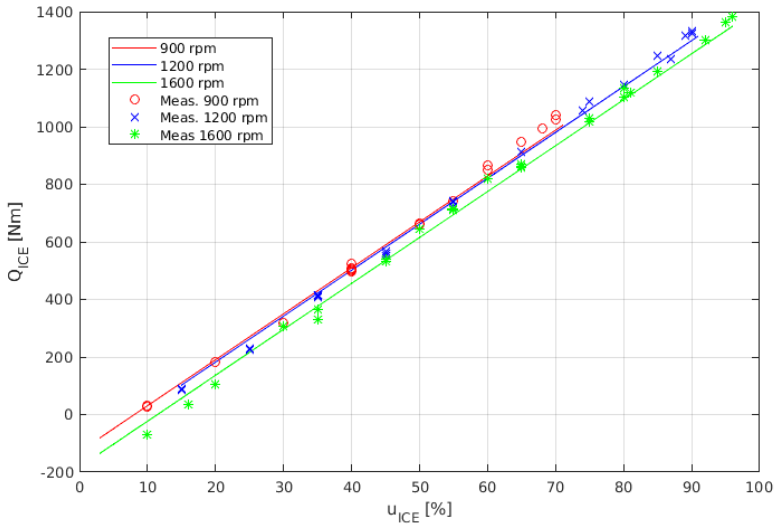

Figure 3-4: Diesel-engine command to brake torque output mapping, Eq. (3.5).

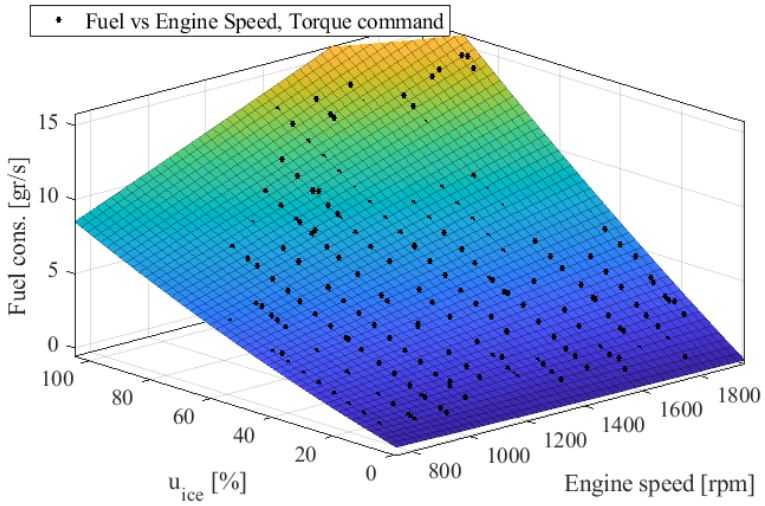

Figure 3-5: Diesel-engine fuel consumption mapping, Eq. (3.6).

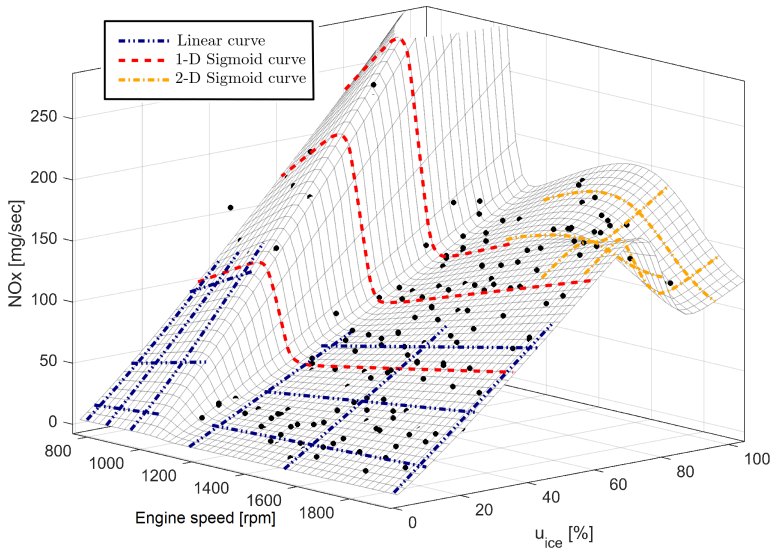

(a) Conceptual approach for NOx model, Eq. (3.7).

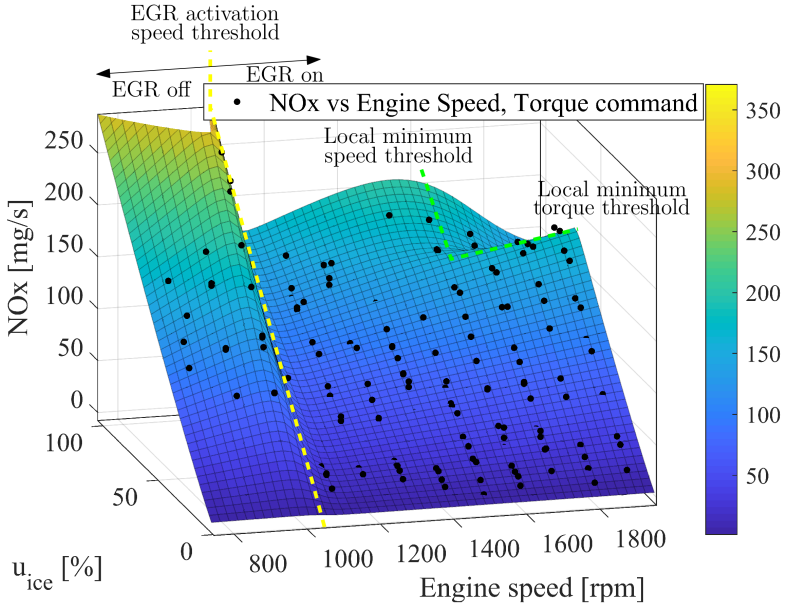

(b) Diesel engine NOx emissions behavior, Eq. (3.7).

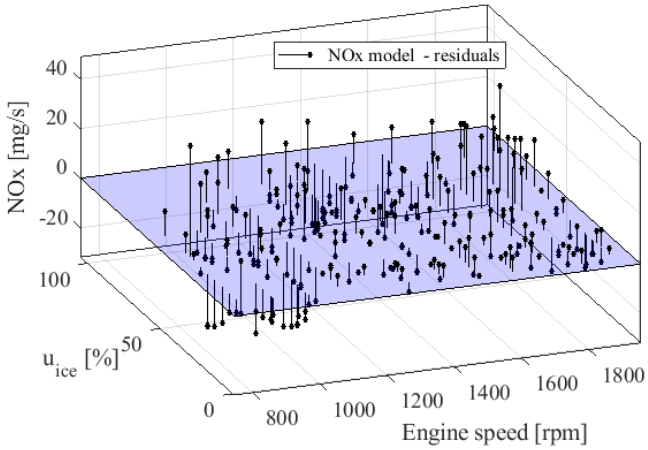

(c) Residual error of NOx emissions model, Eq. (3.7).

Figure 3-6: Diesel engine NOx emissions modeling.

Table 3.1: Fitting results of the engine models

Model	Symbol	R-Square
Torque production	Q_{ice}	0.994
Fuel consumption	$\dot{m}_f$	0.995
NOx emissions	$\dot{m}_N$	0.953

as polynomial models and sigmoid functions. Sigmoid functions are widely used for system modeling, as they can approach accurately non-linear patterns, as the one observed in the NOx emissions of the engine in Fig. 3-6a, according to the engine operation point. As it can be observed in Fig. 3-6b, the NOx behavior follows an increasing trend in higher speed and torque load with two local minima observed near speed $N_{eng,N,0} = 1050\ rpm$, where the EGR system is activated as well as above speed $N_{eng,N,1} = 1750\ rpm$ and $u_{ice,N,1} = 80\%$. Hence, these points were used as threshold values of the sigmoid curves. Overall, the NOx model is formed as

$$\dot{m}_N = b_{N,1}[a_{N,1} - a_{N,2}\sigma_1(z_1)]u_{ice}^{a_{N,4}} N_{eng} - b_{N,2}\sigma_2(z_2)\sigma_3(z_3)u_{ice}N_{eng} \tag{3.7}$$

where

$$\sigma_i(z_i) = \frac{1}{1+e^{-z_i}} \text{ is the sigmoid function}$$

and

$$z_1 = a_{N,3}(N_{eng} - N_{eng,N,0})$$

$$z_2 = a_{N,5}(u_{ice} - u_{ice,N,1})$$

$$z_3 = a_{N,6}(N_{eng} - N_{eng,N,1})$$

Parameters $a_{N,i}$ and $b_{N,i}$ are fitted to the measured data, as it is shown in Fig. 3-6b. The fitting R-square results of the diesel engine models is presented in Table 3.1.

3.2.3 Electric machine

Powertrain's electric interconnection is presented in Fig. 3-2, where the EM operation charges and discharges the battery, without consideration of any auxiliary electric power consumption or generation. The output torque of the EM is regulated via a frequency inverter, which is aligned between the EM and the battery. The response time of the EM torque generation can be neglected in the context of this work since its time scale is much smaller than the controller's sample time.

Although electric machines are considered dynamical systems, dynamic models are rarely used for hybrid power plant simulation and its control-orientated applications, [18]. From the control engineering point of view, the AC motor output which is required for the controller is the power flow, given the output torque and rotational speed as inputs. As such, in the present

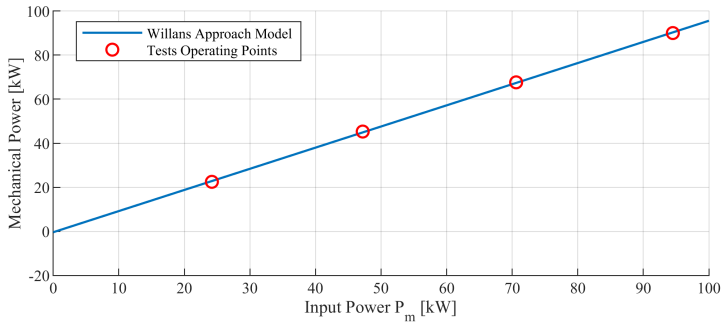

Figure 3-7: Willan's model fitting results, compared to test data from manufacturer.

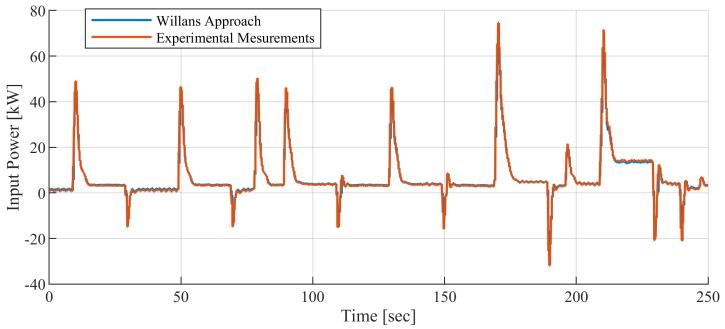

Figure 3-8: Willan's model comparison with experimental data.

work, a quasi-static approach was followed.

Therefore, the EM torque is modeled as the following linear relation

$$Q_{em} = c_{em} \cdot u_{em} \tag{3.8}$$

where u_{em} is the torque command as a percentage of the maximum torque which is fed to the drive and c_{em} expresses the transformation to torque units.

A widely used quasi-static model, which connects the output rotating speed and torque with the required power input, is the Willans approach, [18]. This model considers that the electrical power input and the mechanical power output, have a linear dependency. The model is valid for both motoring and generating modes. consequently, the mechanical torque output Q_{em} of the EM was evaluated as

$$\begin{aligned} Q_{em} \cdot \omega_{eng} &= e \cdot P_m - P_0, \qquad \text{(Motoring)} \\ Q_{em} \cdot \omega_{eng} &= \frac{P_m}{e} - P_0, \qquad \text{(Generating)} \end{aligned} \tag{3.9}$$

where P_{em} is the electric power and e and P_0 are the Willans model coefficients, related with power conversion efficiency. These are considered to be constant. The Willan's model is fitted to HIPPO- 2 AC motor data, and then it is compared to experimental results. The data used for fitting was derived from the manufacturer's data-sheets. The result of Willan's model and its comparison with the experimental results is illustrated in Fig. 3-7 and Fig. 3-8.

Considering the fitting results, it is clear that the model can satisfactorily predict the required power demand, for low and high loads for both motoring and generating modes. Therefore, the model was integrated inside the NMPC controller and was also used in simulations.

Model parameters

The model coefficients that are presented in this chapter were calculated by using data from the testbed and the manufacturers' test sheets. The numerical values are listed in Table B.1.

3.2.4 Battery model

The main function of battery devices in hybrid propulsion plants, is to transform and store electrical energy in chemical form and then re-transform it back to electricity, to be used by the electric motors, when it is required, [75]. Each battery is characterized by the nominal capacity Q_{nom} and the maximum electric power that it can provide. Also, the dimensionless parameter *State of Charge* (SoC) describes the remaining capacity Q_t of the battery, and is expressed as a percentage or fraction of the nominal capacity

$$SoC(t) = \frac{Q(t)}{Q_{nom}} \tag{3.10}$$

The battery charge, and therefore SoC, is difficult to be measured directly. Subsequently, it is calculated indirectly, from the electric current flow as

$$\dot{Q}(t) = -I_b(t) \tag{3.11}$$

Several battery modeling approaches have been presented in the literature. The use of partial differential equations and a large number of unknown parameters, often leads to high computational cost and consequently, these models are not desirable for control-oriented applications in HEV, [76]. Most of the modeling approaches refer to the linear operating region, since the nonlinearities appear mostly outside of the battery operational limits, [77].

In the present work, two Equivalent Circuit Models (ECMs) were finally used, a quasi-static and a dynamic approach, which are presented in Fig. 3-9. Regarding the capacity and model parameters of the battery, they are given in respect to each power-split control system design, where the suitable battery sizing was made.

Quasi-static model for controller design

This model was utilized as a part of the internal model of the controller for SoC prediction. It is based on the widely used equivalent circuit, which is presented in Fig. 3-9a, and was firstly used for lead-acid batteries [18]. The ECM consists of a voltage source and a resistance. The

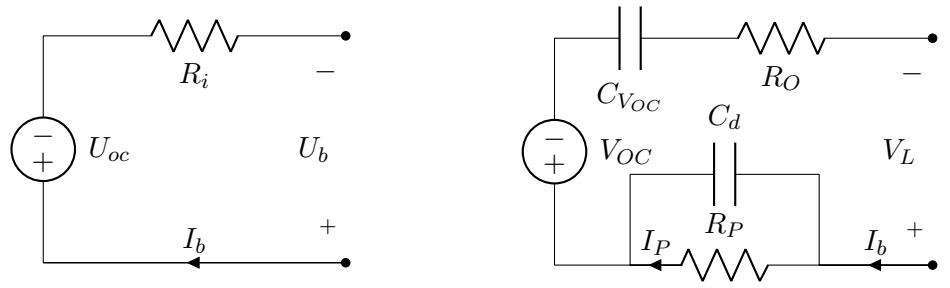

(a) Equivalent circuit of battery model for controller design

(b) Equivalent circuit of battery model for state of charge emulation.

Figure 3-9: Battery models used in this work.

first component refers to the open source voltage U_{oc}, and represents the equilibrium potential of the battery. Since this quantity depends on the charge level, it is parameterized using the following affine relationship

$$U_{oc}(t) = k_2 \cdot SOC(t) + k_1 \tag{3.12}$$

The internal battery resistance R_i, takes into account several phenomena and can be evaluated as a function of SoC. Thus, in HEV optimization problems, internal resistance is considered as a constant quantity [74]. In the present work, the battery modeling is oriented for control purposes, and therefore, the input variable is the required power $P_b(t) = I_b(t)U_b(t)$ that the battery should balance, and the output variable is the SoC of the battery. The terminal battery voltage equation for the quasi-static ECM is calculated via the Kirchhoff voltage law

$$U_b(t) = \frac{U_{oc}(t)}{2} + \sqrt{\frac{U_{oc}^2(t)}{4} - P_b(t) \cdot R_i} \tag{3.13}$$

And the yielding equation for battery current is

$$I_b(t) = \frac{U_{oc}(t) - \sqrt{U_{oc}^2(t) - 4P_b(t) \cdot R_i(t)}}{2R_i} \tag{3.14}$$

Finally the SoC, is calculated by combining Eq. (3.11) and Eq. (3.10). As a result, a differential equation for the state of charge is formulated

$$\frac{dSOC}{dt} = -\frac{100}{Q_{nom}} \cdot \frac{U_{oc}(t) - \sqrt{U_{oc}^2(t) - 4P_b(t) \cdot R_i}}{2R_i} \tag{3.15}$$

The operating limits of the above model, can be derived considering Eq. (3.13), [18]. For the discharge case, the following limitation are applied: $P_b \geq 0$ and $U_b < U_{oc}$, leading to the following expressions for the maximum power, the battery can provide, and the corresponding voltage and current

$$P_{b,max}(t) = \frac{U_{oc}^2(t)}{4R_i(t)}, \qquad U_{b,P_{max}}(t) = \frac{U_{oc}(t)}{2}, \qquad I_{b,P_{max}}(t) = \frac{U_{oc}(t)}{2R_i(t)} \tag{3.16}$$

In the case of control schemes including battery cell components, additional constraints regarding the battery function are applied, such as rate of SoC alteration, maximum current, and voltage, etc., [76, 78]. These constraints refer to battery health management, and are usually defined by the manufacturer. In this work, the battery component is virtual, and therefore, no further analysis is conducted.

Battery model utilization

The quasi-static battery model was integrated inside the NMPC controller. The reason is, that the only output variable of importance considering the battery, for control purposes, is the battery SoC. As for both models, this parameter evolution is almost the same, and the prediction horizon will be a maximum of 10 seconds, the quasi-static approach returns an accurate result. Moreover, the quasi-static model is contains only one differential equation and one algebraic loop. However, there are limitations, as compared to the actual battery behavior.

To generate more realistic conditions, a more complicated model than the one for controller design was used, from [79], which is presented in Appendix A. The virtual battery component is considered to be charged/discharged by the electrical energy that is produced/consumed by the EM of the HIPPO-2 testbed. The battery state of charge is simulated during the experiments. The selection of different battery models for SOC simulation and controller design was intentional, to evaluate the controller performance with modeling inaccuracies.

3.3 Conclusion

In this chapter, the powertrain modeling methodology and fitting results were presented. Each subsystem's outputs, i.e. engine torque and speed, fuel consumption and NOx emissions, electric motor torque, and electric power flow, as well as battery state of charge were modeled. First principle and data-based models were fitted to powertrain measurements and the component interconnection was identified. As inputs, the manipulated variables of the powertrain were primarily used, which are the torque production commands of the engine and the electric motor, and the shaft rotational speed as they determine the operating point within the engine loading envelope. Fitting results showed that the proposed approach can approximate accurately the dynamical system behavior during transient loading, as well as patterns that were observed within the measured data. The powertrain models will be used for control system design and powertrain simulation. In the next chapter, the propeller disturbance modeling and estimation are explained.

THIS PAGE INTENTIONALLY LEFT BLANK

Chapter 4

Load Emulation and Observer Design for Propeller

In the previous chapter, the control-oriented modeling of the ship power plant was presented. The models of the hybrid powertrain are going to be used for the controller design process. This chapter focuses on the modeling of ship and propeller dynamics and also on the estimation of propeller disturbance parameters that are required for optimal control.

This chapter aims to employ a parametric propulsion plant model that fits the experimental facility to apply propeller loading considering several vessel operating scenarios and conditions. For this, the main propulsion plant components and their dynamic interaction are taken into account. Also, a propeller observer is designed and implemented to quantify the propeller load characteristics, as acting disturbance, which are required for the optimal power-split calculation, without knowledge of the uncertain propulsion plant parameters.

4.1 Propulsion Plant Model

As it can be seen in Fig 4-1, propulsive load variation, induced by ship operation and environmental conditions, affects the overall system performance, as it can lead to engine overloading or cause oscillating behavior of the propulsion powertrain. As such, a realistic simulation environment of the ship propulsion plant is a prerequisite for the design and evaluation of the control system. The modeling of the propulsion system of the ship has to be well defined and provide information for the transient effects during system operation as well as the influence from external-environmental disturbances, such as sea waves. Moreover, optimal control systems, also require reliable disturbance models and information, to perform an accurate prediction for the system operation within a short future time horizon.

HIPPO-2 experimental facility is a full-scale prototype hybrid diesel-electric marine powertrain, which could potentially be fitted in a small vessel, as the main or one of the main propeller

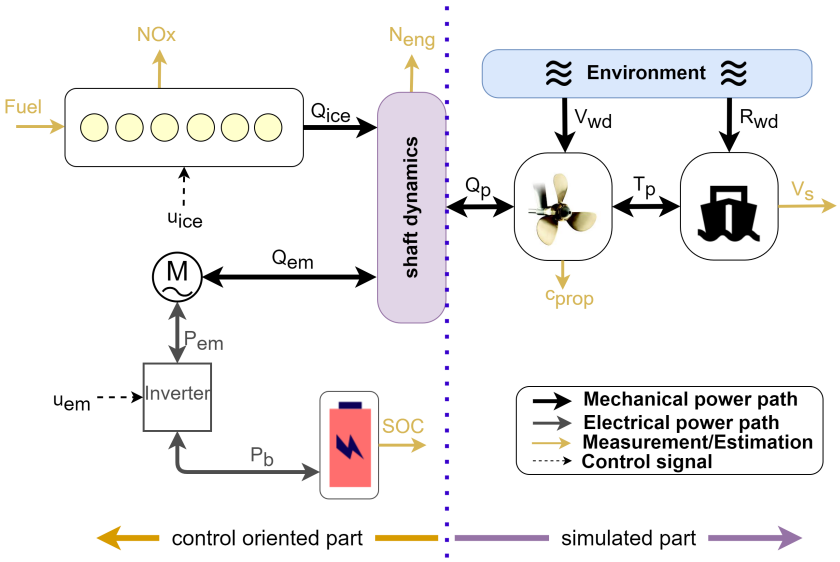

Figure 4-1: Subsystem interaction and modeling approach for the parallel hybrid propulsion plant considered in this Thesis.

prime movers, e.g a port tug vessel. As such, a model for the surge motion of a similar ship (shown in Fig. 4-2) was employed to perform emulation of the propeller load demand during ship maneuvering and cruising conditions under wave disturbance. The importance of considering the *engine-propeller-ship-environment* interaction in propulsion controller design procedure is highlighted in [13]. The aim is to generate realistic loading conditions for the powerplant, to perform control system tuning and robustness evaluation in cases such as

- Engine overloading
- Increased transient load demand due to fast accelerations
- Propeller load fluctuations due to wave disturbance

For this purpose, the basic principles of ship propulsion were considered.

The propulsion plant model includes the shafting components to calculate the delivered power to the propeller, the propeller performance characteristics, the ship dynamics as well as an environmental model for the wave disturbance which affects the mean and the instant propulsion plant equilibrium point. The principal vessel particulars, the propulsion plant model parameters as well as the wave spectral characteristics are summarized in Table B.2.

4.1.1 Gearbox and shaftline

The gearbox reduction ratio i_{gb} projects on the engine side $(load/eng)$ the torques Q_i, the rotating speeds ω_i and the inertias J_i of the connected parts on the propeller shaft side $(shaft/prop)$

Figure 4-2: The tug vessel considered in this work, model DAMEN Stun Tug 1205 from Damen Shipyards Group (NL), $L = 13.8\ m,\ \Delta = 58\ t$.

as follows

$$Q_{load} = \frac{Q_{shaft}}{n_{gb} i_{gb}} \tag{4.1a}$$

$$\omega_{eng} = i_{gb} \omega_{shaft} \tag{4.1b}$$

$$J_{load} = \frac{J_{shaft}}{i_{gb}^2} \tag{4.1c}$$

The gearbox efficiency $n_{gb} = \frac{Q_{shaft}}{Q_{load}} = \frac{Q_{load} - Q_{loss}}{Q_{load}}$ was considered from [80], where the gearbox losses are calculated as

$$Q_{loss} = \alpha_{gb} + b_{gb} \omega_{eng} + c_{gb} Q_{load} \tag{4.2}$$

and the shaft line efficiency was evaluated from [81] as

$$n_s l = 1 - b_{sl} \omega_{shaft} + \frac{\alpha_{sl}}{1 - b_{sl}} (b_{sl} \omega_{shaft} - \omega_{shaft}^2) \tag{4.3}$$

The total mechanical efficiency of the shaftline is calculated as $n_m = n_{gb} n_{sl}$ and the propeller torque is transmitted to the engine as

$$Q_{load} = \frac{Q_{prop}}{n_m i_{gb}} \tag{4.4}$$

4.1.2 Propeller

A ducted, 4-blade, fixed pitch Wageningen Ka 4-40 with Nozzle 19A propeller with a pitch to diameter ratio $\frac{P}{D} = 1.2$ was considered, which is commonly used in small size harbor tugs. The propeller model was obtained from [82].

The propeller performance characteristics, torque demand Qp and thrust production T_p, are

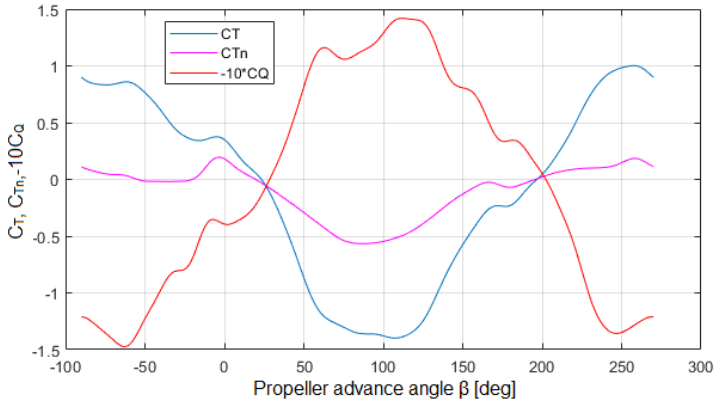

Figure 4-3: Wageningen Ka4-70 P/D=1.2 ducted propeller with Nozzle 19A C_Q, C_T coefficients. C_{Tn} coefficient shows the thrust fraction that is produced from the duct itself.

based on the propeller advance angle β at 70% of the propeller radius, which is defined as

$$\beta = \arctan \frac{V_a}{0.7\pi n_p D} \tag{4.5}$$

where V_a is the propeller effective wake velocity, n_p is the propeller rotational speed (in rps) and D the propeller diameter. V_a is the propeller inflow velocity which is affected by the ship hull shape, therefore it differs from the ship speed V_s by the effective wake fraction w, as

$$V_a = (1 - w)V_s + v_{wd} \tag{4.6}$$

where v_{wd} is the wake field speed disturbance due to waves from Eq. (4.14).

As such the torque and thrust of the propeller are calculated as follows

$$T_p = \frac{\pi}{8} C_T \rho [V_a^2 + (0.7\pi n_p D)^2] D^2 \tag{4.7a}$$

$$Q_p = \frac{\pi}{8} C_Q \rho [V_a^2 + (0.7\pi n_p D)^2] D^3 \tag{4.7b}$$

$C_T = C_T(\beta)$ and $C_Q = C_Q(\beta)$ coefficients are propeller specific, based on the propeller advance angle β, as shown in Fig. 4-3, and are derived from Fourier series models fitted to the propeller open water experimental results, such as in [83]. The actual torque that is absorbed from the propeller shaft depends on the relative rotative efficiency η_r as

$$Q_{prop} = \frac{Q_p}{\eta_r} \tag{4.8}$$

The propeller inertia J_{prop} consists of the rotating mass inertia J_M plus the hydrodynamic mass inertia J_P, as calculated in [82, 84].

4.1.3 Ship dynamics

The propeller loading model depends on the ship advance speed; therefore the ship longitudinal motion was taken into account. The vessel surge dynamics for the ship acceleration are calculated

$$\frac{dV_s}{dt} = \frac{N_p T_p - \frac{R_t}{(1-t)} - R_{wd} - F_{BP}}{M_{disp} + M_{hyd}} \tag{4.9}$$

where M_{disp} is the ship displacement and M_{hyd} is the added hydrodynamic mass of the ship. The above equation depends on the following forces

- $N_p T_p$ is the propellers' thrust force, where N_p is the number of fitted propellers, T_p is the thrust contribution of each propeller.
- R_t is the total ship resistance, which consists of the calm water frictional and wave-making resistance $R_t = R(V_s)$, t is the thrust deduction factor due to hull and propeller interaction.
- R_{wd} is the added mean resistance force due to adverse weather conditions and wave disturbance, which is calculated from Eq. (4.15).
- F_{BP} is the external force that acts on the ship during tug operations.

4.1.4 Wave disturbance

For more realistic simulation scenarios, irregular wave disturbance was considered. The wave disturbance affects the propulsion plant in two ways. The wave orbital motion changes propeller inflow velocity, as presented in Eq. (4.6) and on the other hand a mean wave resistance is considered to act on the hull due to the additional water pressures of the waves acting on the hull, Eq. 4.9.

Irregular waves are formed from N contributing regular monochromatic waves. As such, using the superposition principle, the water surface elevation is calculated

$$\zeta(t) = \sum_{i=1}^{N} \zeta_i \sin(\omega_i t + \epsilon_i) \tag{4.10}$$

where ζ_i, ω_i and ϵ_i are the amplitude, the frequency, and the phase of each contributing regular wave component. A snapshot of the water surface elevation is presented in Fig. 4-4. Assuming deep seawater, the wavenumber k_i is given

$$k_i = \frac{\omega_i^2}{g} \tag{4.11}$$

so the ship moving reference frame with encounter angle χ is excited by the waves with encounter

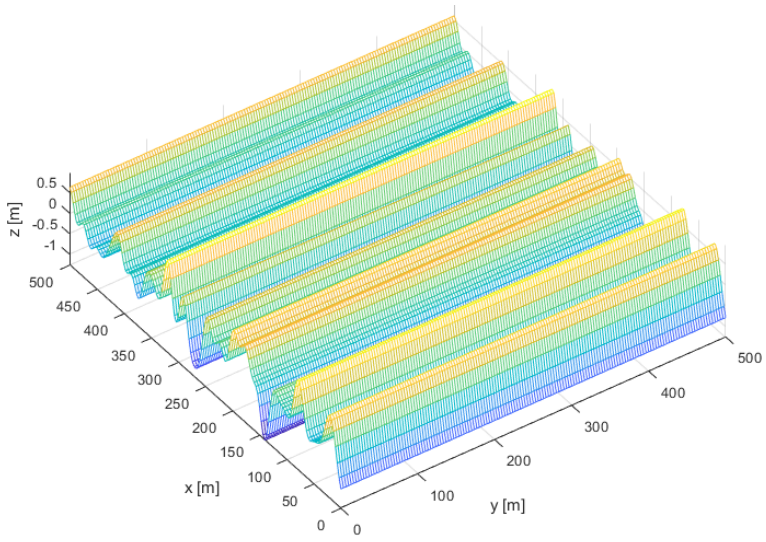

Figure 4-4: Snapshot of water free surface elevation with one-directional irregular waves, $\chi = 180^o$, generated with GNC toolbox [85].

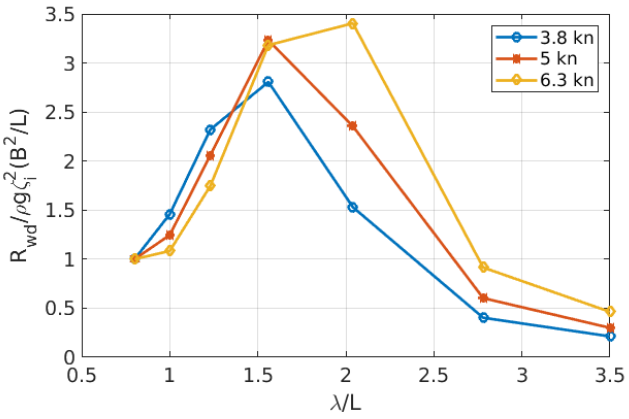

Figure 4-5: Normalized added resistance coefficient for head sea considered in this work.

frequency ω_{e_i}

$$\omega_{e_i} = \omega_i - k_i V_s \cos(\chi) \tag{4.12}$$

At depth h_{prop}, where the propeller hub is immersed, the water orbital velocity is

$$\dot{\zeta}_p(t) = \sum_{i=1}^{N} \zeta_i \omega_{e_i} \cos(\omega_{e_i} t + \epsilon_i) e^{-h_{prop} k_i} \tag{4.13}$$

Finally, the propeller inflow velocity disturbance v_{wd} is evaluated as

$$v_{wd}(t) = -\dot{\zeta}_p \cos(\chi) \tag{4.14}$$

The added resistance can be calculated using experimental or simulation data for the ship seakeeping response at each frequency that contributes to the irregular wave, as shown in Fig. 4-

5. These experimental data are from [86] and are scaled to the ship that is studied here with the Froude similarity principle ($\frac{V_s}{\sqrt{gL}}$ fraction is kept constant). Using the superposition principle

$$R_{wd}(t) = \sum_{i=1}^{N} R_{wd,i}(V_s, \zeta_i, \frac{g}{\omega_i}) \tag{4.15}$$

The characteristics of the regular waves that contribute to the irregular wave formation are selected based on a specific wave spectrum, where the sea state is defined from the significant wave height H_s (that is the mean value of the 1/3 highest free surface elevation observations) and the peak frequency ω_p, which is the wave frequency at which the maximum spectral density occurs. Like sea state, wave spectrum determines, in ocean engineering science, the relation between H_s and ω_p that are observed at a specific sea area. The value of H_s considered in this work corresponds to a sea state condition that is at the upper limit of the sea state that a ship of this size will face during operation.

Remark: In the above propeller and environmental disturbance model, many assumptions have been made and many parameters, such as the ship 6-DOF motions, the propeller immersion or the wind disturbance have not been taken into account. However, the scope of the above model is to generate a control-oriented disturbance scenario, for advanced propulsion control systems development and evaluation. An advanced approach was followed, as compared to the studies that have been made so far, in the related literature of marine powertrain control, which consider simplistic environmental models, such as white noise or monochromatic sinusoidal waves. Engine control systems design is very critical for propulsion plant performance. Sea state and adverse weather conditions can excite the propulsion powertrain system in a wide range of frequencies and above their operational limits as well. Therefore, the advantage of irregular waves simulation, as compared to regular waves oscillating at only one frequency, is that they facilitate the design and evaluation of the control system architecture and tuning using realistic engine loading scenarios.

4.2 Propeller Load Observer

One of the critical questions that always needs to be answered in marine propulsion plant control is how to quantify the propeller load that needs to be satisfied by the ship power plant in an optimal fashion. The underlying physics and the number of systems that interact in a complex and interconnected manner, make the problem difficult to be explicitly solved. The reason is that ship operation is performed mainly in off-design conditions, due to environmental disturbances, operational conditions, system aging, etc., most of which cannot be measured or quantified.

Optimal control methodologies require full quantitative knowledge of the system operating parameters and conditions, which proves to be challenging in complex and uncertain systems, such as a marine propulsion plant. The knowledge of the propeller load disturbance is important for the control system equilibrium. In the same framework, to achieve high vessel control performance and perform energy management, all propulsion system variables that are considered in the problem formulation should be available. In practice, this is often difficult due to reasons such as the inability to place a sufficient number of sensors, the high cost of specialized sensors installation, the uncertainties regarding the propulsion plant, propeller, and ship resistance characteristics over time. On the other hand, observer signals can be more accurate, less expensive to produce, and more appropriate than measured signals, reducing the phase lag inherent in the sensor. In general, observers offer an inviting alternative to adding new sensors or upgrading existing ones. In some cases, the observer can be used to enhance system performance. EKF has been recently the subject of extensive research and application, particularly in the area of autonomous or assisted navigation.

Although propeller load can be measured or calculated using Eq. (4.1)-(4.9), these methods are either unreliable or cannot serve fast real-time control. Taking into account the practical issues, as well as the fact that modeling errors cannot guarantee an offset-free NMPC control, in this work, the use of an extended state observer (ESO) for Q_{load} disturbance and propeller law coefficient $\hat{c}_{prop}$ estimation is proposed. In [87], a propeller load observer is proposed to estimate the propeller torque using the engine speed and engine torque measurements. A load torque observation scheme based on nonlinear parameter estimation using adaptive control techniques is also presented. Moreover, in [88], a generalized form of Extended State Observer (ESO) is proposed regarding non-integral form systems. In [89, 90], methods for state and disturbance estimation are presented, to compensate modeling inaccuracies and guarantee offset-free model-based control with satisfying transient behavior.

Regarding the value of the propeller load disturbance, as the engine speed elevates, it cannot be considered constant within the prediction horizon. According to the propeller law, propeller

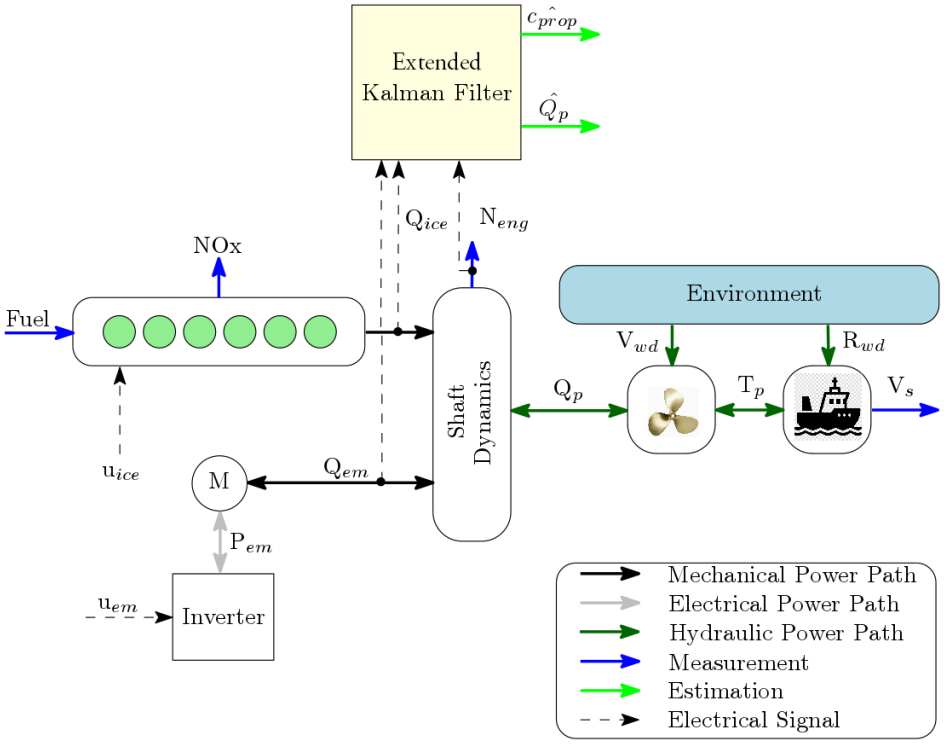

Figure 4-6: Schematic diagram with propeller observer.

power demand P_{prop} is proportional to the cubic power of rotational speed N_{shaft}

$$P_{prop} = Q_{prop}\omega_{shaft} = c_{prop}N_{shaft}^3 \Leftrightarrow \tag{4.16}$$

$$Q_{prop} = \frac{60}{2\pi}c_{prop}N_{shaft}|N_{shaft}| \tag{4.17}$$

This proportional parameter c_{prop} is vessel specific and changes over time depended on ship loading conditions, environmental conditions, aging, etc. However, it is reliable to consider that c_{prop} remains constant within the prediction horizon. As such, in this section, the Extended State Observer (ESO) formulation is utilized to develop a disturbance model and an Extended Kalman Filter (EKF) is designed for non-linear parameter estimation to complement online NMPC control.

4.2.1 Extended state space model formulation

On the engine side of the gearbox, Q_{prop} and N_{shaft} are expressed as Q_{eng} and N_{eng} according to Eq. (4.1). Here, function $Q_{load} = f(N_{eng}) = \frac{60}{2\pi}c_{load}N_{eng}^2$, which describes the propeller law, has varying parameter c_{load} that changes with time, loading condition of ship and environmental disturbance. As such, the system of Eq. (3.4) has to be considered in order to design a disturbance observer using the propulsion plant rotational dynamics, such that $Q_{load} = f(N_{eng}, u_{ice}, u_{el})$. Initially, it is needed to incorporate Q_{load} in the system state equations. The system described

in Eq. (3.4) can be written in a state-space form as follows

$$\dot{x} = Ax + B_u u + B_d d; \quad y = Cx \tag{4.18}$$

where $x = \omega_{eng}$, $u = \begin{bmatrix} Q_{ice} \\ Q_{em} \end{bmatrix}$, $d = Q_{load}$, $A = [0]$, $B_u = \begin{bmatrix} \frac{1}{J_{system}} & \frac{1}{J_{system}} \end{bmatrix}$, $B_d = \begin{bmatrix} -\frac{1}{J_{system}} \end{bmatrix}$ and $C = [1]$.

As d is unknown, the state space model has to be augmented by adding an extended variable $x_{n+1} = d$. As such the state space matrices of the augmented system are

$$\dot{\bar{x}} = \bar{A}\bar{x} + \bar{B}_u u; \quad \bar{y} = \bar{C}\bar{x} \tag{4.19}$$

where variables

$$\bar{x} = \begin{bmatrix} x \\ d \end{bmatrix}; \quad \bar{y} = x$$

and matrices

$$\bar{A} = \begin{bmatrix} A & B_d \\ 0 & 0 \end{bmatrix}; \quad \bar{B} = \begin{bmatrix} B_u \\ \mathbf{0}_{1x2} \end{bmatrix}; \quad \bar{C} = \begin{bmatrix} C & 0 \end{bmatrix}$$

System Eq. (4.19) is observable and can be used for observer design.

4.2.2 Disturbance model

The propeller torque load can be calculated from Eq. (4.7b). In this equation, however, it becomes necessary to know both the C_Q coefficient and the propeller inflow velocity V_a. Equation (4.7b) can be rewritten in the following form

$$Q_p = K_Q \rho D^5 n_p |n_p| = \frac{K_Q \rho D^5}{4\pi^2} \omega_{shaft} |\omega_{shaft}| \tag{4.20}$$

where

$$K_Q = \frac{\pi}{8} C_Q \left[\left(\frac{V_a}{n_p D} \right)^2 + (0.7\pi)^2 \right]$$

In this formula, the propeller torque calculation is based on the propeller rotational speed, which is available from rotational speed sensors. As such, by estimating the $K_Q = f(n_p(t), V_a(t))$ coefficient, the propeller load torque can be calculated without the knowledge of any further parameter from the propulsion plant. Thus, Eq. (4.20) is used instead of Eq. (4.7b).

The control model of the plant, described in Eq. (3.4), is rewritten using Eq. (4.20) and the unknown parameter θ, as defined in [87], as follows

$$\dot{\omega}_{eng} = \frac{1}{J_{system}} (Q_{ice} + Q_{em} - \theta i_{gb}^{-3} \omega_{eng} |\omega_{eng}|) \tag{4.21}$$

where

$$\theta = \frac{K_Q \rho D^5}{4\pi^2} \tag{4.22}$$

Using the ESO formulation, unknown parameter θ is considered as disturbance input $d = \theta$ and $\dot{d} = 0$ is the state equation of the augmented system that has to be estimated. Also d includes any modeling inaccuracies. The control plant model presented in Eq. (4.21) can be written using augmented state vector $\bar{x} = [x, d]^T$, input u, output y, including process noise w, and measurement noise v, as follows

$$\begin{aligned} \bar{x}_{k+1} &= f(\bar{x}_k, u_k) + w_k \ , \quad w_k \sim (0, Q_k) \\ y_k &= h(\bar{x}_k, u_k) + v_k \ , \quad v_k \sim (0, R_k) \end{aligned} \tag{4.23}$$

where $\bar{x} = \begin{bmatrix} x \\ d \end{bmatrix}$, $u = \begin{bmatrix} Q_{ice} \\ Q_{em} \end{bmatrix}$, $x = \omega_{eng}$, $d = \theta$ and $y = \omega_{shaft}$.

4.2.3 Observation scheme

For the disturbance estimation, an EKF is designed. The EKF method is a two-step process: the first step predicts the state of the system, and the second step uses the measurements to refine the estimate of the system state. The EKF operates by propagating the mean and covariance of the state through time. The algorithm computes the state estimates $\hat{x}$ of the nonlinear system using state transition and measurement functions.

Regarding Eq. (4.23), f is a nonlinear state transition function that describes the evolution of states $\hat{\bar{x}}$ from one time step to the next. The measurement function h relates $\bar{x}$ to the measurements y at time step k. w and v are the zero-mean, uncorrelated process and measurement noises, respectively. The noise terms in both equations are additive. $\bar{x}_k$ is linearly related to the process noise w_{k-1}, and y_k is linearly related to the measurement noise v_k. The two-step Extended Kalman Filter observation algorithm includes the estimation step

$$\begin{aligned} \hat{\bar{x}}_k^- &= f(\hat{\bar{x}}_{k-1}, u_{k-1}) && \text{state estimation} \\ P_k^- &= La_k P_{k-1} La_k^T + Lb_k Q_{k-1} Lb_k^T && \text{error covariance} \end{aligned}$$

followed by the correction step

$$\begin{aligned} K_k &= P_k^- Lc_k^T (Lc_k P_k^- Lc_k^T + Ld_k R_k Ld_k^T)^{-1} && \text{Kalman gain} \\ \hat{\bar{x}}_k &= \hat{\bar{x}}_k^- + K_k (y_k - h(\hat{\bar{x}}_k^-)) && \text{estimate update} \\ P_k &= (I - K_k Lc_k) P_k^- && \text{error covariance update} \end{aligned}$$

where

$$La = \left.\frac{\partial f}{\partial x}\right|_{\hat{\bar{x}}} \quad Lb = \left.\frac{\partial f}{\partial w}\right|_{\hat{\bar{x}}} \quad Lc = \left.\frac{\partial h}{\partial x}\right|_{\hat{\bar{x}}} \quad Ld = \left.\frac{\partial f}{\partial v}\right|_{\hat{\bar{x}}}$$

It is noted that the "-" superscript denotes the estimates from the previous time instant which are a priori known. All measurements before (but not including) time k are available for use in an estimate of x_k and a priori estimation of $\hat{x}_k$ can be calculated. I is the identity matrix. As it can be seen from the EKF algorithm, given the state transition and measurement functions, Q_k and R_k are the corresponding noise covariances that are used as tunning parameters of the observer. The input u that is fed to the Kalman filter is $u = \hat{u} = [\hat{Q}_{ice}\ \hat{Q}_{em}]^T$, where $\hat{Q}_{ice}$, $\hat{Q}_{em}$ are the torque outputs of the engine and the EM calculated using NMPC commands and Eq. (3.5) and Eq. (3.8).

4.2.4 Propeller law parameter calculation and utilization

Using the above method to gather the disturbance estimation, $\hat{\theta}$ is used for the propeller law parameter using Eq. (4.24).

$$\hat{c}_{load} = \frac{\hat{c}_{prop}}{i_{gb}^3} = \frac{2\pi\rho D^5}{60^3 i_{gb}^3}\hat{K}_q = \frac{8\pi^3}{60^3 i_{gb}^3}\hat{\theta} \tag{4.24}$$

The propeller law parameter value is utilized in run-time in order to solve the online optimization problem. In more detail, at sampling instant k parameter $\hat{c}_{load}$ is calculated and assuming that c_{load} is kept constant within a future prediction window $k...k+N$, within which a model-based controller must calculate future $x[k+i|k],\ i = 1...N$. As such, it is needed to estimate resulting propeller torque as follows

$$Q_{load}[k+i|k] = \frac{60}{2\pi} c_{load}[k] N_{eng}[k+i|k]^2 \tag{4.25}$$

instead of assuming that $Q_{load}[k+i|k] = \hat{Q}_{load}[k]$.

4.3 Simulation Results

To demonstrate the engine-propulsion plant-environment dynamic interaction and evaluate the observer performance, the model of the propulsion plant was coupled with the engine model, so that the engine, in speed control mode, serves the propeller load demand and follow the desired engine speed reference. The main ship particulars, as well as the propulsion model parameters, are presented in Table B.2. In Fig. 4-7 the simulation results of a fast and a slow engine and

Table 4.1: Design parameters of EKF propeller observer

Parameter	Symbol	Value
EKF Scheme - Model		
State noise covar. matrix	$Q[k]$	$7\ 10^{-4}$
Input noise covar. matrix	$R[k]$	5

ship transient acceleration in waves are presented.

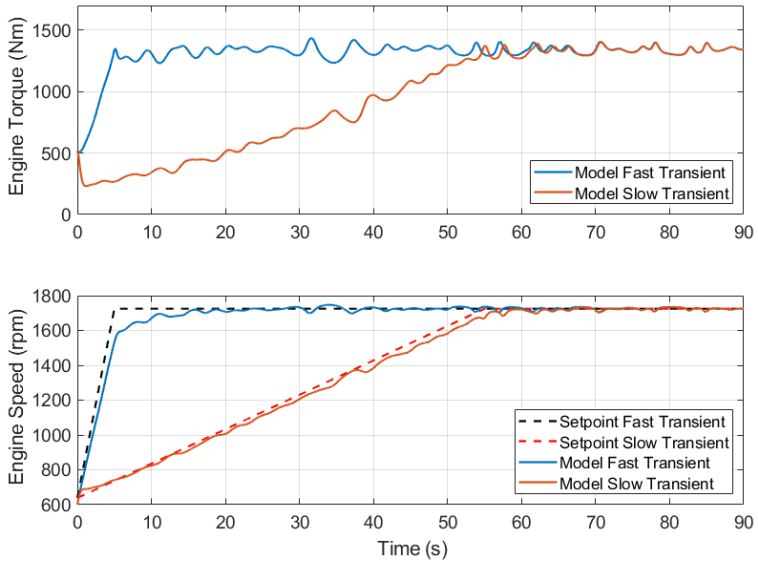

(a) Engine performance during slow and fast ship acceleration with wave disturbance.

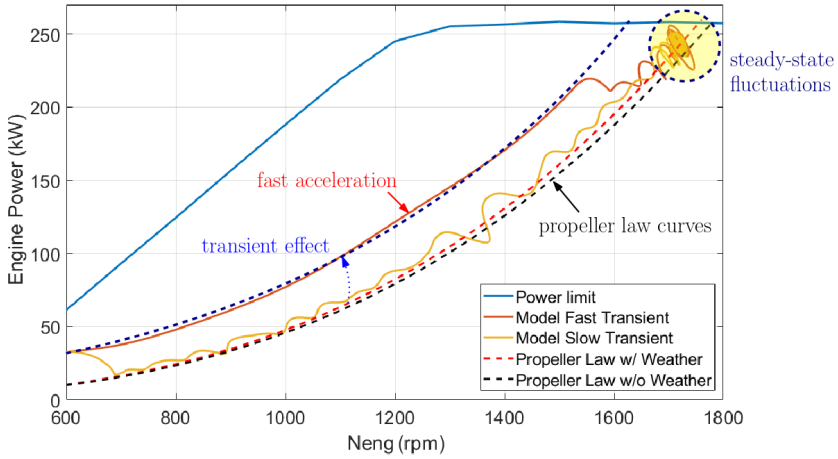

(b) Engine loading envelope and propeller load at engine crankshaft during slow and fast ship acceleration with wave disturbance, compared to the propeller load curve with 15% power margin due to bad weather.

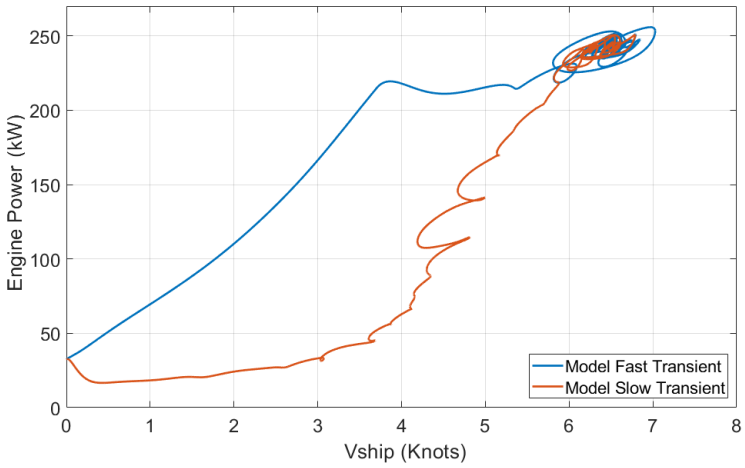

(c) Engine power-ship speed phase in slow and fast ship acceleration with wave disturbance.

Figure 4-7: Engine-propulsion plant interaction in slow and fast ship acceleration with wave disturbance.

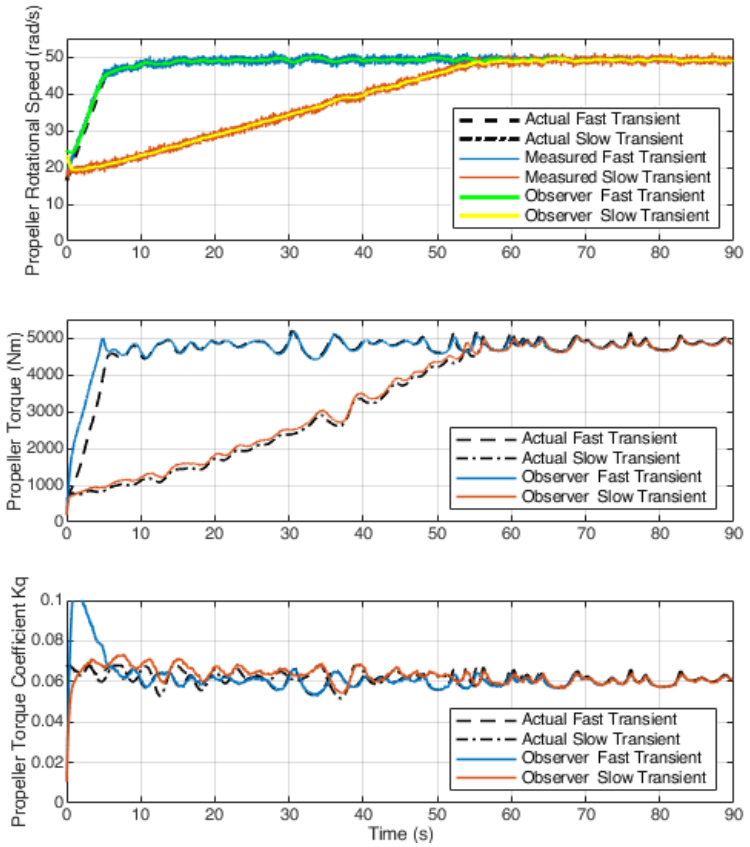

(a) Propeller torque, speed and torque coefficient K_Q estimation.

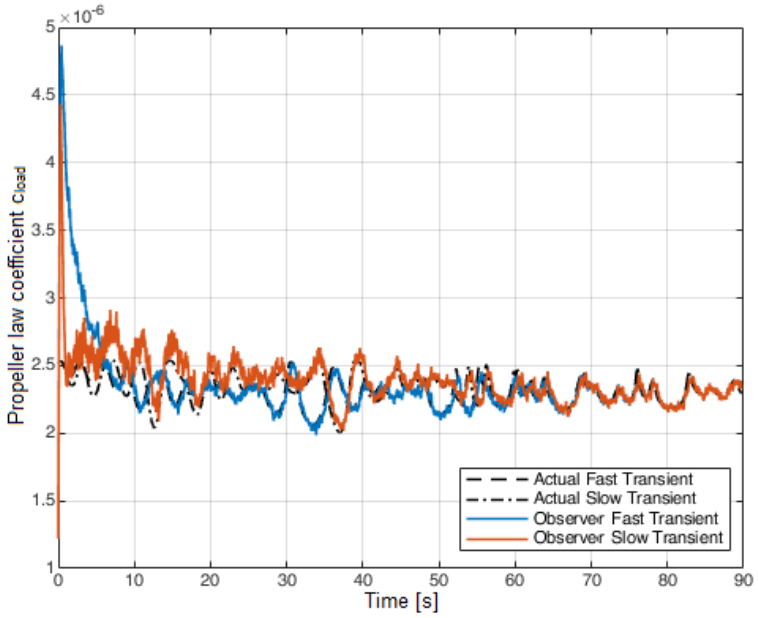

(b) Propeller law coefficient c_{load} at the engine side calculation.

Figure 4-8: Propeller observer performance in fast and slow ship acceleration, with wave disturbance.

Fig 4-7a shows the resulting engine load, as the engine speed follows the desired speed reference in slow and fast acceleration scenarios. In Fig. 4-7b the engine loading in respect to the engine operating envelope is shown. Regarding the transient system response, it can

be noted from Fig. 4-7b and 4-7 that the ship speed affects the propeller inflow speed, and thus the propulsion plant loading. In fast transients, propeller load is increased up to 30% as compared to the propeller law (power is proportional to the cube of the rotational engine speed, $P = cN_{eng}^3$), where c is constant for static and steady-state operation points. Thus, the c parameter is increased during transient loading or in adverse weather conditions, as it is presented in Fig. 4-7b. Besides, it can be seen in Fig. 4-7a that the propeller load fluctuates around an increased mean value. The wave disturbance results in increased engine power and fluctuations of the engine and vessel speeds as well as decreased vessel speed due to the added resistance, as it can be observed in the engine operating envelope and the engine power-vessel speed phase diagram in Fig. 4-7b.

The Extended Kalman Filter estimation results of the propeller rotational speed and torque during slow and fast acceleration (with wave disturbance) are shown in Fig. 4-8. As it can be seen, the observed values follow the course of the corresponding real values with small error and small time shift. A very good performance of the observer is achieved in transient and steady-state operation. Particularly, in Fig. 4-8b it can be seen that the estimation propeller load parameter follows the actual value, which fluctuates due to the wave disturbance. During the engine acceleration, an overshoot can be observed. Finally, as it can be noted from the results, the mean value of the propeller law parameter c_{load} remains constant, even though propeller rotational speed and load elevate. As such, it can be utilized to perform calculation and prediction of the future propeller load, based on rotational speed elevation.

4.4 Conclusion

In this chapter, the emulation and estimation of the propeller load and its characteristics were investigated. At the initial stage, the ship surge motion was modeled, based on the basic principles of ship propulsion. The purpose was to use a realistic emulation model during control system development and experimental testing, to evaluate the interaction of the system *controller-powertrain-propulsion plant-environment*. In the second step, the propeller load characteristics should be estimated, as the calculation of the propeller load demand is essential for the system equilibrium. The approach was based on the propeller law principle (power is proportional to the cubic power of shaft speed).

Through simulations in cases of slow and fast accelerations, it was shown that the modeling adequately corresponds to the actual sizing and operating conditions of a small tug vessel and the observer can respond efficiently, giving accurate estimates, in steady-state and transient loading conditions. The observer was used to develop and implement the predictive control schemes and provide online information regarding the disturbance response.

This chapter responded to research questions 1 and 2.

THIS PAGE INTENTIONALLY LEFT BLANK

Chapter 5

Transient Operational Profile Identification and Prediction

In the previous chapter, the emulation and identification of propeller load characteristics were investigated. Load demand can be calculated using the engine rotational speed and the propeller law coefficient, which is estimated and can be considered as constant within a short time horizon. In this chapter, the focus is on the identification and prediction of the operator's reference input during ship cruising and maneuvering. The first step is to recognize typical marine loading profiles, so as to perform the design and performance evaluation of the EMS. Secondly, a prediction model for the operator's speed reference input is developed, which utilizes past operator's inputs and its output will be provided as online information to the optimization algorithm. These objectives were achieved, following a data-based identification methodology and using Machine Learning (ML) techniques.

5.1 Marine Transient Profile Identification

Marine driving cycles have not been developed and investigated to the same extent as automotive driving cycles. There is not sufficient literature about marine diesel engine loading cycles that can be used for the scientific research that is relative to the objective of this Thesis. Therefore, concepts of automotive driving cycle analysis are examined and taken into consideration for the identification of marine loading cycles.

A driving cycle, or driving schedule, is represented by vehicle speed versus time. Some examples are the European certification driving cycle for light-duty vehicles and the New European Driving Cycle (NEDC), which are used for test approval that the vehicle manufacturers follow the legislation. Driving cycles are important components for evaluating vehicles and have a fundamental role in vehicle design, since they affect the cost, lifetime performance, fuel consumption, and pollutant emissions of vehicles, [91]. Driving cycles have been widely used to assess exhaust gas emissions of vehicles, [92], but they are also used to evaluate different control

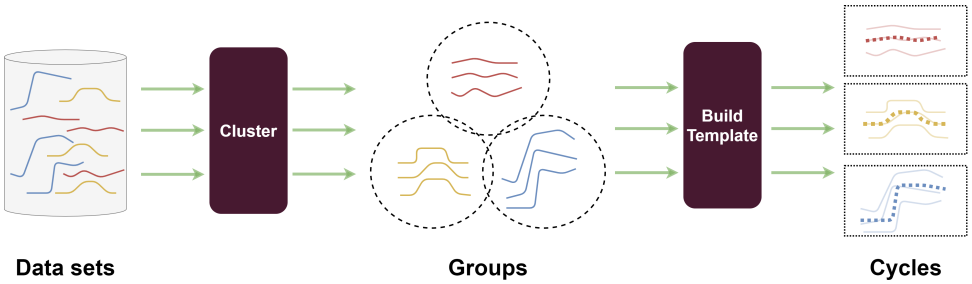

Figure 5-1: Silhouette score graph

strategies for vehicles, [93, 94], as well as, during vehicle design and sizing of components, [95]. There are several approaches to generate new driving cycles that are representative for a certain region of interest. There have been many proposals of new driving cycles that are representative of a certain region of interest in [96, 97]. Recently, pattern recognition in time-series using data analytics and machine learning methodologies has been investigated, [98, 99].

This section presents the generation of standard (or representative) load cycles using concepts of automotive driving cycle analysis and machine learning methods such as unsupervised pattern recognition in time-series data. This is achieved by finding and grouping similar load profiles and, then, a proper averaging procedure is applied to create representative templates (cycles), [100]. The main aspects of the proposed methodology can be summarized to

- dimensionality reduction
- similarity matching
- hierarchical clustering
- prototype creation

using time-series averaging methods. The methodological approach is graphically presented in Fig. 5-1.

5.1.1 Preprocessing of data

Data available from the legacy of the Laboratory (LME/NTUA), measured at 200 Hz from marine engines during maneuvering and before the stop of the vessel, for different vessels, with different engines were utilized. Data contain 638 time-series in total. Measurements include

- Engine Speed (N_{eng})
- Engine Speed Reference (N_{ref})
- Electronic Fuel Index (u_{ice})

The measurements are normalized signal values. A filter with cut-off frequency 2 Hz was applied on raw data.

The first step of preprocessing is dimensionality reduction. From the correlation analysis between each pair of variables, which is calculated and presented in Table 5.1, it can be seen that the correlation between each pair of variables is higher than 0.8, so it is concluded that all variables are highly correlated with each other and their representative variable is selected to be the engine speed reference, which is the most reliable and easily implementable variable in simulation and experiments.

Table 5.1: Correlation matrix for each pair of measured variables.

	N_{eng}	N_{ref}	u_{ice}
N_{eng}	1	0.8706	0.8997
N_{ref}	0.8706	1	0.9759
u_{ice}	0.8997	0.9759	1

Also, time-series with a percentage of empty cells greater than 4%, a relative difference from the average length greater than 2% or the ones that have only zero values were eliminated from the process. The remaining time-series were cut-off at average length and any empty cells were replaced with the value of the previous measurement. Additionally, time-series with only zero values are excluded because they do not offer any valuable information for the clustering procedure. After all, the resulted dataset contains 584 time-series out of 638 that were initially before preprocessing; 8.46% of the initial time-series data is excluded from the analysis.

The preprocessing process resulted in time-series with a length of $17 \cdot 10^4$ samples each. Most algorithms in literature need extreme processing time and computational resources to handle such datasets. Therefore, resampling at the frequency of 2 Hz, was performed before analysis can take place that will reduce the computational effort without causing loss of information.

5.1.2 Time-series clustering

Such a database of time-series is difficult to be processed and evaluated by human means, it is necessary to use grouping methods to group the available data and extract a number of representative time-series that can be then human-managed. Visualization and scalar measurements are major techniques for the evaluation of clustering quality, which is also known as clustering validity, [101]. Clustering is a method for classifying a big amount of data when there is not any earlier knowledge about data grouping. Since it is an unsupervised clustering problem, in this Thesis the silhouette score metric [102], was employed to identify the optimal quantity of clusters.

The average silhouette approach briefly, measures the quality of a clustering procedure. It determines how well each object lies within its cluster. A high average silhouette magnitude

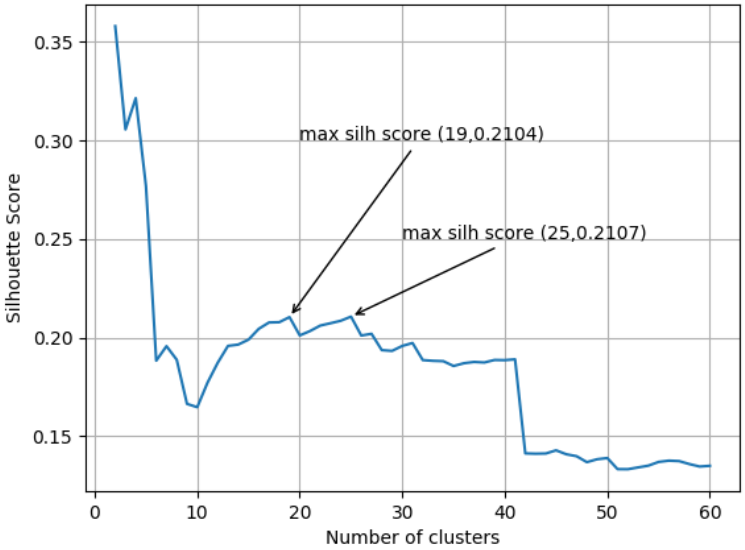

Figure 5-2: Silhouette score graph

indicates a good clustering. Specifically, the average silhouette method computes the average value of silhouette of the individual observations for a different total number of clusters k. The optimal number of clusters k is the one that maximizes the average silhouette over a range of possible k values. The silhouette coefficient is defined for each profile and is composed of the following two features

1. the mean distance between a profile and all other profiles in the same class a.
2. the mean distance between a profile and all other profiles in the next nearest cluster b.

The Silhouette Coefficient s for a single profile is then given as:

$$s = \frac{b - a}{\max(a, b)} \tag{5.1}$$

The optimal number of clusters may be in a range of values and appears where the Silhouette score is maximized. Based on Fig. 5-2, the optimal number of clusters is between 19 and 25. The maximums in the range from 2 to 8 are considered inappropriate because this number of clusters is considered very low (risk of overfitting). Also at 41 clusters, a step is observed, which is explained as the upper bound of classes where the data can be grouped.

In the clustering procedure, using a summed distance metric $\mathbb{R}^n \to \mathbb{R}$, where n is the number of samples in each profile, shape similarities between the measured time-series are identified and the time-series with similar time profile are categorized in the same cluster. Hierarchical clustering is an approach to cluster analysis that makes a hierarchy of clusters. This work focus is on agglomerative clustering, where each sample starts as an individual cluster and the closest pairs of clusters merge until only one cluster remains (bottom-up approach).

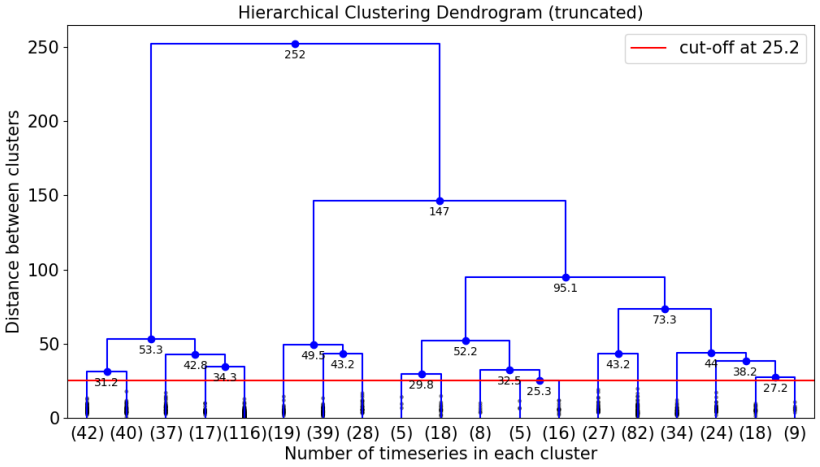

Figure 5-3: Hierarchical clustering dendrogram

A commonly used algorithm for agglomerative hierarchical clustering is Ward's linkage method, [103]. In Ward's linkage, the two clusters that lead to the minimum increase of the total within-cluster sum of squared errors (SSE) distance are merged during every iteration of the clustering algorithm. It is calculated as follows: let $d(s,t)$ be the distance between two clusters s and t in a dendrogram. When two clusters s and t from this dendrogram are combined into a single cluster u, then s and t are removed from the initial data dendrogram, and u is added to the dendrogram until only one cluster remains in the dendrogram. A distance matrix is maintained at each iteration. The $d[i,j]$ corresponds to the distance between cluster i and j in the original dendrogram.

The new entry $d(u,v)$ in each iteration is computed as follows

$$d(u,v) = \sqrt{\frac{|v|+|s|}{T}d(v,s)^2 + \frac{|v|+|t|}{T}d(v,t)^2 + \frac{|v|}{T}d(s,t)^2} \tag{5.2}$$

where u is the newly joined cluster consisting of clusters s and t, v is an unused cluster in the dendrogram, $T = |v| + |s| + |t|$, and $|*|$ is the cardinalityof its argument. This is also known as the incremental algorithm.

The results of hierarchical clustering, where Ward's method was used, are presented using a hierarchical tree, as shown in Fig. 5-3. In the x axis, the volume of time-series grouped in each cluster are denoted and the y axis refers to the summed Euclidean distance between neighbor clusters. The clustering is performed by cutting off the hierarchical tree in a specific distance (marked with a horizontal red line in Fig. 5-3), resulting in a specified number of clusters.

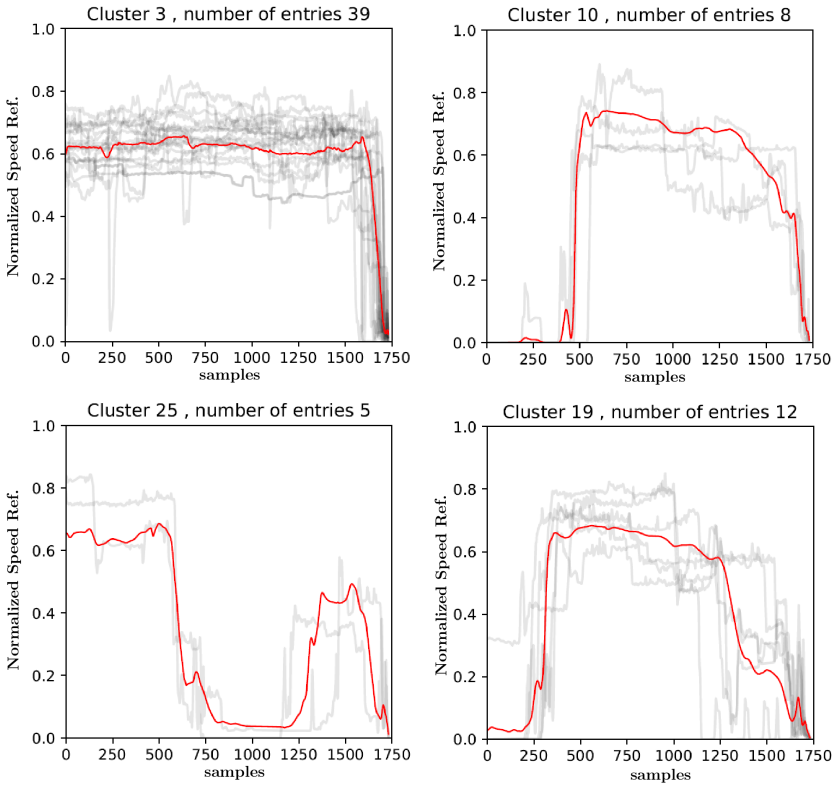

Figure 5-4: Averaging results, templates derived with Soft-DTW method, $\gamma = 0.5$.

5.1.3 Time-series averaging

For the time-series that were classified in each cluster, a template profile was extracted, which represents the average behavior of the time-series in the specific cluster. The representative average profile was created with Soft Dynamic Time Warping (Soft DTW) averaging method.

Dynamic time warping (DTW) finds the optimal non-linear alignment between two time-series. Its advantage is that it allows distortion in the time axis, as compared to the euclidean distance metric. However, dynamic time warping is quadratic in the length of the time-series used and it is very slow to compute. Dynamic programming is used for the calculation of the path that minimizes the distance between the time-series. The advantage of DTW based against euclidean distance methods is that DTW can produce a geometrical, shape average result.

Additionally, modifications of the recursive function to define smoothed dynamic programming distances have been proposed, [104]. When applied to the DTW discrepancy, that regularization results in a soft-DTW output, which considers the soft-minimum of the distribution of all costs spanned by all possible alignments between two time-series. In short, Soft-DTW proposes to replace the minimum in DTW with a soft minimum. The main advantage of soft-DTW comes from the fact that it is differentiable everywhere and that its gradient can also be computed in quadratic time. Variable γ is used in the recursive function to smoothen the average result. γ is a positive regularization parameter in the range $[0, 1]$, with lower values resulting in less

smoothing. The closer the value to zero, the closer are the results to those of the DTW method.

In Fig. 5-4, averaging results derived from clustered time-series are presented. In each sub-figure, time-series of the corresponding cluster are plotted on the background and the resulting average template is demonstrated with red color. It can be noted that the template averages the shape of the time-series contained in each class.

5.1.4 Marine loading cycles extraction

To preserve as much of the information contained in the initial data, a two-step methodology was followed, where iteratively clustering and averaging were applied

1. The available preprocessed 584 time-series are clustered in 40 clusters and templates for each of these clusters are produced with the Soft-DTW method.

2. The 40 produced templates will be clustered in 20 clusters and templates for every cluster will also be created, resulting in 20 templates, shown in Fig. 5-5.

Based on the results, shown in Fig. 5-5, the output of the averaging step is 20 templates (representative profiles). These templates can be evaluated as follows

- The templates that were derived with the soft-DTW method are favorable in terms of smoothness and representation of realistic marine loading profiles.

- These templates contain patterns that can be identified in vessels' operating profiles. As such, they can be utilized as marine loading cycles.

- Some templates, such as clusters 2, 3, and 14 in Fig. 5-5, contain useful information for steady-state engine operation and may be used for system design.

- Some templates, such as clusters 15, 17, and 20 in Fig. 5-5, contain information for transient marine engine behavior and are more appropriate for control systems evaluation.

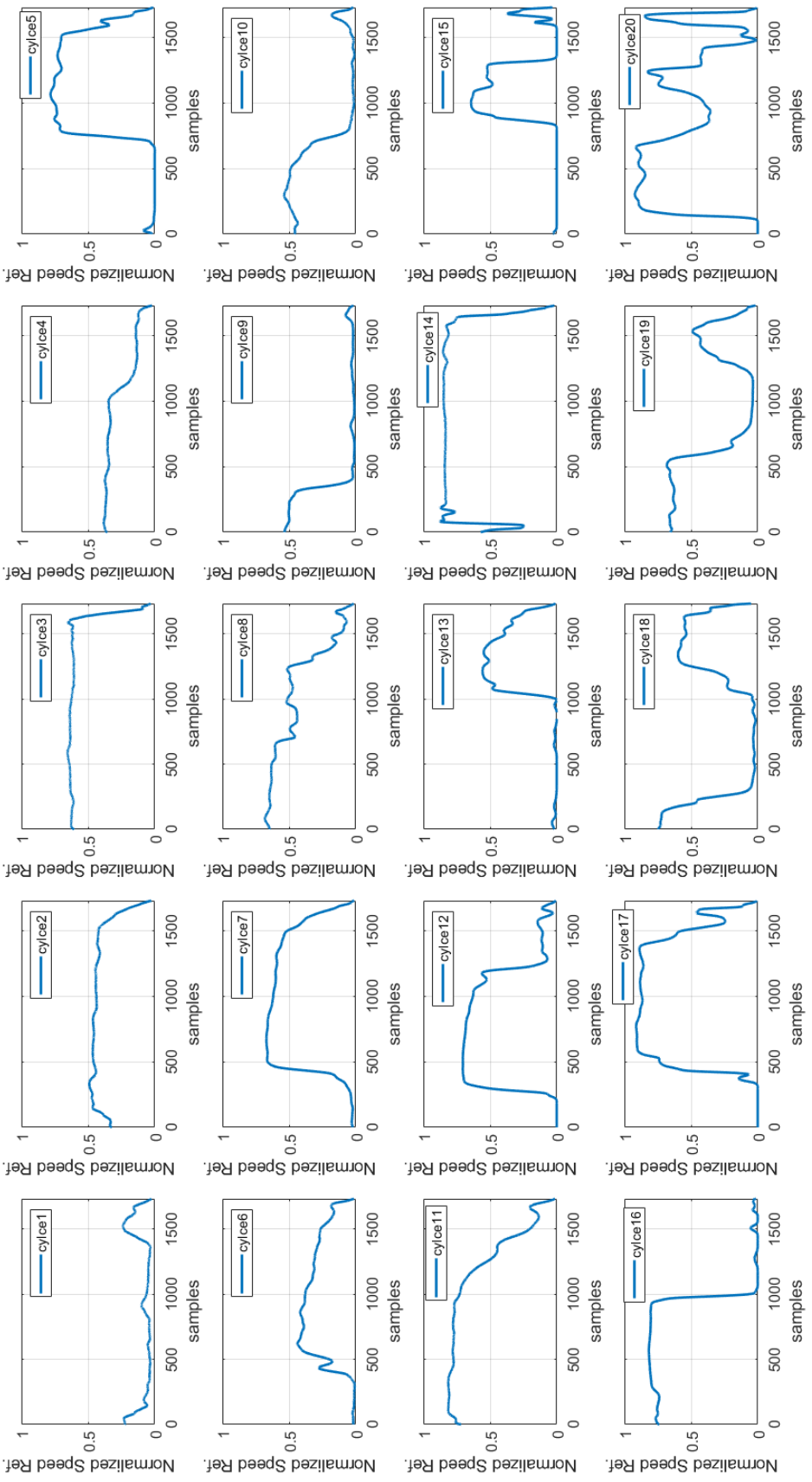

Figure 5-5: Averaging results, loading cycles representing typical ship operational profiles.

5.2 Reference Input Predictor

5.2.1 Problem statement

To perform optimal energy management control, the knowledge of the operating profile in terms of speed and load variations over time is favorable to calculate the global optimal strategy. However, the profile is not a priori known and actual loading conditions differ from these that may have been considered during system design. The optimality of the EMS algorithm's solution is not totally dependent on the optimization algorithm itself but on the availability and reliability of the information that the EMS receives in run-time, based on which the optimal energy management planning is performed. Therefore, the expected operator's reference input over a short-term future time window would be useful to aid the optimization procedure.

The proposed EMS, which is an NMPC-based scheme, is used to optimize the powerplant performance while satisfying the operator's desired engine speed. In the automotive industry, the reference of vehicle velocity is used as prediction input to the EMS. However, in the marine industry, due to the scale differences between ships, each vessel has its nominal conditions (time constants and top speed); Additionally, ship cruising conditions are greatly affected by ship loading and environmental conditions, e.g. the propulsion power demand may differ by over 20% between two different cruising conditions at the same vessel speed. As such estimation of powertrain dynamics should be decoupled from ship dynamics.

The objective of the operator's demand prediction module is to provide an estimation, at each sampling interval k, of the future propeller operational points within a time window of length T, which are determined by shaft rotational speed $N_{eng}[k+t|k]$ and torque load $Q_{load}[k+t|k]$, $t \in (0...T]$. Using the propeller observer, developed in section 4.2, Q_{load} can be calculated as a function of N_{eng}. As such, only N_{eng} needs to be estimated, and particularly $N_{eng,ref}$ is selected, as it is the operator's reference input to the EMS.

Engine speed reference prediction within the prediction time window is particularly important to ensure maximum energy efficiency and fuel economy. Reference predictors have been used for marine energy management applications. In [47], probabilistic operating load estimation is performed to adapt the energy management controller. In [45], for each prediction window, the operating load estimation is performed based on the percentage of time on low- medium- and high- power demand of the vessel. Moreover, in [48] the load prediction is made by a neural network with wavelet excitation functions.

The parameters that determine the appropriate model structure selection and development are the availability of measurements and computational complexity. When referring to design cases based on the restricted availability of information, approaches based on artificial neural networks (NN) have gained attention. Usually, historical data of vehicle velocity are utilized to predict the future vehicle velocity request, [105, 106]. Moreover, in [107], various stochastic

and deterministic prediction models of vehicle velocity are compared. It is shown that Neural Networks (NN) can outperform other types of models and perform very accurate predictions. In this work, a feedforward NN is used for the prediction of future engine speed reference.

5.2.2 Prediction model design

The focus is on engine rotational speed predictions over the 1 to 10 steps prediction horizon. The engine speed was chosen as the NN output variable as it is also the reference input to the controller. To train the neural network, it became necessary to provide sufficient relevant data. The dataset was provided from MarineTraffic platform. Specifically, speed data of tugboats were taken during four consecutive days of operation, located worldwide. Using the propulsion plant model, these data were converted to engine rotational speed. The data were normalized and time-scaled according to the Froude similarity principle for ship time constant T_s, [82].

The neural network function that was fitted using the available data is

$$\hat{\xi} = f(\xi) = W_{x2}\phi_x(W_{x1}\xi + b_{x1}) + b_{x2} \tag{5.3}$$

where $f, \hat{\xi}, \xi \in \mathbb{R}^{10}$, $\xi = [x_{k-1}, ..., x_{k-10}]^T$ and f produces $\hat{\xi} = [\hat{x}_{k+1|k}, ..., \hat{x}_{k+10|k}]$, x_i is the normalized $N_{eng,ref}$, ϕ_x is the *tansig* activation function and $W_{xi,10\times10}$, $b_{xi,10\times1}$ are the fitted weights of the ith network layer. The structure of the NN hidden layer is composed of 10 nodes. As such the computational complexity of the model is kept simple, in contrast to deep neural network structures that require great computational effort.

For training, MATLAB neural network toolbox was used and Levenberg-Marquardt optimization algorithm was employed to minimize the mean squared prediction error over the actual values. To increase online prediction robustness and produce a transferable result, the data were populated with 3 different time scales [$0.8T_s$ T_s $1.2T_s$]. Data points were derived from ship operational profiles with sample time 0.5 s. In total, 56700 data points were used for training and 24300 for testing.

Fig. 5-6 shows the speed predictions of the neural network on a horizon of 1 to 10 steps forward, in relation to the corresponding real values, for a specific period of the tugboat operation. It can be observed that as the prediction step increases, so does the deviation from the corresponding real values. However, the overall performance of the neural network is particularly high. It can also be noted that the neural network predictions follow the course of the target values, with both small error and small time shift. The largest deviations are observed in the very high and very low-speed values and in speed abrupt alternations. This is due to the speed variation in the collected dataset, which consists of constant speed segments and intense accelerations and decelerations due to the tugboat operation. In conclusion, for the operation of the MPC presented in this work, the neural network described above gives satisfactory predictions

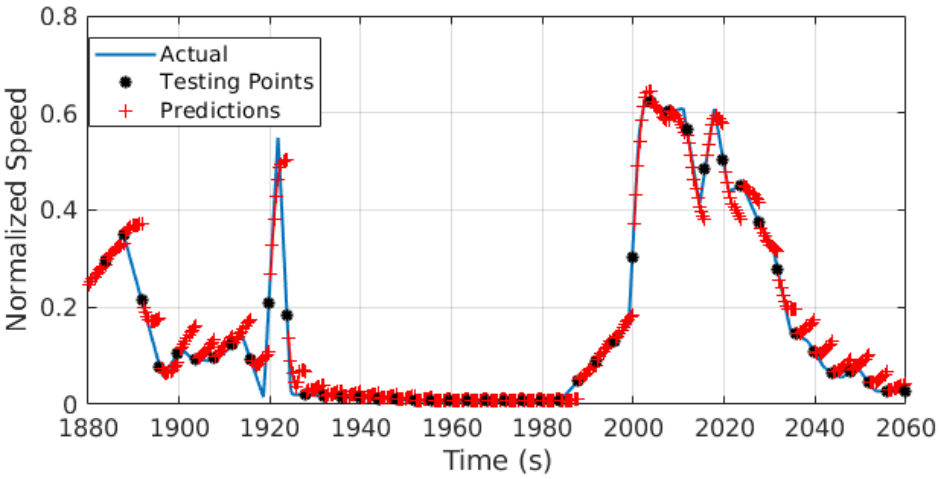

Figure 5-6: Neural Network velocity predictions up to 10 steps forward.

up to 10 samples ahead.

5.3 Conclusion

This chapter dealt with the operating profile of a marine propulsion plant in transient operating conditions. Shaft speed was determined as the representative system variable for the operational profile. Initially, 20 marine loading cycles were extracted and evaluated as typical marine operational profiles. Cycles that contain rich information about the transient operation are utilized in the next chapter for control system tuning and evaluation. Moreover, to ensure optimal energy management planning, a prediction model for the future operator's reference was designed. From the possible model structure candidates, the neural network gives the most accurate predictions within a horizon of 10 sampling instants ahead. The online information generated by the prediction model is used along with the propeller observer, to calculate future propeller load disturbance.

This chapter responded to research question 3.

THIS PAGE INTENTIONALLY LEFT BLANK

Chapter 6

Transient Power-Split Controller

The application of Model Predictive Control (MPC) is attractive for problems related to optimal power-split and energy management of hybrid power plants. In this chapter, the theoretical and implementation framework of NMPC is discussed. Then, the problem formulation of the torque-split control during transient operation of the hybrid propulsion powertrain under investigation is performed. A power management, NMPC-based control scheme is designed and experimentally evaluated in transient propeller loading conditions.

6.1 NMPC Theoretical Framework

Model Predictive Control is an advanced, model-based, control method, which is intuitively able to deal with multiple input and output constrained systems, complex interconnected dynamics and in particular, offers a systematic design procedure for constrained control. Model Predictive Control (MPC) solves an optimization problem online to compute the optimal sequence of control commands over a finite time window, called prediction horizon. The problem is formulated based on (i) the available plant measurements, (ii) the plant prediction model, (iii) control objectives, and (iv) plant/actuator limitations. Only the first control command of this sequence is applied to the plant in closed-loop in a receding-horizon planning. An illustrative representation of the MPC application is shown in Fig. 6-1.

In this section, elements of basic theoretical background for the NMPC controller schemes which are applied in the context of this Thesis are presented.

6.1.1 Nonlinear Model Predictive Control

Nonlinear Model Predictive Control (NMPC) is based on the principal MPC idea, however, it can tackle problems with nonlinear dynamics and constraints, and is not known to be convex as well. Due to the increased complexity, these problems are considered to be difficult to be solved, and it is suggested that there is no global efficient way to solve them, but only a few approaches under

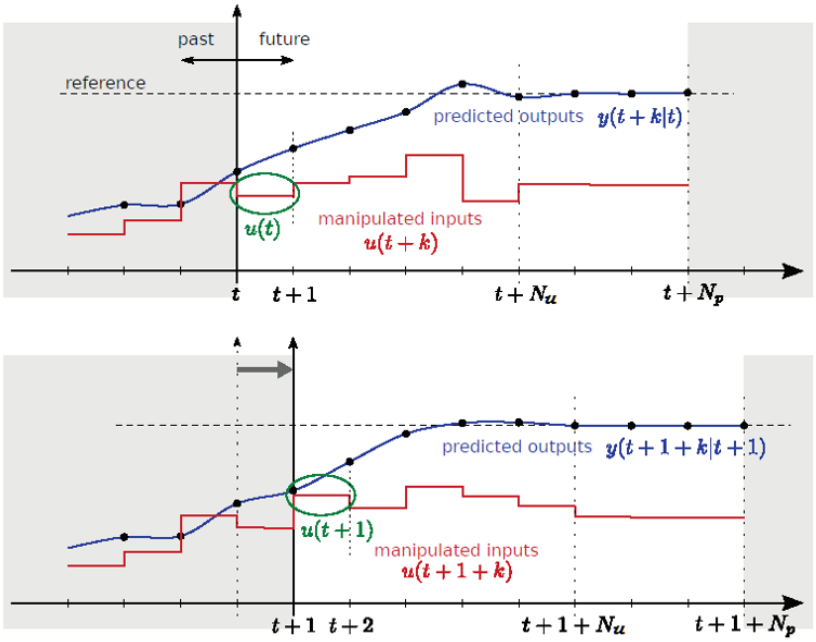

Figure 6-1: Concept of Model Predictive Control.

a number of compromises. NMPC was first introduced in the chemical industry where systems evolve at a very slow rate, giving time to the controller to complete the required calculations. In recent years, the development of optimization algorithms and embedded control platforms have greatly reduced the required time for the NMPC algorithms to solve the optimization problem, leading to an increased number of implementations and faster applications [108].

Before the Nonlinear Model Predictive Control (NMPC) scheme is analyzed, it is appropriate to describe the basic structure of the finite horizon Optimal Control Problem (OCP). In this class of problems, the objective is to compute the best control strategy, for the given horizon, which would not violate the physical constraints of the problem and would minimize a specific cost function. The optimal problem can be defined as

$$\min_{x(\cdot),u(\cdot)} \int_{t_0}^{t_N} F(T_k, x(t_k), u(t_k))dt_k + E(t_N, x_(t_N), x(t_N))$$

subject to

$$x(t_0) = x_0 \qquad (Initial\ Values)$$

$$x_{k+1} = f(t_k, x(t_k, u(t_k)) \qquad (System\ Dynamics)$$

$$h(x_{t_k}, u_{t_k}) \leq 0 \qquad (Stage\ Constraints)$$

$$r(x(t_N)) \leq 0 \qquad (Terminal\ Constraints)$$

where F is the stage cost function and E is the terminal cost function, which form the objective function J. The objective function is minimized in interval $t_0, ..., t_N$. $x = x_0, ..., x_n$ denotes the

state vector and $u = u_0, ..., u_m$ denotes the control vector of the system. Solving the problem gives the best sequence of controls u_k that delivers the sequence of states x_k, for every time interval $k = t_0, ..., t_{N-1}$, satisfying the stage constraints $0 \geq h(x_{t_k}, u_{t_k})$ and ending up such that x_N satisfies the terminal constraint $0 \geq r(x_{t_N})$.

Model predictive control (both linear and nonlinear) is a procedure that aims to solve the above optimal problem recursively online. To give a better illustration of the procedure, and since the chosen algorithm for this work depends on the linear approach, the principles of both schemes are described.

To implement and solve NMPC in fast real-time applications, several algorithmic approaches have been proposed. In the present work, the implementation is performed using the widely used approach of the *Real Time Iteration (RTI) Scheme* [108]. Since the NMPC problem is approximated with the RTI scheme by solving one properly structured linear Quadratic Problem (QP) per sampling time, the NMPC here can be conceived as a special case of linear time-varying MPC, with the particularity that system dynamics are linearized online, according to the current state and control prediction and a numerical integration scheme is employed to simulate the system dynamics.

6.1.2 NMPC problem formulation and solution via Real Time Iteration

The RTI approach for the NMPC problem is based on the Quadratic Programming (QP) structure of MPC for nonlinear systems. In order to illustrate the approach, a time-invariant discrete nonlinear dynamic system $x^+ = f(x, u)$, with inequality constraints $h(x, u) \leq 0$, is considered. The NMPC problem can be formulated as

$$NLP(\hat{x}_i, \mathbf{x}_i^{ref}, \mathbf{u}_i^{ref}) = \underset{\mathbf{x},\mathbf{u}}{argmin} \sum_{k=0}^{N-1} \begin{bmatrix} x_{i,k} - x_{i,k}^{ref} \\ u_{i,k} - u_{i,k}^{ref} \end{bmatrix}^T W_{i,k} \begin{bmatrix} x_{i,k} - x_{i,k}^{ref} \\ u_{i,k} - u_{i,k}^{ref} \end{bmatrix} \tag{6.1}$$

$$\begin{aligned} &s.t. \\ &x_{i,0} = \hat{x}_i, \\ &x_{i,k+1} = f(x_{i,k}, u_{i,k}), \quad k = 0, ..., N-1 \\ &h(x_{i,k}, u_{i,k}) \leq 0, \quad k = 0, ..., N-1 \end{aligned}$$

At every time instant, the problem provides the NMPC control solutions in the following form

$$u_i^{NMPC} = u_{i,0}, \ (\mathbf{x}_i, \mathbf{u}_i) = NLP(\hat{x}_i, \mathbf{x}_i^{ref}, \mathbf{u}_i^{ref}) \tag{6.2}$$

The above problem is a structured Nonlinear Program (NLP), which can be solved with various approaches. In this work, the Sequential Quadratic Programming (SQP) algorithmic approach is used. It is noted that the stage cost matrix is considered to be quadratic positive and semi-definitive. According to [108], although more generic costs could be more suitable, closed-loop stability and algorithmic issues might occur. Moreover, for sake of simplicity, the terminal cost is omitted.

Sequential Quadratic Programming (SQP) for NMPC

The SQP approach for NMPC occurs from QPs delivering Newton directions for performing steps towards the solution starting from an available guess. The iteration is repeated performing Newton steps until convergence. At guess $[x_i^{guess}, u_i^{guess}]$, the nonlinear problem is formulated as

$$\begin{aligned} &QP_{NMPC}(\hat{x}_i, \mathbf{x}_i^{guess}, \mathbf{u}_i^{guess}, \mathbf{x}_i^{ref}, \mathbf{u}_i^{ref}) = \\ &\qquad arg\min_{\Delta\mathbf{x},\Delta\mathbf{u}} \sum_{k=0}^{N-1} \frac{1}{2} \begin{bmatrix} \Delta x_{i,k} \\ \Delta u_{i,k} \end{bmatrix} H_{i,k} \begin{bmatrix} \Delta x_{i,k} \\ \Delta u_{i,k} \end{bmatrix} + J_{i,k}^T \begin{bmatrix} \Delta x_{i,k} \\ \Delta u_{i,k} \end{bmatrix} \end{aligned} \tag{6.3}$$

$$\begin{aligned} \text{s.t.} \quad & \Delta x_{i,0} = \hat{x}_i - x_{i,0}^{guess}, \\ & \Delta x_{i,k+1} = A_{i,k}\Delta x_{i,k} + A_{i,k}\Delta u_{i,k} + r_{i,k}, \quad k = 0, ..., N-1 \\ & C_{i,k}\Delta x_{i,k+1} + D_{i,k}\Delta u_{i,k} + h_{i,k} \leq 0, \quad k = 0, ..., N-1 \end{aligned}$$

where $\Delta x_{i,k} = x_{i,k} - x_{i,k}^{ref}$ and $\Delta u_{i,k} = u_{i,k} - u_{i,k}^{ref}, \quad k = 0, ..., N-1$.

The matrices $A_{i,k}, B_{i,k}, C_{i,k}, D_{i,k}$ are derived from the linearization of system dynamics and dynamic constraints. Contrary to the linear MPC for nonlinear systems, the linearization occurs at the initial guess $[x_i^{guess}, u_i^{guess}]$. Therefore, the sensitivity matrices are

$$\begin{aligned} A_{i,k} &= \left.\frac{\partial f(x,u)}{\partial x}\right|_{x_i^{guess}, u_i^{guess}} & B_{i,k} &= \left.\frac{\partial f(x,u)}{\partial u}\right|_{x_i^{guess}, u_i^{guess}} \\ C_{i,k} &= \left.\frac{\partial h(x,u)}{\partial x}\right|_{x_i^{guess}, u_i^{guess}} & D_{i,k} &= \left.\frac{\partial h(x,u)}{\partial u}\right|_{x_i^{guess}, u_i^{guess}} \end{aligned} \tag{6.4}$$

$$r_{i,k} = f\left(x_i^{guess}, u_i^{guess}\right) - x_{i,k+1}^{guess} \quad h_{i,k} = h\left(x_i^{guess}, u_i^{guess}\right), \qquad J_{i,k} = W_{i,k} \begin{bmatrix} x_{i,k}^{guess} - x_{i,k}^{ref} \\ u_{i,k}^{guess} - u_{i,k}^{ref} \end{bmatrix} \tag{6.5}$$

The matrix $H_{i,k}$ is the Hessian approximation of the Lagrangian of Eq. (6.3). The popular Gauss-Newton Hessian approximation is given directly by assuming $H_{i,k} = W_{i,k}$. Therefore, the SQP procedure for time instant i, is given by Algorithm 1.

Algorithm 1: SQP for NMPC at discrete time i

Input: current state estimate $\hat{x}_i$, reference trajectory $(\mathbf{x}_i^{ref}, \mathbf{u}_i^{ref})$ and initial guess $(\mathbf{x}_i^{guess}, \mathbf{u}_i^{guess})$

while *Not converged* **do**

- Evaluate $r_{i,j}$,$h_{i,k}$, and the sensitivities $A_{i,k}, B_{i,k}, C_{i,k}, D_{i,k}, H_{i,k}, J_{i,k}$ using Eq. (6.4);
- Construct and solve $QP_{NMPC}(\hat{x}_i, \mathbf{x}_i^{guess}, \mathbf{u}_i^{guess}, \mathbf{x}_i^{ref}, \mathbf{u}_i^{ref})$ as in Eq. (6.3) to get the Newton direction $(\Delta\mathbf{x}_i \ \Delta\mathbf{u}_i)$;
- Compute step - size $\alpha \in [0, 1]$ to guarantee descent;
- Update $(\mathbf{x}_i^{guess}, \mathbf{u}_i^{guess})$ with the Newton step

$$(x_i^{guess} \ u_i^{guess}) \leftarrow (x_i^{guess} \ u_i^{guess}) + \alpha(\Delta\mathbf{x}_i \ \Delta\mathbf{u}_i)$$

end

return: NMPC solution $(x_i, u_i) = SQP(x_i, u_i) = x_i^{guess}, u_i^{guess}$

The NMPC solution of the $NLP(\hat{x}_i, \mathbf{x}_i^{ref}, \mathbf{u}_i^{ref})$ is the obtained from the SQP Algorithm 1, starting from the initial guess $(x_i^{guess}, u_i^{guess})$, as follows

$$u_i^{NMPC} = u_{i,0}, \quad (\mathbf{x}_i, \mathbf{u}_i) = SQP(\hat{x}_i, \mathbf{x}_i^{guess}, \mathbf{u}_i^{guess}, \mathbf{x}_i^{ref}, \mathbf{u}_i^{ref}) \tag{6.6}$$

The choice of appropriate initial guess input is of great importance since they play a major role in the convergence and reliability of the SQP iterations. While for linear MPC, the initial guess is chosen to be the reference trajectory, in the present context of SQP for NMPC, a good initial guess for the discrete time instant i can be obtained, provided that a good solution has been obtained at the previous time instant $i-1$. This procedure assumes that the evolution of system dynamics follows the predicted trajectory (i.e. $\hat{x}_i \approx x_{i-1,1}$), and can be expressed as

$$x_{i,k}^{guess} = x_{i-1,k+1}, \quad k = 0, ..., N-1 \tag{6.7}$$

$$u_{i,k}^{guess} = u_{i-1,k+1}, \quad k = 0, ..., N-2 \tag{6.8}$$

$$x_{i,N}^{guess} = f(x_{i,N-1}^{guess}, u_{i,N-1}^{guess}) \tag{6.9}$$

It is suggested that if the solution (x_{i-1}, u_{i-1}) is feasible, then the shifted solution should be also feasible, regarding the dynamic constraints. Furthermore, if the guess which was obtained from the shifting procedure is close enough to the real solution of the NMPC problem, then full Newton steps can be selected for SQP iterations and the first iteration would be a close approximation of the exact solution to the NMPC problem, [109]. Several approaches have been proposed to select the control input guess $u_{i,N-1}^{guess}$, with the most common being that the last control input is equal to the previous i.e $u_{i,N-1}^{guess} = u_{i,N-2}^{guess} = u_{i-1,N-1}$.

The SQP procedure starts when the new state estimate is obtained. While the iterations of the algorithm are performed, the physical system evolves, and consequently, when the SQP finally converges, the information which was used to compute the state estimate $\hat{x}_i$ are outdated.

This problem can be overcome by employing prediction algorithms to estimate the state when the iterations have been completed. However, since the update of the control law requires the completion of the SQP algorithm and thus large computational delays can occur. The RTI approach which is presented here chooses to begin the SQP algorithm and constantly incorporate the latest information of the system evolution in the iterations.

Real Time Iteration approach (RTI)

The RTI approach is a method that efficiently solves the NMPC problem via the SQP, via performing the Newton steps always using the latest information of the system evolution. The RTI procedure is based on Algorithm 1 which was previously presented, with some modifications. At first, it is considered that the initial guess is derived from the shifting procedure. Secondly, the NMPC solution is updated via a single Newton step for every time instant, on the previously constructed initial guess, instead of applying the SQP to full convergence. Assuming, that the solution which was obtained at time instant $i-1$ is a good initial guess, then according to the previous, the solution of the NMPC with $\alpha = 1$ (in Algorithm 1) is an excellent approximation of the fully converged solution. Thirdly, besides the above, the RTI, divides the calculations into two phases, to reduce the feedback time. Considering the fact that the shifting procedure and calculation of the sensitivities (linearization of the system) on the initial guess, does not require the knowledge of the state estimate $\hat{x}_i$, and therefore they can be performed before the state estimate is available. Therefore, the RTI procedure consists of two phases which are

1. The *preparation phase*, in which shifting and sensitivity calculations occur prior obtaining the state estimate

2. The *feedback phase*, in which the rest of the calculations occur after obtaining the state estimate

For the above scheme, the Hessian approximation, i.e. $H_{i,k} = W_{i,k}$ is usually used in order not to calculate second order derivatives, receive a positive semi-definite approximation. The RTI algorithm is presented below [108].

As it was mentioned before, NMPC optimization is non-convex, and therefore the computation of global solution for each time instant is not guaranteed. However, according to [108], under some specific assumptions, the solution provided from the RTI, can be proved to be global.

The above algorithm applies to discrete-time systems. RTI procedure requires to compute the dynamic sensitivities, $\nabla f(x, u)$, which for the above systems is straightforward. However, in most cases, the controlled systems are described by continuous time ordinary differential equations, in form of $\dot{s}(t) = F(s(t), v(t))$, where $s(t)$ and $v(t)$ are the states and controls respectively.

Algorithm 2: RTI for NMPC at discrete time i

1 *Preparation Phase* performed over time interval $[t_{i-1}, t_i]$;
Input: previous NMPC solution $(\mathbf{x}_{i-1}, \mathbf{u}_{i-1})$, reference $(\mathbf{x}_{i-1}^{ref}, \mathbf{u}_{i-1}^{ref})$
2 Shift $(\mathbf{x}_{i-1}, \mathbf{u}_{i-1})$ in order to construct $(\mathbf{x}_i^{guess}, \mathbf{u}_i^{guess})$;
3 Evaluate $r_{i,j}$,$h_{i,k}$, and sensitivities $A_{i,k}, B_{i,k}, C_{i,k}, D_{i,k}, H_{i,k}, J_{i,k}$ at $(\mathbf{x}_i^{guess}, \mathbf{u}_i^{guess})$ using 6.4;
4 Form QP omitting $\hat{x}_i$, prepare all possible calculations (e.g. condensing, matrices factorization) **return:** QP
5 *Feedback Phase* performed at time t_i upon availability of $\hat{x}_i$;
Input: $\hat{x}_i$,prepared QP
6 Compute $(\Delta x_i, \Delta u_i)$ by introducing $\hat{x}_i$ in QP and solving it ;
7 Apply the full Newton step

$$(x_i^{guess}\ u_i^{guess}) \leftarrow (x_i^{guess}\ u_i^{guess}) + (\Delta \mathbf{x}_i\ \Delta \mathbf{u}_i) \tag{6.10}$$

return: NMPC solution (x_i, u_i)

Therefore, discretization of the system should be conducted before the RTI algorithm proceeds. To do this, several methods have been proposed. However, the accuracy and the computational efficiency of each method mainly depend on the application. In [108], several methods are presented and analyzed. In the present work, it is chosen that the discretization is conducted first using a 4th order implicit Runge-Kutta method and then the linearization to take place at every time instant the previous solution, as it is proposed by the RTI algorithm. The NMPC controller and the RTI scheme were implemented with the *ACADO Toolkit*, [110, 111].

6.1.3 Feasibility and stability

The stability of systems controlled by MPC is in generality not trivial. Feasibility and stability are explicitly ensured by introducing terminal cost and terminal constraints, which guarantee that a solution exists and that the system trajectories will converge to the origin. However, the terminal constraint usually reduces the region of attraction. Regarding the stability of NMPC without terminal constraints see [112]. In relation, a sufficient long prediction horizon is usually selected in practice to ensure recursive feasibility. Additionally, soft constraints using slack variables in the cost function can enlarge the feasibility set that the state converges to the origin and enhance robust stability, [113].

In this Thesis, MPC design practices that are proposed in the literature were followed. The weights of the stage and terminal cost values are scaled considering the prioritization of the control objectives. In addition, a higher terminal cost for each state variable is selected to ensure the recursive feasibility of the NMPC problem. Also, system states are soft-constrained, as due to load disturbance in marine applications, a violation can often be tolerated for short time periods. Regarding the terminal constraints, they remain the same as state constraints, in order not to reduce the region of attraction. The stability was also practically proved during

simulations and experiments, as the proposed control schemes were tested in multiple operating scenarios and a variety of disturbance excitation amplitudes.

The RTI scheme performs the preparation and the feedback steps in different time instants, to maximize the time efficiency of the solution, [108]. RTI scheme introduces a dynamic interaction between the system and the optimizer. The stability of the RTI scheme was initially proved in [114] for problems in the absence of inequality constraints. The stability of the RTI scheme for optimization problems with inequality constraints is discussed further in [115].

6.2 Transient Power-Split Controller Design

Marine propulsion plants are complex MIMO systems, as the installed power-sources diversify in terms of the underlying technology, principles of operation, size, and physical limitations. On the other hand, system performance specifications strive for competitive objective satisfaction, such as immediate power availability at the propeller shaft, maximized engine energy efficiency, and minimized emissions. In this context, the control system has to explicitly tackle the non-linear system behavior, respect system input and operating limits, and ensure system operation in a manner that is a) optimal according to the desired objectives and b) comfortable in e.g. disturbance rejection.

In relation to powertrain control, the **objectives** could be prioritized as follows

1. *Dynamic torque delivery:* Follow the desired operators speed reference changes without lags and delays.

2. *Disturbance rejection:* Reject speed and load disturbances and avoid oscillating behavior.

3. *Robustness against external load:* Robust behavior against steady-state and dynamic disturbances.

4. *Smooth ICE loading:* Avoid shock loads of the diesel engine that lead to overshoot in fueling and emissions production (inertial load take-up and turbo-charger lag phenomena).

5. *Minimum electric energy usage:* Minimize EM engagement to avoid electric energy conversion losses and long period electric operation which requires increased battery capacity.

6. *Battery charge sustainability:* Maintain in the long term the battery state of charge regardless of the vessel operational profile.

Also, system input and state constraints should be respected. These objectives should be achieved by determining the optimal control inputs, which are the torque output commands supplied to the ICE ECU and the EM inverter system.

The application of an NMPC controller requires the solution of a nonlinear Optimal Control Problem (OCP) at each time step. The solution provides an optimal sequence of control inputs that minimize an appropriate cost function over a short horizon window and the first value is applied to the system at each sampling instant. The **optimization model** that was integrated in the problem formulation was presented in Chapter 3. Equations (3.4), (3.5), (3.8)-(3.15) are utilized as information about the evolution of system behavior over time for the variables of interest. NMPC problem is structured considering the following four differential states

$$\mathbf{x} = [N_{eng}, SOC, u_{ice}, u_{EM}]^T \tag{6.11}$$

two controlled outputs

$$\mathbf{y} = [N_{eng}, SOC]^T \tag{6.12}$$

three control variables

$$\mathbf{u} = [\dot{u}_{ice}, \dot{u}_{em}, \varepsilon]^T \tag{6.13}$$

and the disturbance variable

$$\mathbf{d} = c_{load} \tag{6.14}$$

As it can be noted, the system inputs are considered as differential states and their derivatives as control inputs. In this way, the rate of change of the system inputs can be weighted and constrained to control the transient behavior of the power sources and avoid sudden changes of the ICE and EM torque outputs.

The **constraints** in consideration and the controller tuning guarantee that Q_{load} is mainly satisfied by the diesel engine in steady-state operation and the EM is motoring only in transient loads to mitigate diesel engine fast accelerations and load fluctuations. This power smoothing strategy, achieves a quasi-steady like operation for the diesel engine and can achieve further emissions reduction, with minimum battery usage, [20, 33]. Moreover, the slack variable ε is introduced as an additional control input, to implement soft constraints formulation, with which the limit violation within the prediction horizon is heavily penalized in the cost function. As such, the optimization problem remains feasible.

The load disturbance Q_{load}, is not measured. Here, the observed propeller law parameter projected on the engine side $\hat{c}_{load}$, which is calculated using the propeller load observer presented in Section 4.2, is provided to the NMPC and $Q_{load} = \hat{Q}_{load}$ is calculated over the prediction horizon according to the predicted engine speed elevation, from Eq. (4.25). As explained before, the developed observer guarantees an offset-free tracking of the operator's desired speed reference, given the fact that none of the system constraints is violated.

The **cost function** J, which is required to be minimized to solve the OCP is the following

$$\begin{aligned} J(\dot{u}_{ice}, \dot{u}_{em}, u_{em}, N_{eng}, SOC, \varepsilon) = \\ = \sum_{i=0}^{N-1} W_i \begin{bmatrix} (N_{eng,i} - N_{eng,ref})^2 \\ (SOC_i - SOC_{ref})^2 \\ u_{em,i}^2 \\ \dot{u}_{em,i}^2 \\ \dot{u}_{ice,i}^2 \\ \varepsilon^2 \end{bmatrix}^T + \\ W_N \begin{bmatrix} (N_{eng,N} - N_{eng,ref})^2 \\ (SOC_i - SOC_{ref})^2 \end{bmatrix}^T \end{aligned} \tag{6.15}$$

where W_i is the stage cost matrix and W_N is the final cost matrix. The **optimization problem** is formulated as follows

$$\begin{aligned} & \min_{\dot{u}_{ice}, \dot{u}_{em}, \varepsilon} J(\dot{u}_{ice}, \dot{u}_{em}, u_{em}, N_{eng}, SOC, \varepsilon) \\ s.t. \quad & \text{Equations (3.4), (3.5), (3.8)-(3.15)} \\ & Q_{load,i} = \frac{60}{2\pi} \hat{c}_{load,i=0} N_{eng,i}^2 \\ & SOC_{min,hard} \leq SOC \leq SOC_{max,hard} \\ & u_{em,min} \leq u_{em} \leq u_{em,max} \\ & 0 \leq u_{ice} \\ & Q_{ice} \leq Q_{ice,max}(N_{eng}) \\ & \dot{u}_{ice,min} \leq \dot{u}_{ice} \leq \dot{u}_{ice,max} \\ & \dot{u}_{em,min} \leq \dot{u}_{em} \leq \dot{u}_{em,max} \\ & N_{eng,min,soft} - \varepsilon \leq N_{eng} \leq N_{eng,max,soft} + \varepsilon \\ & SOC_{min,soft} - \varepsilon \leq SOC \leq SOC_{max,soft} + \varepsilon \\ & \varepsilon \geq 0 \\ & U_{oc}^2 - 4 P_b R_i \geq 0 \end{aligned} \tag{6.16}$$

where $Q_{ice,max}(N_{eng})$ is the maximum ICE torque curve from the engine envelope (Fig. 2-2) and the last equation refers to battery overloading, as described by Eq. (3.16). By solving the above optimization problem over the prediction horizon, the appropriate commands for power-split are calculated that satisfy the control objectives. To realize that, a real-time NMPC scheme was designed and generated with ACADO toolkit, [110], where the Sequential Quadratic Programming (SQP) method is deployed and qpOASES3 [116] is selected as solver.

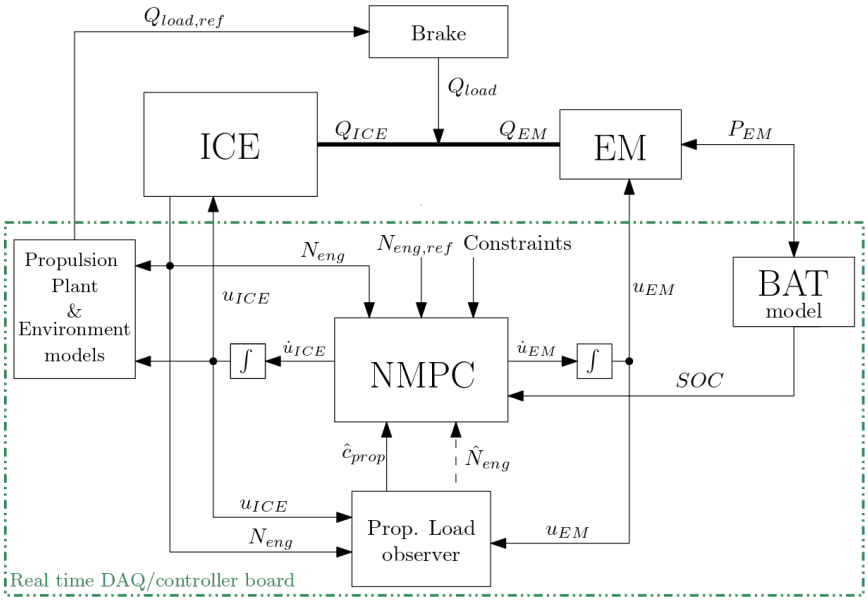

Figure 6-2: NMPC architecture and experimental implementation.

To reduce testbed hours, controller tuning and evaluation were performed in simulation. Also, the controller was experimentally implemented and evaluated in extreme transient loading, where it coped with step disturbance application and step reference tracking. Although such aggressive conditions are rarely faced in real operation, step input is commonly used to test the transient behavior of the system. The experimental results of this procedure are extensively presented in [5, 6] and [7].

6.3 Experimental Testing

6.3.1 Experimental implementation

For the evaluation of the transient power-split controller, a number of experiments were performed using the HIPPO-2 experimental facility at the Laboratory of Marine Engineering (NTUA/LME) (seen in Fig. 2-1). The control set up consists of the controller scheme (NMPC and observer), the propulsion plant, wave disturbance and battery emulation models, as shown in Fig. 6-2.

The NMPC, based on the information provided by measurements, the propeller observer, and the reference from the operator, calculates the optimal control commands (i.e. load rate of ICE and EM), which are provided to the power sources. The parameters of the internal model are summarized in Table B.1. The controller tuning was performed in simulation. In simulation and experiment the same control system tuning was used. Simulation results are similar to experimental results leading to the same conclusions and as such, they are omitted. The numerical values of the tuning parameters, as well as the constraints of the NMPC problem, are presented in Table 6.1.

Table 6.1: Parameters and tuning of the NMPC.

Parameter	Symbol	Value
NMPC Sample Time	T_s	0.1 s
Prediction Horizon	H_p	10 steps
Control Horizon	H_c	10 steps
Cost Matrix	W_i	$diag(15\ 200\ 0\ .5\ 5\ 0.5\ 10^3)$
Terminal Cost Matrix	W_N	$diag(15\ 1000)$
	Constraints	
Soft SOC	SOC_{soft}	[25 75] %
Soft N_{eng}	$N_{eng,soft}$	[700 2000] rpm
EM cmd	u_{em}	[-90 90] %
EM cmd rate	$\dot{u}_{em}$	[-50 50] %/s
ICE cmd rate	$\dot{u}_{ice}$	[-20 3] %/s
	Prop. observer	
State noise covar. matrix	$Q[k]$	$7\ 10^{-4}$
Input noise covar. matrix	$R[k]$	5

The propulsion plant and environmental disturbance emulation model, developed in Section 4.1 (its parameters are summarized in Table B.2), was utilized for the propeller load calculation that is applied to the experimental testbed by the electric dynamometer. It interacts dynamically with the physical system and the controller behavior. On the other hand, the propeller observer is based on the information that would be available onboard a vessel, which refers to the controller commands and the engine speed measurement, provided by the ICE ECU.

Finally, the battery SOC calculation is based on the electric power flow measurement, received by the power electronics (inverter system) of the EM. A 3.5 kWh battery pack was considered for the present scenario, to avoid long-term electric operation. The numerical parameters of the quasi-static and dynamic battery models are presented in Table 6.2. As it was explained in subsection 3.2.4, different battery models for SOC simulation and controller design was intentional, to evaluate the NMPC behavior with modeling inaccuracies and the fact that actual or experimental battery performance deviates from the modeled parameters.

6.3.2 Experimental results

During experiments, two consecutive propeller speed accelerations were applied. The two accelerations have different slopes. The first profile applied includes a 900-1600 rpm ramp in 10 s ($\dot{N}_{eng} = 70\ rpm/s$), and the second a 900-1600 rpm ramp in 5 s ($\dot{N}_{eng} = 140\ rpm/s$). These scenarios resemble a typical propeller acceleration profile during ship maneuvering. During experimental testing, it is intentional to make a comparison between the proposed control scheme and a standard industrial controller. Therefore transient behavior of the proposed NMPC control scheme (NMPC experiment) is evaluated against the operation of the conventional set-up, without operation of the EM, where the powertrain is controlled by the diesel engine ECU speed

Table 6.2: Battery models sizing for Transient Controller testing.

Description	Parameter	Value and Unit
Battery Dynamic Model Parameters		
Open Source Voltage	V_{OC}	696 V
Ohmic Resistance	R_O	0.241 Ω
Polarization Resistance	R_P	0.271 Ω
Open Source Capacitance	$C_{V_{OC}}$	17600 F
Polarization Capacitance	C	960 F
Nominal Capacity	Q_{nom}	5 Ah / 3.5 kWh
Battery Internal Model Parameters		
Open Source Voltage Coeff.	k_1	696 V
Open Source Voltage Coeff.	k_2	1.022 $Volts/\%SOC$
Internal Resistance	R_i	0.512 Ω

controller, which has its industrial calibration (ICE ECU experiment). The experimental results are presented in Fig. 6-3, 6-4 and 6-5.

The engine speed profile, the resulting propeller load for NMPC and ICE ECU experiments and the battery state of charge, the propeller load observation, the power-split are shown in Fig. 6-3. As it can be observed in the first subplot, during the acceleration intervals the NMPC regulates the ICE and EM torques to accelerate the shaft and to satisfy the propeller load demand. The EM immediately provides torque, while the diesel engine load transition is performed according to the $\dot{u}_{ice}$ constraint. In the second acceleration, the EM maximum torque limit is reached and a small speed error is observed until the ICE can balance the load demand at the reference speed.

During steady speed intervals, EM operates in generating mode to recharge the battery, while ICE works near its torque limit to satisfy the propeller load and generate battery power for battery charging. The EM torque value is controlled to reject speed disturbance that is caused by the propulsion plant environment and achieve reduced engine power fluctuations. At decelerations, EM operates in regenerating mode to balance the excess power generated by the engine while unloading, as well as absorb kinetic energy of the shaft and reduce the rotational speed. Finally, it can be noted that offset-free speed reference tracking is achieved.

As compared with the loading in the ICE ECU experiment, which is shown in Fig. 6-3 second subplot, the diesel engine is forced to perform extreme transient operations, that need power margin availability at low engine speeds, where diesel engines in general under-perform. In addition, at higher speeds, the system *"controller-power train-propulsion plant-vessel-environment"* interaction leads to high amplitude power oscillations that affect the ICE performance and system safety, in contrast to the NMPC case where this interaction is smoothened.

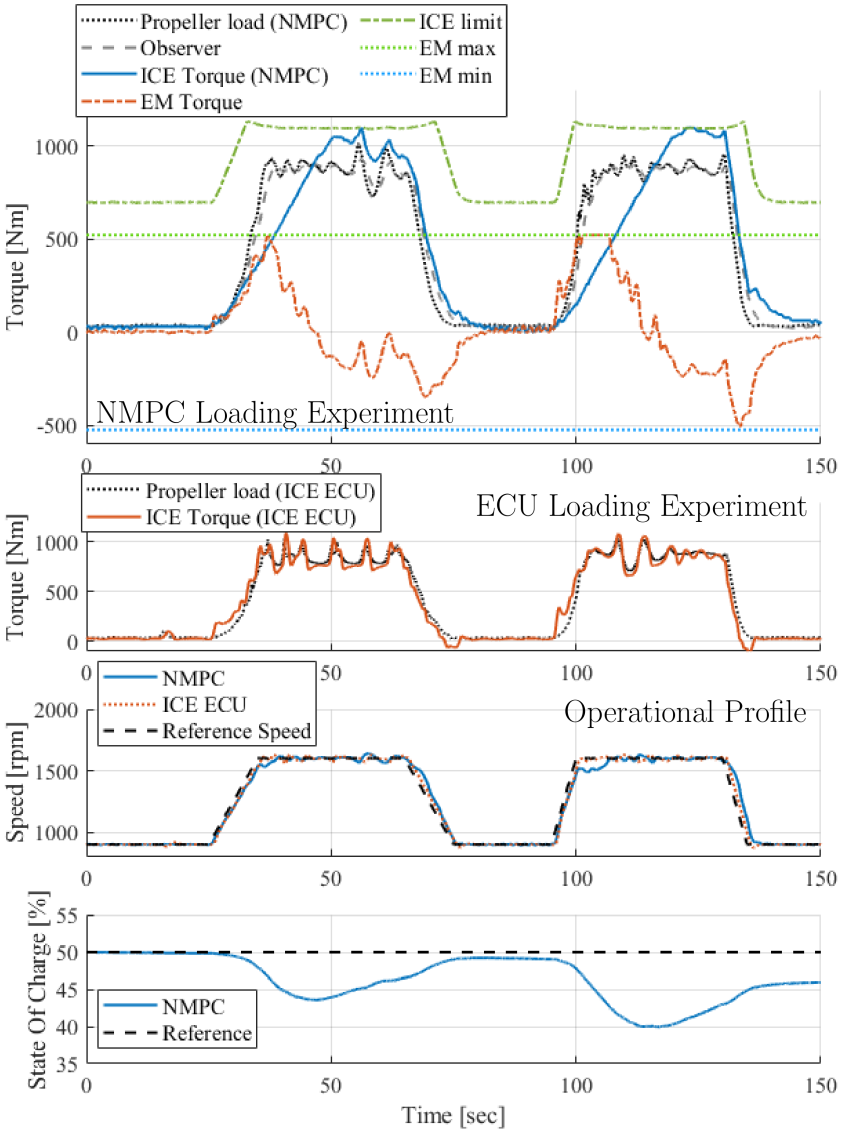

Figure 6-3: Loading, power-split, shaft speed and battery state of charge at experimental testing.

In Fig. 6-4 the ICE performance during the NMPC and ICE ECU experiments is presented. As it can be seen, with NMPC, ICE obtains a quasi-steady like operation, as compared to the ICE ECU experiment where more aggressive behavior is observed, in terms of fuel feed overshoots and oscillations, more exhaust gas pollutants during fast accelerations, and worse emissions efficiency in deceleration and lower speeds. In total, the calculated cumulative NOx emission is 10.10 gr with NMPC as compared to 10.35 gr that were emitted during the ICE ECU experiment. The cumulative fuel consumption was 0.80 l in both experiments.

In Fig. 6-5, the speed-power phase diagram for each acceleration-deceleration slope for each experiment is presented. In the left column, the transient engine loading can be seen during acceleration and deceleration, as well as the steady-state power fluctuations of the engine power due to environmental disturbance. On the right column diagrams, the total load-split during acceleration and deceleration is plotted. As it can be noted, the acceleration path has increased

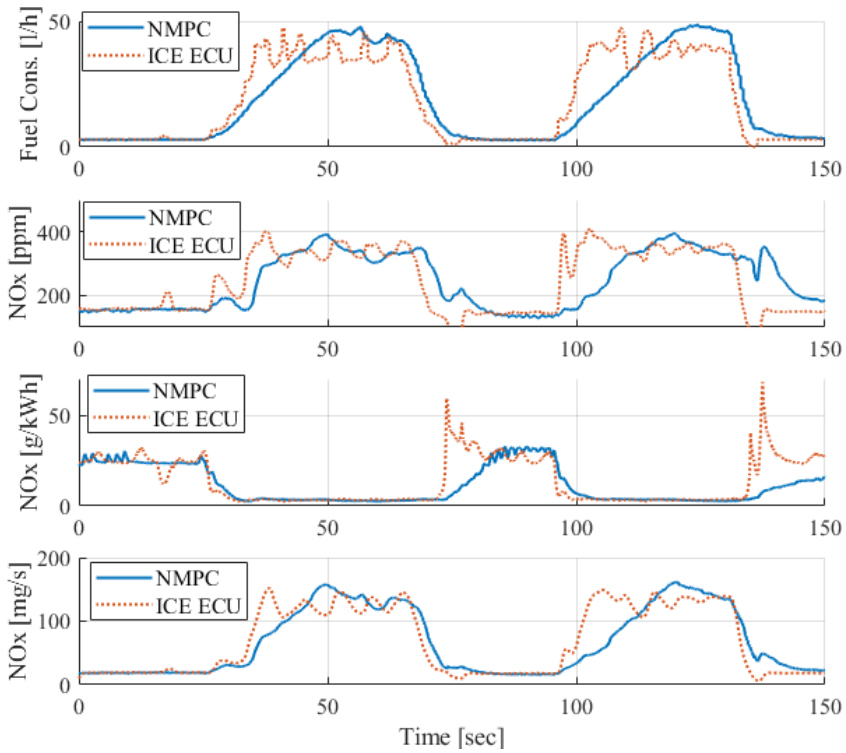

Figure 6-4: Diesel engine performance at experimental testing.

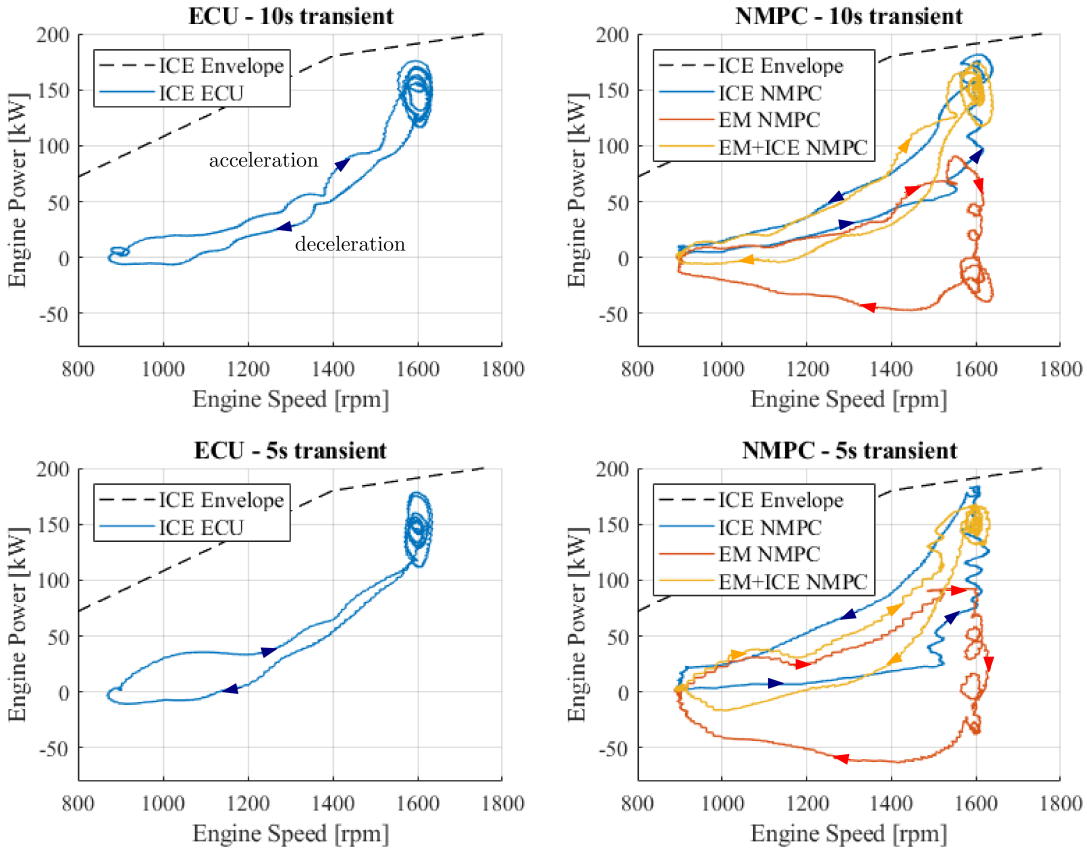

Figure 6-5: Phase plots of power vs. engine speed at experimental testing.

power demand, as compared to the power path during deceleration. As such different propeller law constant is observed. Furthermore, during the 5 s transient which occurs between time 80-150 s, increased power has to be delivered at engine speed range 900-1200 rpm, as compared to the 10 s transient which occurs in the time interval between 0-80 s, as it can be seen in Fig. 6-3.

The ICE in NMPC experiments, as compared to the ICE ECU experiment, follows a different power-speed path to balance the total propeller load demand in cooperation with the EM. As a result, during acceleration, the ICE accelerates on lower load, according to the $\dot{u}_{ice,max}$ constraint and decelerates on higher load, since EM is in generating mode. Finally, as it can be observed, the EM power limit is reached during acceleration between 1400-1600 rpm in the NMPC - 5 s transient diagram.

During experimental testing, NMPC achieved a 2.4% reduction in mean and 3.3% total NOx emissions, while the mean specific NOx production was decreased by 20.2% as compared to the system operation with conventional control. At the end of the experiment, The EM cumulative energy flow was 73.58 kJ and the battery was discharged by 4% at the end of the experiment.

6.4 Conclusion

When referring to powertrain control, NMPC is one of the appropriate control methods that can inherently deal with system non-linearity, manage physical and operational limitations and utilize knowledge of system and disturbance response to produce an optimal result. In relation, this chapter proposed a Nonlinear Model Predictive Control (NMPC) scheme for solving the optimal transient power-split problem of a parallel hybrid diesel-electric marine propulsion plant, considering transient propeller load and environmental disturbance, from the viewpoint of achieving smooth power transitions and mitigation of power fluctuations of the internal combustion engine.

The developed power-split strategy utilized EM to deal with the powertrain fast dynamics to deliver the required torque load at the propeller shaft and achieves quasi-static loading of the ICE that leads to suppression of ICE fast acceleration, as well as mitigation of ICE load oscillations that produce overshoots in NOx emissions and fueling. In addition, indirect energy management was performed, i.e the fuel consumption and NOx emissions models were not utilized by the controller internally. At the same time, battery charge sustaining, in the long-term, was achieved.

Finally, the proposed control scheme is robust to disturbance load characteristics, meaning that it achieves offset-free reference tracking independently of the propulsion plant size, the uncertainty of the propeller and ship characteristics, as well as the modeling errors between the actual powertrain behavior and the internal NMPC model. As such, it is concluded that the problem of transient power-split control was well defined and properly formulated.

This chapter responded to research question 4.

Chapter 7

Energy Management and Emissions Minimization Control System

In the previous chapter, an integrated torque-split control scheme was proposed for the operation of ship hybrid propulsion plants in transient loading conditions. The main performance specifications were torque availability as well as mitigation of ICE fast accelerations and load oscillations, that lead to NOx and fueling overshoots. In this way, a robust but indirect energy management was achieved. The *contribution* of the present Chapter is the development and implementation of an integrated, real-time capable, Energy Management and Emissions Minimization System (EMEMS) for parallel hybrid ship propulsion plants, that is able to satisfy the current and predicted propeller load and maximize both fuel consumption and NOx emissions efficiency of the system according to the selected criteria.

7.1 Energy Management System Design

Along this line, the optimal control problem is reformulated so as to perform energy management planning according to a weighting factor which determines the trade-off between fuel consumption and NOx emissions minimization. The EMEMS calculates the optimal power-split strategy, based on the internal model information for system performance in addition to operator's reference prediction, which is received online. A simulation study is performed to investigate the trade-off between fuel efficiency and NOx performance for different weighting factors and evaluate results in respect to the solution of the optimal control problem, where the loading profile is known in advance. Finally, for the validation of the control concept, the control scheme is experimentally implemented and tested under realistic operating conditions.

As compared to section 6.2, the control system **objectives** are modified, as follows:

1. *Dynamic torque delivery:* Follow the desired speed reference changes without lags and delays.

2. *Disturbance rejection:* Reject speed and load disturbances and avoid oscillating behavior.

3. *Robustness against external load:* Robust behavior against steady-state and dynamic disturbances.

4. *Smooth ICE loading:* EM deals with fast system dynamics and ICE follows in a quasi-static manner.

5. *Minimized weighted energy consumption and emissions production:* The weighted cumulative equivalent fuel consumption and NOx emissions production m_{ec} over the prediction time window should be minimized.

6. *Battery charge sustainability:* In the nominal test-case, the battery charge should be equal at the end of the operational cycle in order to evaluate the capabilities of the EMS regarding fuel savings and emissions reduction.

7. *Constraints satisfaction:* Ensure that the physical and operating constraints, such as the engine overloading, of the hybrid system are not violated.

Regarding the above objectives, items 1-4 and 7 were explained in Section 6.2. As such, here only the aspects regarding the reformulation of the optimal control problem will be discussed.

With the use of the **equivalent consumption formulation**, the battery energy flow is penalized with an equivalence factor λ which depends on the battery state of charge and the electric energy consumption of the EM, which is expressed in equivalent fuel mass consumption when divided with the lower heating value of the engine fuel Q_f. Also, NOx emissions are scaled with maximum fuel consumption to maximum NOx emissions ratio λ_N in order to be comparable with the range of fuel consumption values. As such, the equivalent consumption $\dot{m}_{ec}$ is defined as

$$\begin{aligned} \frac{dm_{ec}}{dt} =& \dot{m}_{ec} \\ \dot{m}_{ec} =& (1-A)\dot{m}_f + A\lambda_N \dot{m}_N + \lambda \frac{1}{Q_f} P_b \end{aligned} \tag{7.1}$$

where

$$\begin{aligned} \lambda &= \lambda_{SOC}\lambda_{ecems} \\ \lambda_{SOC} &= 1 - \left(\frac{2SOC - (SOC_{min} + SOC_{max})}{SOC_{max} - SOC_{min}} \right)^3 \\ \lambda_N &= \frac{\max(\dot{m}_f)}{\max(\dot{m}_N)} \end{aligned} \tag{7.2}$$

where λ_{ecems} is a tuning parameter which is determined in simulation to derive the same initial and final battery state of charge. In this way, the savings regarding the hybrid operation can be evaluated in relation to the achieved energy efficiency and battery energy conservation.

The optimality of **energy management planning** does not depend only on the particular optimization methods deployed to solve the minimization problem, but on the availability and reliability of the information received in run-time. As such, the propeller observer, from Section 4.2, as well as the results of Chapter 5 were utilized to provide off- and online information that are required in order to produce the nearest-optimal possible result.

The **optimization model** that was integrated into the problem formulation was presented in Chapter 3. Equations (3.4)-(3.15), (7.1) and (7.2) are utilized as information about the evolution of system behavior over time for the variables of interest. NMPC problem is restructured considering the following five deferential states

$$\mathbf{x_c} = [N_{eng}, SOC, m_{ec}, u_{ice}, u_{em}]^T \tag{7.3}$$

two controlled outputs

$$\mathbf{y} = [N_{eng}, m_{ec}]^T \tag{7.4}$$

three control variables

$$\mathbf{u_c} = [\dot{u}_{ice}, \dot{u}_{em}, \varepsilon]^T \tag{7.5}$$

and the disturbance variable

$$\mathbf{d} = c_{load} \tag{7.6}$$

The system input variables are considered as differential states, and their derivatives as control inputs. Hence, the rate of change of the system inputs can be weighted and constrained in order to control the transient behavior of the power sources. Moreover, the slack variable ε is used as additional control input, in order to consider soft constrained variables, with which the limits violation within the prediction horizon is heavily penalized in the cost function. As such, the optimization problem remains feasible.

To solve the OCP, the following **cost function** J is considered

$$\begin{aligned} &J(N_{eng}, m_{ec}, \dot{u}_{ice}, \dot{u}_{em}, \varepsilon) = \\ &= \sum_{i=0}^{N-1} W_i \begin{bmatrix} (N_{eng,i} - N_{eng,ref,i})^2 \\ \dot{u}_{ice,i}^2 \\ \dot{u}_{em,i}^2 \\ \varepsilon^2 \end{bmatrix}^T + \\ &+ W_N \begin{bmatrix} (N_{eng,N} - N_{eng,ref,N})^2 \\ m_{ec,N}^2 \end{bmatrix}^T \end{aligned} \tag{7.7}$$

where W_i is the stage cost matrix and W_N is the final cost matrix. $N_{eng,ref,0}$ is the operator's speed reference input and $N_{eng,ref,i},\ i = 1 : N$ are predictions of the future operator's input

provided by the neural network prediction model, (5.3), developed in Section 5.2, utilizing past values of $N_{eng,ref}$.

The mathematical **formulation of the OCP** is

$$\begin{aligned}
&\min_{u_{ice},u_{em},\varepsilon} J(N_{eng}, m_{ec}, \dot{u}_{ice}, \dot{u}_{em}, \varepsilon) \\
s.t.\ &\text{Equations (3.4)-(3.15),(7.1),(7.2)} \\
&Q_{load,i} = \hat{c}_{load,i=0} N_{eng,i}^2 \\
&SOC_{min,hard} \leq SOC \leq SOC_{max,hard} \\
&u_{em,min} \leq u_{em} \leq u_{em,max} \\
&0 \leq u_{ice} \leq u_{ice,max}(N_{eng}) \\
&\dot{u}_{ice,min} \leq \dot{u}_{ice} \leq \dot{u}_{ice,max} \\
&\dot{u}_{em,min} \leq \dot{u}_{em} \leq \dot{u}_{em,max} \\
&N_{eng,min,soft} - \varepsilon \leq N_{eng} \leq N_{eng,max,soft} + \varepsilon \\
&SOC_{min,soft} - \varepsilon \leq SOC \leq SOC_{max,soft} + \varepsilon \\
&\varepsilon \geq 0 \\
&U_{oc}^2 - 4P_b R_i \geq 0
\end{aligned} \tag{7.8}$$

where $u_{ice,max}(N_{eng})$ is the maximum ICE torque curve and the last equation refers to battery overloading. By solving the above optimization problem over the prediction horizon, the appropriate commands for power-split are calculated, in order to track the reference shaft speed based on a mid-term plan to minimize the weighted fuel consumption and NOx emissions. Then, the first control value is applied to the system at each sampling instant. To achieve a mid-term prediction horizon, it is defined as 10 s within which reliable predictions can be made. NMPC sample time must be prolonged to 0.5 s as compared to the transient NMPC controller of Section 6.2. As such, the computational effort is kept low and the sampling interval sufficient in order to solve the online optimization problem. For off-line system tunning and evaluation in simulation and experiments, the marine load emulation model as well as the created loading cycle 20 from Fig 5-5 will be used.

Remark 1: Speed reference prediction refers to $N_{ref}[k+i|i],\ i = 1...N$ and is relevant to the energy management planning. As such, a wrong prediction, does not affect tracking of $N_{ref}[k|k]$ which is the actual set-point requested by the operator; only the energy management planning is affected.

Remark 2: m_{ec} was selected to be implemented as terminal term, as it is the integral of $\dot{m}_{ec}$ at each instant $k+i|k$ within the prediction horizon. This formulation has an economic perspective

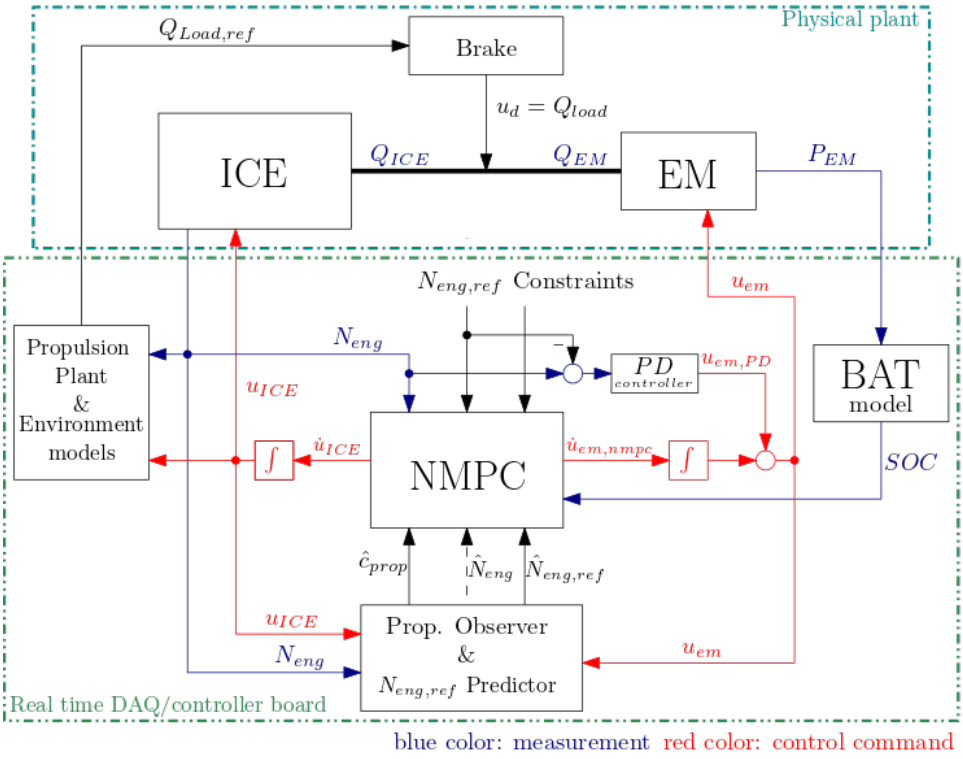

Figure 7-1: Control scheme architecture and experimental implementation.

and was preferred instead of using integral of squared $\dot{m}_{ec}$ that has a tracking meaning. The first proved to be more efficient in order to find the minimal m_{ec} power path.

To implement the controller, *ACADO toolkit* , [110], was used to create an implementable and real-time capable NMPC algorithm. In order to perform the power-split calculation over a sufficient long time horizon and at the same time keep the computational effort low, the NMPC sample time was set to 0.5 s. The control architecture and implementation is presented in Fig. 7-1, where the essential information flow between software and hardware subsystems is presented.

The NMPC sample time is not sufficient for speed reference tracking when wave disturbance acts on the system. For this reason, a PD controller was used in parallel to the NMPC in order to regulate the u_{em} between the NMPC sampling intervals. Input to the PD controller is the speed tracking error. The control command that was provided to the EM was $u_{em} = u_{em,nmpc} + u_{em,PD}$. The PD controller was tunned in order to minimize the speed reference tracking error. According to seakeeping theory, irregular wave disturbance has zero mean value. As such, the PD controller regulates the EM and the mean value of u_{em} is $u_{em,nmpc}$ at steady state conditions. $u_{em,PD}$ is saturated to $\pm 10\% u_{em,max}$ so that u_{em} does not exceed the physical limits of the EM.

7.2 Benchmark Controller Design

Predictive control is considered as a (sub-)optimal control method, that is appropriate for online implementation of optimal control. It is very popular, as its concept combines optimization and online adaptation to alterations of its environment. When designing and tuning MPC, the aim is to achieve a performance similar to the optimal result, that would be achieved if all the input, disturbance, and system response information were available *a priori*.

However, it is common that an optimal controller is used as a benchmark problem, to evaluate and improve, off-line, the performance of MPC designs. As such, using [117], an off-line optimal controller was designed, which is solved using Dynamic Programming (DP). In the DP case, the operation profile is a-priori known and the power-split has to be decided to minimize the term $(1-A)m_f + A\lambda_N m_N$ over the known speed and load profile.

To reduce problem complexity and calculation time (solution time increases quadratically to the number of system states), only battery dynamics were taken into account. In DP problem formulation, only the quasi-static characteristics of the powertrain were considered, neglecting the transient performance of the power sources that was not weighted or constrained. This is commonly considered in automotive and energy applications. As such, the benchmark problem is mathematically formulated as follows

$$
\begin{aligned}
&\min_{u_{ice},u_{em}} \ (1-A)m_f + A\lambda_N m_N \\
s.t.\ &\text{Equations (3.5)-(3.15)} \\
&N_{eng,ref,i} - N_{eng,i} = 0 \\
&Q_{load,nmpc,i} - Q_{ice,i} - Q_{em,i} = 0 \\
&SOC_{min,hard} \leq SOC \leq SOC_{max,hard} \\
&u_{em,min} \leq u_{em} \leq u_{em,max} \\
&0 \leq u_{ice} \leq u_{ice,max}(N_{eng}) \\
&U_{oc}^2 - 4P_b R_i \geq 0 \\
&SOC_{i=0} = SOC_{i=N_f}
\end{aligned}
\tag{7.9}
$$

where $u_{ice,max}(N_{eng})$ is the maximum ICE torque curve and the last equation refers to battery overloading. By solving the above optimization problem, the optimal control inputs $\mathbf{u}^\star = [u_{ice}^\star, u_{em}^\star]^T$ over the provided operational profile $[N_{eng,nmpc,i}, Q_{load,nmpc,i}]^T,\ i = 1...N_f$ are calculated. In order to create a truly comparable result against the same conditions, the operational profile consists of the speed $N_{eng,ref}$ and disturbance $Q_{eng,nmpc}$ that the system produced in simulation under closed-loop control. The discretization interval in DP problem formulation was same as the NMPC sample time.

7.3 Controller Implementation

The control architecture and implementation are presented in Fig. 7-1. As it can be seen, the controller scheme (NMPC, observer, and NN predictor), the propulsion plant, wave disturbance as well as the dynamic battery emulation models were integrated into the prototype controller board of the experimental facility. The essential information flow between the software and hardware subsystems is also depicted in Fig. 7-1.

The NMPC, based on the information provided by measurements, the propeller observer as well as the reference received by the operator and the NN predictor, calculates the optimal control commands (rate of ICE and EM commands), which are integrated and provided to the power sources. The NMPC internal model parameters are summarized in Table B.1. The controller tuning was performed in simulation, based on cycle 20 from Fig. 5-5 as reference input and without application of wave disturbance. Cycle 20 was selected as it has the most transient operating profile and covers almost the whole shaft rotational speed range. In simulation and experiment the same control system's tuning parameters were used. The numerical values of the tuning parameters, as well as the constraints of the NMPC problem, are presented in Table 7.2.

The battery SOC calculation is based on the electric power flow measurement, received by the power electronics (inverter system) of the EM. A 27.84 kWh battery pack was considered for the present scenario, in order to avoid long-term electric operation. The numerical parameters of the quasi-static and dynamic battery models are presented in Table 7.1. As it was explained in subsection 3.2.4, different battery models for SOC simulation and controller design was intentional, in order to evaluate the NMPC behavior with modeling inaccuracies and the fact that actual or experimental battery performance deviates from the modeled parameters. The difference between the simulation model and the model used for NMPC design is depicted in Fig. 3-9a and Fig. 3-9b.

The propulsion plant and environmental disturbance emulation model, developed in Section 4.1, which parameters are summarized in Table B.2, was utilized for the propeller load calculation that is applied to the experimental testbed by the electric brake. It interacts dynamically with the physical system and the controller behavior. On the other hand, propeller observer and NN predictor are based on the information that would be available onboard a vessel, which is the operator's input, the controller commands, and the engine speed measurement, provided by the ICE ECU., the propulsion plant, and environmental disturbance emulation model, developed in Section 4.1 and its parameters summarized in Table B.2, was utilized for the propeller load calculation that is applied to the experimental testbed by the electric brake. It interacts dynamically with the physical system and the controller behavior. On the other hand, propeller observer and NN predictor are based on the information that would be available onboard a vessel, which is the operator's input, the controller commands, and the engine speed

Table 7.1: Sizing of control oriented and simulation models.

Description	Parameter	Value
Battery Dynamic Model Parameters		
Open Source Voltage	V_{OC}	696 V
Ohmic Resistance	R_O	0.0301 Ω
Polarization Resistance	R_P	0.0339 Ω
Open Source Capacitance	$C_{V_{OC}}$	140800 F
Polarization Capacitance	C_p	7680 F
Battery Internal Model Parameters		
Open Source Voltage Coeff.	k_1	696 V
Open Source Voltage Coeff.	k_2	1.022 $Volts/\%SOC$
Internal Resistance	R_i	0.0640 Ω
Nominal Capacity	Q_{nom}	40 Ah / 27.84 kWh
Shafting and Propeller		
Gear Ratio	i_{gb}	4 : 1
Propeller type (for C_Q, C_T)		Wageningen C 4-40
Pitch to diameter ratio	$\frac{P}{D}$	1.2
Propeller Diameter	D	1.05 m
Shaftline and propeller inertia	J_{shaft}	16.52 kgm^2
Environment		
Sea state condition (for experimental testing)		3

measurement, provided by the ICE ECU.

7.4 Simulation Analysis

The control system tuning and off-line performance evaluation were performed in Simulation, using the created cycle 20, from Fig. 5-5, without application of wave disturbance. Parameter λ_{ecems} of the controller was tuned to achieve the same initial and final Battery SOC. The numerical values of model and tuning parameters, as well as the constraints of the NMPC problem, are presented in Table 7.1 and Table 7.2 accordingly. The cumulative results of fuel consumption and NOx emissions by varying fuel to NOx weighting parameter A were derived. In this way, the trade-off performance between fuel and emissions efficiency was investigated.

In Fig. 7-2 and Fig. 7-3, the simulation power-split results for $A = 0.7$ are presented. In the same plots, also the solution of the dynamic programming (DP) optimization algorithm are shown. In Fig. 7-2 it can be seen that NMPC follows a smoother power path with fewer power fluctuations, as compared to the DP solution. Moreover, NMPC is able to adapt to different situations that will face online, such as application of external disturbance or an alternative loading profile, while DP result is produced over a certain, "prerecorded" loading cycle. Despite

Table 7.2: Control scheme parameters.

Parameter	Symbol	Value
Sample time	T_s	0.5 s
Prediction horizon	N	20 steps
Cost matrix	W_i	$diag(1\ 5\ 0.5\ 10^2)$
Terminal cost matrix	W_i	$diag(2\ 0.1)$
Equivalent cons. cost	λ_N	0.067
	λ_{ecems}	1.56
Prop. gain (cont. time)	P	0.3
Deriv. gain (cont. time)	D	-0.02
Constraints		
Soft SOC	SOC_{soft}	[25 75] %
Hard SOC	SOC_{hard}	[20 80] %
Soft N_{eng}	$N_{eng,soft}$	[700 2000] rpm
EM cmd	u_{em}	[-95 95] %
EM cmd rate	$\dot{u}_{em}$	[-50 50] %/s
ICE cmd rate	$\dot{u}_{ice}$	[-20 10] %/s
Prop. observer		
State noise covar. matrix	$Q[k]$	$7\ 10^{-4}$
Input noise covar. matrix	$R[k]$	5

the fact that NMPC and DP do not produce exactly the same solution, the ICE operational areas of attraction, where the cost function can be minimized are common in both cases, especially in the time interval between $t = 150\ s$ and $350\ s$. Also, NMPC follows a different transient loading path between time $t = 70\ s$ and $150\ s$. While in DP solution the EM torque steps from motoring to generating values forcing ICE to a big loading step, with NMPC the EM torque is regulated to assist ICE acceleration before converging at the same negative value as DP at $t = 150s$. In addition, in Fig. 7-3, first subplot, it can be noted that NMPC and DP utilize the same range of battery capacity during the loading cycle.

In Fig. 7-4, the simulation results in terms of fuel consumption and NOx emissions for A values in the range of 0 (fuel optimal) to 1 (NOx optimal) are presented. It is noted that the trade-off follows an exponential trend, where the results for $A > 0.6$ converge to similar powerplant overall performance characteristics. Also, it is noted that up to 2% fuel reduction with the fuel optimal strategy is achieved, while the NOx emissions reduction that can be achieved in this specific profile is up to 6.5% as compared to the conventional, non-hybrid plant operation and 8.5% as compared to the fuel optimal strategy. As it can be observed from Fig. 7-4, the EMS achieves the same NOx emissions reduction and better performance in fuel consumption as compared to DP results. Although that DP is considered to produce the global optimal, NMPC seems to perform better in Fig. 7-4. This occurs as the DP problem a) does not consider the inertial loads in acceleration and deceleration and b) DP and NMPC performance evaluation was performed against different battery models, the quasi-static and the dynamic

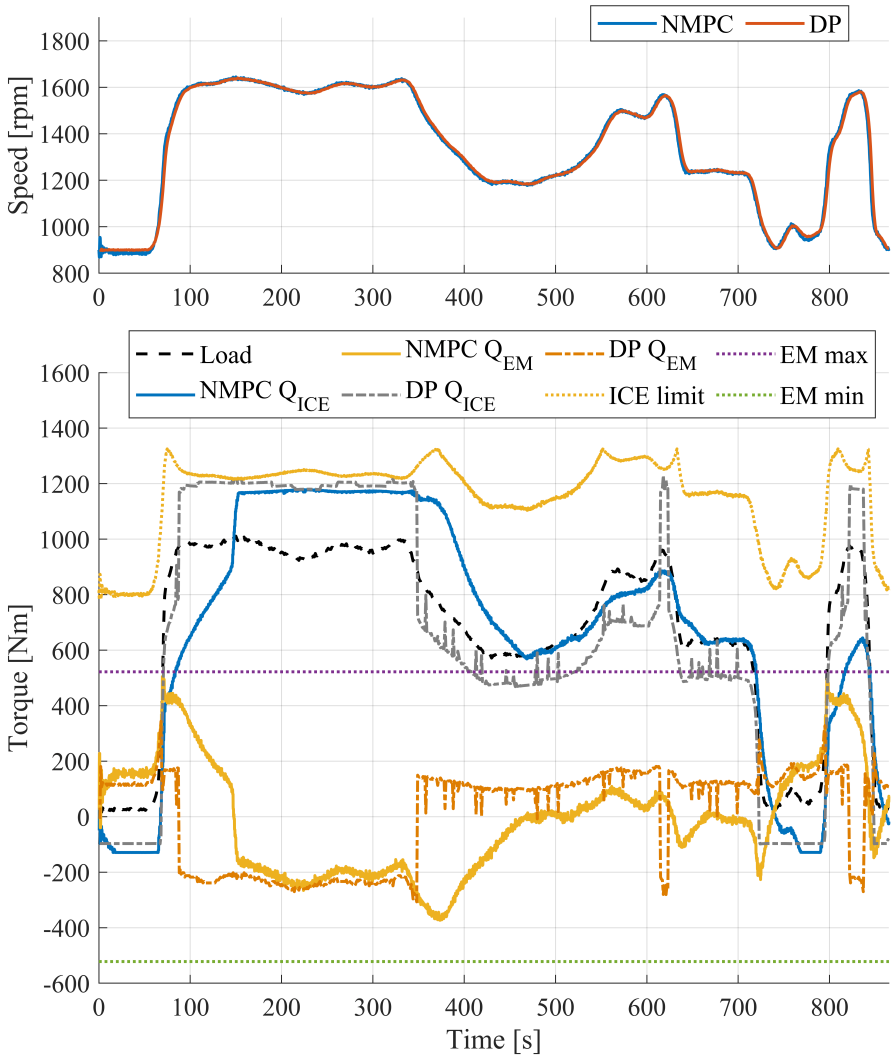

Figure 7-2: NMPC (A=0.7) simulation results in comparison to DP solution. Loading Profile and power-split control are presented.

respectively and c) any positive speer tracking error would result in decreased magnitude of the load disturbance, leading to slightly lower consumption.

It is noted that these results refer to the propeller load power-split, without consideration of any additional electric load consumption, e.g from the ship's grid. Also, the system under investigation does not accommodate any decoupling mechanism between ICE and the gearbox. As such, when EM satisfies the propulsion load, ICE is idling at zero output brake torque, or excess battery energy is consumed to overcome ICE rotating friction, e.g between time $t = 0$ and $t = 70\ s$, leading to higher fuel consumption.

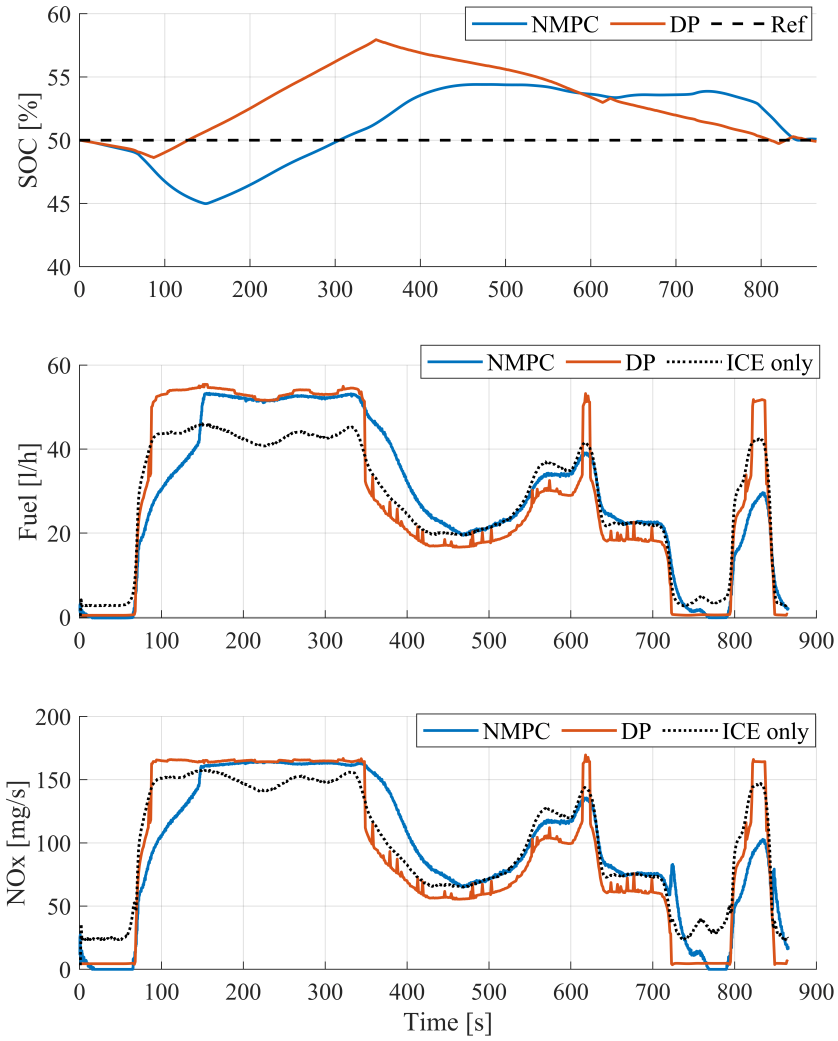

Figure 7-3: NMPC (A=0.7) simulation results in comparison to DP solution. Battery and engine performance over time are shown.

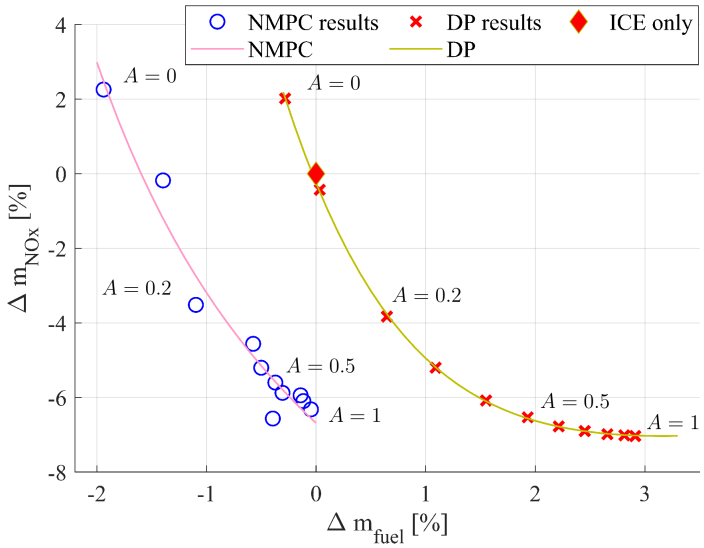

Figure 7-4: NMPC simulation results in comparison to DP solution. Trade-off performance between fuel consumption and NOx emissions for different values of fuel to NOx weighting A.

7.5 Experimental Testing

For the evaluation of the transient power-split controller, various experiments were performed on the hybrid propulsion powertrain HIPPO-2 experimental facility at the Laboratory of Marine Engineering (LME/NTUA) (seen in Fig. 2-1). During experimental testing, the EMS was tested in real-time operation to evaluate its performance in realistic loading conditions applied using the marine load emulation model. For the experiment set-up, the same loading profile with simulation was used so that comparable results are produced. Between experiments, parameter A was varied in order to test different fuel to emissions weighting strategies. The A values that were tested are shown in Table 7.3, which summarizes the experimental results as well. Also, an experiment was carried out without EM operation, where the engine speed and load were controlled by the engine ECU which has the manufacturer calibration. For the considered scenario, where the aim was to have a charge sustaining strategy at the end of the load cycle, fuel consumption and NOx emissions reduction up to 6 and 8%, respectively, were achieved during experimental testing.

In addition, in experiments, the load that was applied by the dynamometer contained environmental disturbance characteristics, in order to emulate realistic conditions and evaluate how the control scheme would mitigate severe load fluctuations and engine speed disturbance. The environmental model emulates irregular wave disturbance which affects the instant and the mean propeller torque load.

The results from experiments with $A = 0$ (fuel optimal) and $A = 0.5$ (Experimental NOx optimal) are presented and compared in this Thesis. In Fig 7-5, the engine speed loading profile, the power-split decisions as well as the battery SOC for the two experiments are presented and in Fig. 7-6 the respective diesel engine performance is shown. As it can be noted in the first subplot of Fig 7-5, the two NMPCs performed different power-split decisions. In the beginning, at low speed, the fuel optimal strategy $NMPC$ $(A = 0)$ operated the EM in generating mode, while $NMPC$ $(A = 0.5)$ operated the plant in full electric mode. At high speed and load (time interval between $t = 150$ s and 350 s) $NMPC$ $(A = 0)$ regulated the ICE torque in a fuel-

Table 7.3: Experimental results analysis for different fuel to NOx weighting factors.

Experiment	Weight A (Fuel to NOx)	Description of result	Cumulative fuel [l]	Cumulative NOx [g]	SOC Difference (%)
1.	$A = 0$	Fuel optimal	6.71	94.7	2.82
2.	$A = 0.2$	Disturbance 1	6.31	95.4	-3.44
3.	$A = 0.2$	Disturbance 2	6.23	92.7	-5.42
4.	$A = 0.5$	Exp. NOx optimal	6.83	91.8	3.41
5.	$A = 0.8$	Sim. NOx optimal	6.85	94.1	3.41
6.	ICE only	Non-hybrid setup	6.62	100.4	-

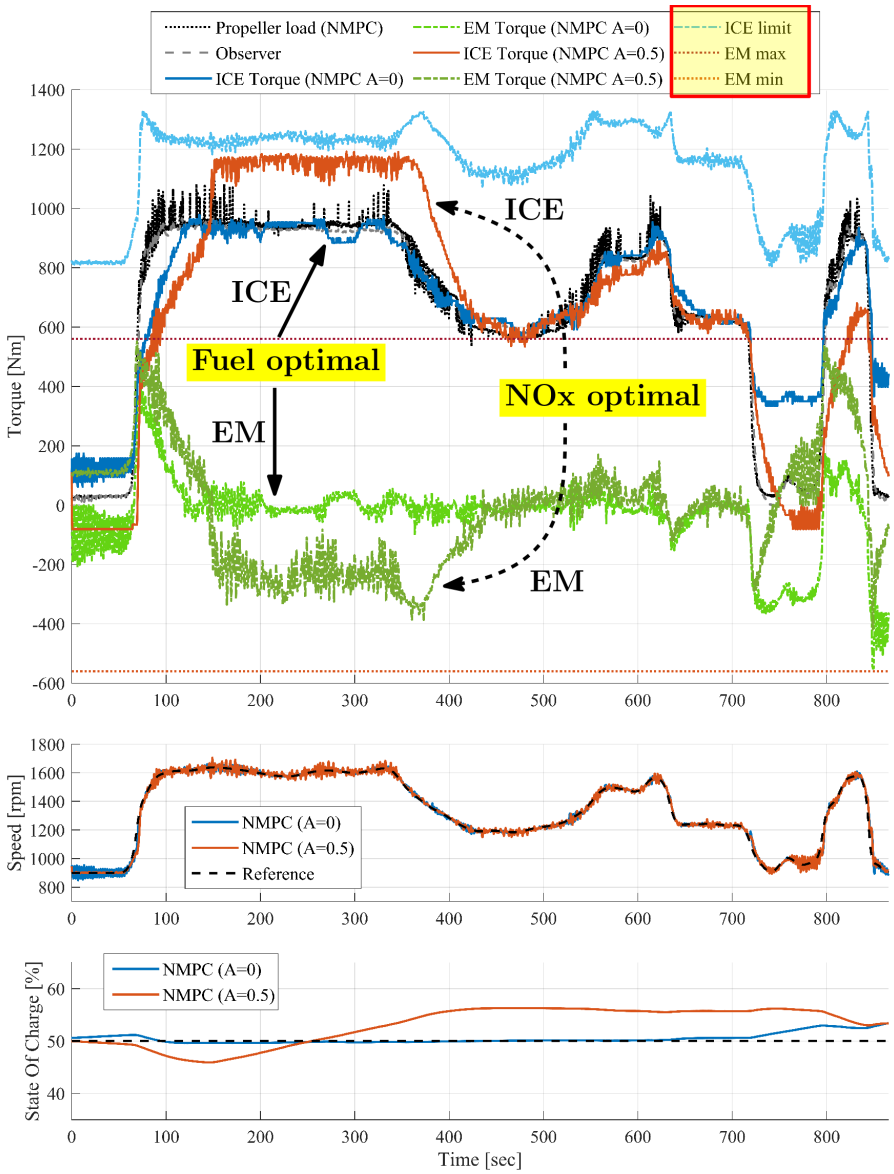

Figure 7-5: Loading, power split, shaft speed and battery state of charge during experiments for two different fuel to NOx weighting factors.

efficient point, while $NMPC$ $(A = 0.5)$ chose an ICE operating point which is NOx efficient in order to charge the battery. Moreover, in Fig. 7-5, first subplot it can be seen that both NMPCs perform the power-split with respect to the powerplant limits as well as that they make use of the EM to reject speed disturbances, to mitigate ICE power fluctuations caused by wave disturbance.

The diesel engine performance is presented in Fig. 7-6. The measured fuel consumption and NOx emissions depend on the diesel engine operational point. NOx, in addition, depends also on the operation of the EGR system, which is shown in the bottom subplot. For $NMPC$ $(A = 0.5)$ some NOx production oscillations are observed during experimental testing. These are produced from the EGR valve oscillating behavior which is self-regulated from the engine ECU. Although this behavior affected NOx emissions, it did not change $NMPC$ $(A = 0.5)$ behavior. As it

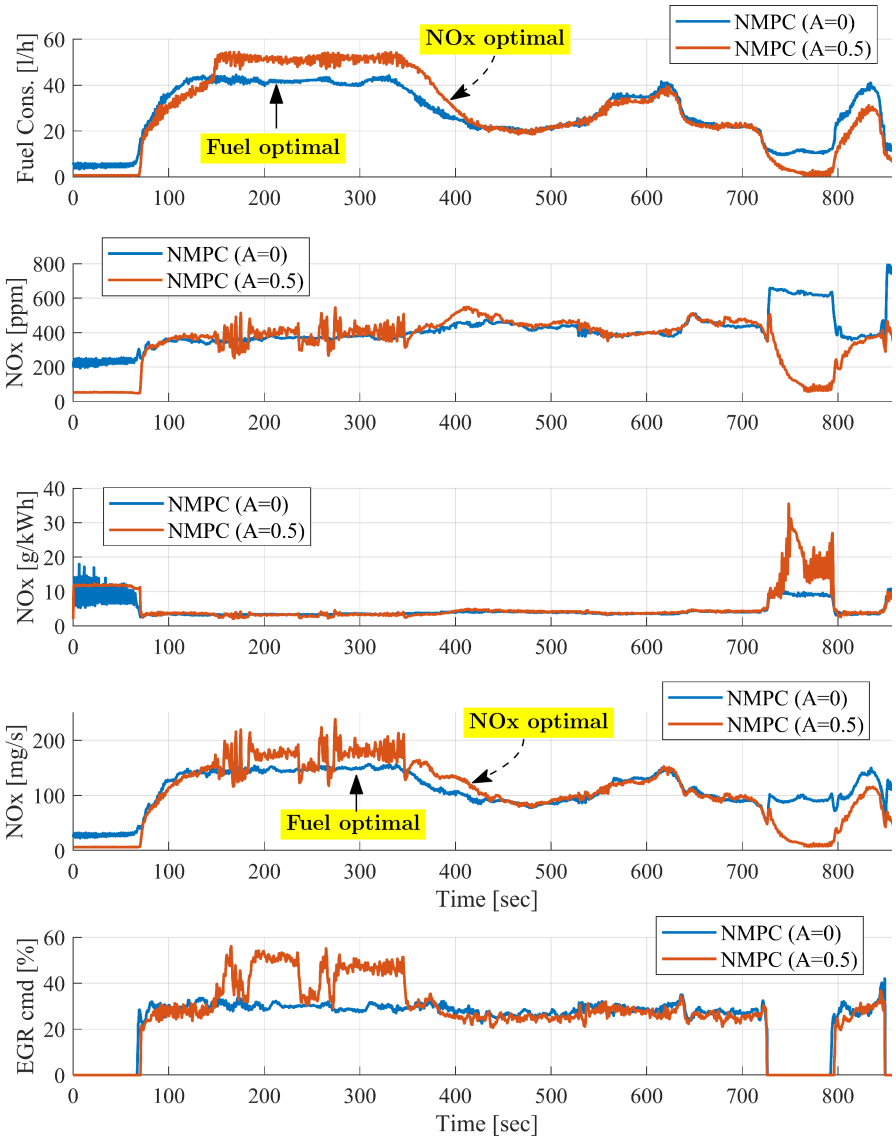

Figure 7-6: Diesel engine performance in experimental testing for two different fuel to NOx weighting factors.

can be noted from Table 7.3, $NMPC$ $(A = 0)$ was more fuel-efficient while $NMPC$ $(A = 0.5)$ resulted in lower cumulative NOx production. In both experiments, the final SOC was greater than the initial, although the same NMPC tunning was used in simulations and experiments.

In Fig. 7-7, two phase plots of engine speed and load are presented, where the control commands of the NMPCs to the diesel engine are shown with respect to the engine fuel efficiency and NOx emissions performance. Diesel engine loading path within the engine specific fuel consumption and engine specific NOx emissions production maps are shown in Fig. 7-7a and Fig. 7-7b accordingly. As it can be observed, the density of $NMPC$ $(A = 0)$ control commands is greater in operating points with lower specific fuel consumption (fuel-efficient) as compared with $NMPC$ $(A = 0.5)$. On the contrary, $NMPC$ $(A = 0.5)$ operated the diesel engine either

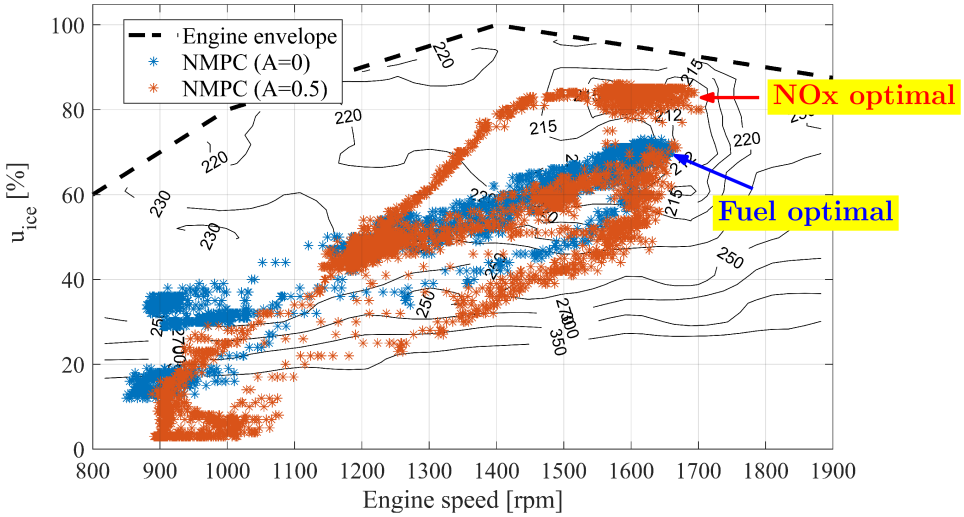

(a) Diesel engine loading path within brake specific fuel consumption map [g/kWh].

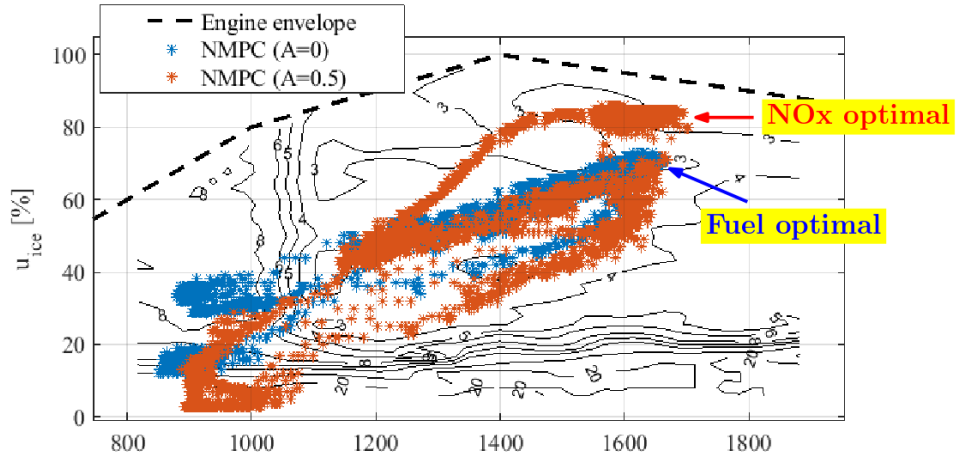

(b) Diesel engine loading path within brake specific NOx map [g/kWh].

Figure 7-7: NMPC commands within diesel engine envelope for A=0 and A=0.5 NOx to fuel weighting.

in zero torque or in operating points where NOx emissions are minimized, such as the local NOx minimum in high speed and torque (1700 rpm, 80%).

Finally, as far as the behavior of the control scheme is concerned, Fig. 7-8 shows the propeller observer performance and the speed reference predictions within the prediction horizon. Both subsystems have the desirable steady-state and transient performance. In the first subplot, only a few predictions are shown, covering at each time interval k the whole range of the prediction time window $k+i|k,\ i=1:N$. The predictions have satisfying accuracy although the experimental speed profile was not used in the training and validation process of the prediction model. The disturbance estimation of the propeller observer and the load calculation are accurate and follow the actual values, as it can be noted in the second and third subplot of Fig. 7-8.

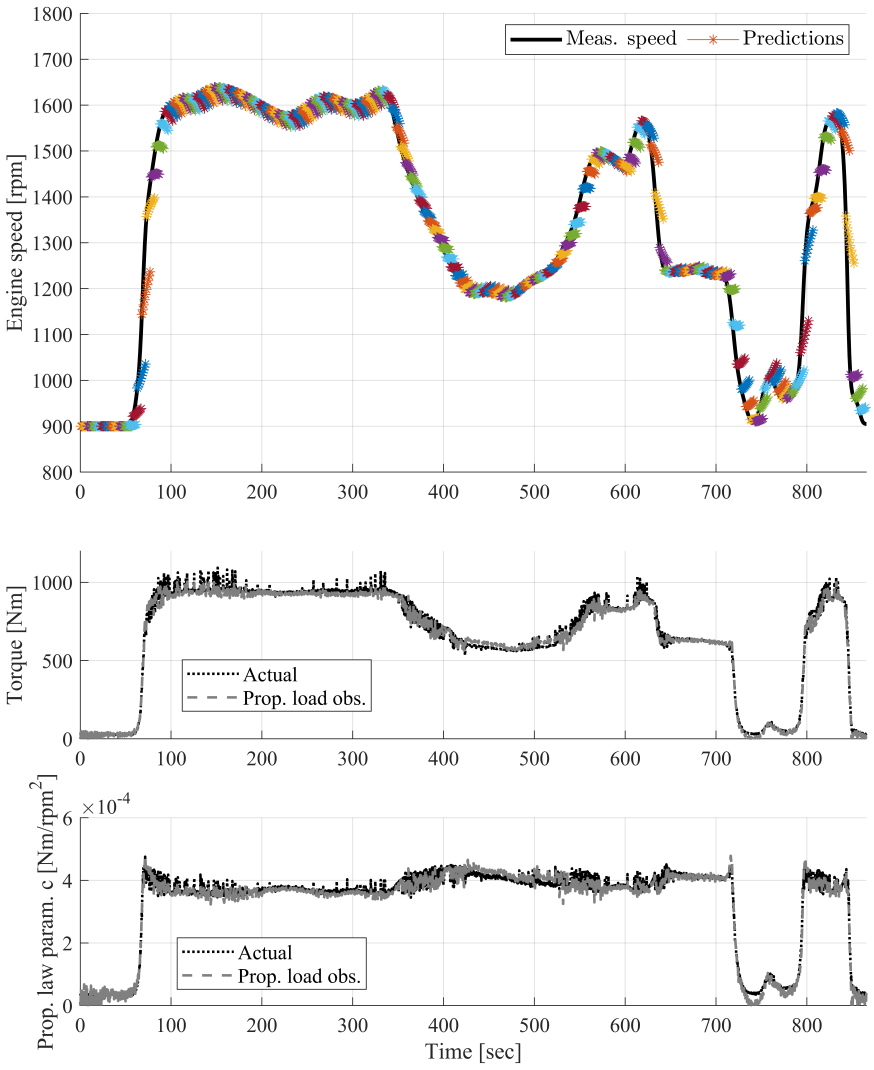

Figure 7-8: NN predictions and observer performance in experiment.

7.6 Discussion

With respect to the control system design that was proposed and evaluated in this chapter, some remarks can be summarized. Firstly, the energy management problem was formulated with respect to the design constraints of a real application. This means that the estimation - prediction - optimization scheme should utilize only the measurements and information that would be available onboard. Also, the NMPC tuning, λ_{ecems} was determined easily in simulation for the presented loading profile in order to have a charge sustaining strategy and evaluate controller effect on fuel consumption and NOx emissions. Further work would consider an optimization-based calculation of λ_{ecems} as well as its online adaptation, in order to be more effective in the real world.

Furthermore, the problem formulation in dynamic programming considers the quasi-static problem and was formulated as the benchmark DP formulations in the literature. Only SOC was considered as state, while the operating profile $N_{eng,ref}$ and the resulting disturbance profile

Q_{load} were given as constraints. Although theoretically, DP solution should be the optimal and NMPC a sub-optimal approximation of it, in the present study NMPC outperformed DP in fuel consumption reduction. This result occurs as the DP problem a) does not consider the inertial loads in acceleration and deceleration, b) DP and NMPC performance evaluation was performed against different battery models, the quasi-static and dynamic respectively, c) any positive tracking error in NMPC would reduce the resulting Q_{load} amplitude and lead to less power generation (and resulting fuel consumption).

Finally, from the simulation and the experimental results it is shown that for the given set-up, the fuel consumption reduction capabilities are limited, as compared to the NOx reduction merits. This can be explained by the fact that a) in the usual vessel cruising conditions, the engine is operated near the maximum fuel efficiency operating point, b) there is not any decoupling mechanism between the engine and the propeller shaft. As such, an engine on/off functionality in order to avoid idling consumption and would lead to greater fuel reductions (about 10%) cannot be considered. Finally, c) in marine applications, there is no "braking" action, where the ship kinetic energy could be recovered and stored in the battery. As such, the whole energy demand over any operation profile should be covered by the internal combustion engine.

7.7 Conclusion

In this chapter, an integrated and real-time capable Energy Management and Emissions Minimization System (EMEMS) was developed. It addresses the optimal power-split control problem and handles the multi-variable control objectives regarding the performance specifications of the powertrain and minimization of fuel consumption and emissions that are produced by the internal combustion engine. The optimal control problem was restructured to perform an energy management planning according to a weighting factor that determines the trade-off between fuel consumption and NOx emissions minimization.

To aid the optimization problem, estimation of the propulsion plant characteristics as well as a prediction for future input by the operator were provided to the NMPC, in order to perform the optimal energy management planning. Despite the fact that the proposed control scheme contains numerous sub-systems that have to cooperate, the optimal problem formulation was simply and plainly defined. Fuel consumption, NOx emissions as well as battery energy utilization and restoration were expressed with the common variable of equivalent consumption.

The control scheme was tuned to perform similarly to the benchmark optimal control problem utilizing an operational profile that was created by ship operational data. In this framework, the trade-off performance between fuel consumption and NOx emissions was investigated. Experimental results proved the robustness of the control scheme regarding the disturbance input

as well as its capability to perform efficiently the power-split, leading to fuel consumption and NOx emissions minimization over the considered profile.

This chapter responded to research question 5.

Chapter 8

Conclusions and Future Work

Marine propulsion plants are complex MIMO systems, as the installed power-sources diversify in terms of the underlying technology, principles of operation, size, and physical limitations. On the other hand, system performance specifications strive for competitive objective satisfaction, such as immediate power availability at the propeller shaft, maximized engine energy efficiency, and minimized emissions.

The objective of this Thesis was to develop a real-time Energy Management and Emissions Minimization System (EMEMS) with optimal transient and steady-state performance in regards to energy consumption and emissions as well as robust behavior against external disturbances. HIPPO-2 experimental facility at LME/NTUA was used for the implementation and evaluation of the developed power-split control schemes. As such, the modeling methodology and the control system were adapted to the specific configuration and the particular specifications of the experimental system. First principle and data-based models were fitted to powertrain measurement data. Fitting results showed that the derived models approximated accurately the system behavior during transient loading, as well as the patterns that were observed within the data and were simple enough in order to reduce the online computational cost.

In order to evaluate the interaction of the system *controller - powertrain - propulsion plant - environment*, a parametric propulsion plant model that matches the experimental facility was employed, to apply propeller loading considering several vessel operating scenarios and conditions. In addition, a propeller observer is designed and implemented in order to quantify the propeller load characteristics, as acting disturbance, which is required for the optimal power-split calculation, without knowledge of the uncertain propulsion plant parameters. The approach was based on the propeller law principle (power is proportional to the cubic power of shaft speed). Through a number of simulations with slow and fast accelerations and irregular wave disturbance, it was shown that the modeling adequately corresponds to the actual sizing and operating conditions of a small tug vessel and the observers can perform efficiently, giving accurate estimates, in both steady-state and transient loading conditions.

For the design and evaluation of the EMEMS, identification and prediction of the operator's reference input during ship maneuvering was performed. These objectives were achieved, following a data-based identification methodology and using machine learning techniques. Profiles that contain rich information about the transient operation were identified and utilized for control system development. Regarding the prediction model for the future operator's reference, a neural network model was designed, which showed adequate performance over unknown operational conditions. The online information generated by the prediction model is used along with the propeller observer by the controller, so as to calculate future propeller load disturbance.

The application of Model Predictive Control (MPC) is attractive for problems related to optimal power-split and energy management of hybrid power plants. In this Thesis, non-linear, MPC (NMPC) based, load-split control schemes were designed, implemented, and experimentally evaluated. At first, an NMPC-based control scheme was proposed to deal with the load-split between the power sources during transient loading conditions, ensuring the dynamic torque delivery with respect to the powertrain physical and operating limits. The energy management was performed indirectly, i.e fuel consumption and NOx emissions models were not incorporated in the controller design. In this design, the electric motor dealt with the powertrain fast dynamics to deliver the required torque load at the propeller shaft; the quasi-static loading of the internal combustion engine that was achieved, led to damping of ICE fast acceleration, as well as mitigation of ICE load oscillations that produce overshoots in NOx emissions and fueling.

In the second control scheme, the optimal control problem was reformulated and extended to develop an energy management and emissions minimization strategy, which is calculated based on the internal model for system performance, as well as the information received online. The energy management planning is performed according to a weighting factor that determines the trade-off between fuel consumption and NOx emissions minimization. Despite the fact that the proposed control scheme contains numerous sub-systems that have to co-operate, the optimal energy management problem formulation was simply and plainly defined. Fuel consumption, NOx emissions, and battery energy utilization, and restoration were expressed with the common variable of equivalent consumption. The control scheme was tuned to perform similarly to the benchmark optimization problem and the trade-off performance between fuel consumption and NOx emissions was investigated in simulation.

The developed control schemes were experimentally tested in real-time operation, where the controllers coped with environmental disturbance rejection, followed the desired rotational speed reference, and operated the plant within the desirable constraints. The control strategies proved their robustness to disturbance load characteristics, achieving offset-free reference tracking independently of the propulsion plant size, the uncertainty of the propeller and ship characteristics, as well as the modeling errors between the powertrain components and the internal model. In parallel, with the EMEMS design, the power-split control was performed with respect to

the energy management and emission minimization targets, and the target to achieve a charge sustaining strategy at the end of the load cycle. The capabilities of the control system were exploited for the considered scenario, where fuel consumption and NOx emissions reduction up to 6.5 and 8%, respectively, were achieved.

In conclusion, the power-split strategies that were proposed in this Thesis align with the state-of-the-art trends and methodologies that are followed in the marine and automotive industry. To exploit the system capabilities for optimal performance, optimal control and novel data-based methodologies for the energy management system design were employed. Moreover, even though the proposed design is based on sophisticated methodologies, it is integrated, real-time capable, and easy to interface with existing vessel powertrain setups. As such, there is potential to be implemented in full-scale propulsion plants.

Suggestions for Future Work

- In this Thesis, a deterministic approach was followed regarding a) the future operational profile prediction, b) the disturbance load characteristics c) the control system tuning. It would be interesting if the optimal control problem was realized following a stochastic approach and system learning methodologies were followed to learn and adapt online for the optimal power-split decisions during ship operation.

- For proof of concept, only one operating profile (cycle) was used to perform the fine-tuning and the evaluation of the energy management and emissions minimization strategy. This cycle was chosen as it contains the richest information about transient ship operation and greater excitation amplitude, as compared to other profiles. It is suggested as a future work extension, that the optimal equivalent consumption parameter tuning for each profile is defined through optimization. Further to this, it is suggested that during ship operation, classification to a specific cycle can be performed in order to apply the appropriate tuning parameters.

- In this Thesis, a centralized control system was designed, aligned with the specific experimental set-up and sizing. The EMS design has the potential for practical application onboard ships. However, during vessel life span and among the several vessel designs, system complexity and size may vary (i.e. integration of photo-voltaic panels and fuel cells). In this case, each power-source needs to be controlled by a local optimal control module in respect to the optimal operation of the whole system. Here, in order to achieve a more robust control system design, it would could be proposed to follow modular and decentralized control approaches after powertrain modifications in design during lifetime.

THIS PAGE INTENTIONALLY LEFT BLANK

Appendix A

Dynamic model for battery emulation

The experimental facility does not accommodate any battery set yet, and therefore a virtual battery emulation model was employed. The ECM of the dynamic battery model is a linear lumped parameter battery model presented in Figure 3-9b. The model is based on a set of parameters, which can be estimated by conducting several test to the cell, involving, mainly, load pulses in several operating conditions, which are described in the PNGV testing procedure.

The equations which describe the model derives from the Kirchhoff voltage law

$$V_L = V_{OC} - \frac{1}{C_{V_{OC}}} \int I_b dt - R_O I_b - R_P I_P \tag{A.1}$$

where V_{OC} is the open circuit battery voltage, R_O is the internal ohmic resistance, R_P is the internal polarization resistance (e.g., due to concentration gradients), C_d is the shunt capacitance around R_P, $\tau = R_P C_d$ is the polarization time constant, I_b is the battery load current, the current through polarization resistance,is the battery terminal voltage, $1/OCV'$ is a capacitance that accounts for the variation in open circuit voltage with the time integral of the load current I_b. OCV is not usually equal to the slope of V_L measured open circuit vs. battery state of charge. The polar current, can be derived by solving the following deferential expression, with a specified initial conditions $I_P = 0$ at $t = 0$

$$\frac{dI_P}{dt} = \frac{I_b - I_P}{\tau} \tag{A.2}$$

where $I_b = \frac{P_b}{V_L}$. The battery SOC can be calculated using Eq. (3.10) and Eq. (3.11).

The above parameters are considered to be constant for a given SoC, temperature, etc. In this evidence, in literature [79], it is proposed for each voltage calculation step, the parameters of the model should be recalculated according to the most recent measurements of SoC and temperature. In this Thesis, due to lack of data and for simplification, this is disregarded.

THIS PAGE INTENTIONALLY LEFT BLANK

Appendix B

Model Parameters

Table B.1: Parameters of the control-oriented powertrain models.

Description	Parameter	Value
Moment of inertia	J_{system}	12.047 kgm^2
ICE torque coef.	θ_Q	$[15.96\ 238.75\ 0.2343\ 0.1247]^T$
ICE fuel cons. coef.	θ_f	[23.18 14.3 4.678 2.668... ... 0.622 $-0.09324]^T$
Fuel density	ρ_f	825 kgm^{-3}
ICE NOx em. coef.	$a_{N,i}$	[0.79 0.5 0.051 1.1 0.4 0.01]
	$b_{N,1}$	2.9 10^{-3}
	$b_{N,2}$	8 10^{-5}
ICE torque norm. coef.	$u_{ice,m}$	45.61
	$u_{ice,std}$	25.98
ICE torque norm. coef.	$N_{eng,m}$	1382
	$N_{eng,std}$	320.6
EM torque coef.	c_{em}	5.8
EM Power Parameter	e	0.9598
	P_0	385.18

Table B.2: Parameters of the propulsion plant emulation model.

Description	Parameter	Value and Unit
Length overall	L	13.8 m
Beam overall	B	5.28 m
Draught aft	T	1.8 m
Depth at sides	$Depth$	2.30 m
Vessel displacement	M_{disp}	58 t
Added hydrodynamic mass	M_{hyd}	5% M_{disp}
Propeller Diameter	D	1.05 m
Number of propellers	N_p	2
Mean propeller Depth	h_{prop}	1.4
Gear Ratio	i_{gb}	3.8 : 1
Gearbox losses	a_{gb}	0.5
Gearbox losses	b_{gb}	0.4
Gearbox losses	c_{gb}	0.1
Shaftline and propeller inertia	J_{shaft}	16.52 kgm^2
Shaftline efficiency	a_{sl}	0.01
Shaftline efficiency	b_{sl}	0.01
Effective wake fraction	w	0.15
Thrust deduction factor	t	0.13
Relative rotating efficiency	η_r	1.02
Water density	ρ	1025 kgm^{-3}
Wave spectrum	$S(\omega)$	ITTC
Wave spectrum peak frequency	ω_p	0.8 rad/s
Significant wave height	H_s	1.2 m
Sea state condition		3

Bibliography

[1] N. Planakis, G. Papalambrou, and N. Kyrtatos, "Predictive power-split system of hybrid ship propulsion for energy management and emissions reduction," *Control Engineering Practice*, vol. 111, p. 104795, 2021.

[2] N. Planakis, G. Papalambrou, N. Kyrtatos, and P. Dimitrakopoulos, "Recurrent and time-delay neural networks as virtual sensors for nox emissions in marine diesel powertrains," *SAE Tecnical paper*, no. 2021-01-5042, 2021.

[3] N. Planakis, G. Papalambrou, and N. Kyrtatos, "Integrated Load-Split Scheme for Hybrid Ship Propulsion Considering Transient Propeller Load and Environmental Disturbance," *Journal of Dynamic Systems, Measurement, and Control*, vol. 143, 10 2020. 031004.

[4] N. Planakis, G. Papalambrou, and N. Kyrtatos, "A real-time power-split strategy for a hybrid marine power plant using mpc," in *Int. J. Modelling, Identification and Control*, vol. 34 (2), pp. 147–157, 2020.

[5] N. Planakis, V. Karystinos, G. Papalambrou, and N. Kyrtatos, "Transient energy management controller for hybrid diesel-electric marine propulsion plants using nonlinear mpc," in *21st IFAC World Congress, Berlin, Germany*, 2020.

[6] N. Planakis, V. Karystinos, G. Papalambrou, and N. Kyrtatos, "Nonlinear model predictive control for the transient load share management of a hybrid diesel-electric marine propulsion plant," in *2020 American Control Conference (ACC)*, pp. 1955–1960, 2020.

[7] N. Planakis, V. Karystinos, G. Papalambrou, and N. Kyrtatos, "A predictive energy management system for a hybrid diesel-electric marine propulsion plant," in *2020 European Control Conference (ECC)*, pp. 693–698, 2020.

[8] N. Planakis, G. Papalambrou, and N. Kyrtatos, "Power-split strategies for hybrid diesel-electric marine power plant using predictive control and transient load preview," in *29th CIMAC World Congress, Vancouver, Canada*, p. paper 042, 2019.

[9] N. Planakis, G. Papalambrou, and N. Kyrtatos, "Predictive control for a marine hybrid diesel-electric plant during transient operation," in *2018 5th International Conference on Control, Decision and Information Technologies (CoDIT)*, pp. 989–994, 2018.

[10] R. Geertsma, R. Negenborn, K. Visser, and J. Hopman, "Design and control of hybrid power and propulsion systems for smart ships: A review of developments," *Applied Energy*, vol. 194, pp. 30 – 54, 2017.

[11] M. Jaurola, A. Hedin, S. Tikkanen, and K. Huhtala, "Optimising design and power management in energy-efficient marine vessel power systems: a literature review," *Journal of Marine Engineering & Technology*, vol. 18, no. 2, pp. 92–101, 2019.

[12] M. Martelli, M. Viviani, M. Altosole, M. Figari, and S. Vignolo, "Numerical modelling of propulsion, control and ship motions in 6 degrees of freedom," *Proceedings of the Institution of Mechanical Engineers, Part M: Journal of Engineering for the Maritime Environment*, vol. 228, no. 4, pp. 373–397, 2014.

[13] R. Geertsma, R. Negenborn, K. Visser, M. Loonstijn, and J. Hopman, "Pitch control for ships with diesel mechanical and hybrid propulsion: Modelling, validation and performance quantification," *Applied Energy*, vol. 206, pp. 1609 – 1631, 2017.

[14] K. Yum, S. Skjong, B. Taskar, E. Pedersen, and S. Steen, "Simulation of a hybrid marine propulsion system in waves," in *2016 CIMAC Congress, Helsinki*, 06 2016.

[15] X. Gong, H. Wang, M. R. Amini, I. V. Kolmanovsky, and J. Sun, "Integrated optimization of power split, engine thermal management, and cabin heating for hybrid electric vehicles," in *2019 IEEE Conference on Control Technology and Applications (CCTA)*, pp. 567–572, 2019.

[16] J. van Schijndel, M. Donkers, F. Willems, and W. Heemels, "Dynamic programming for integrated emission management in diesel engines," *IFAC Proceedings Volumes*, vol. 47, no. 3, pp. 11860 – 11865, 2014. 19th IFAC World Congress.

[17] A. Chasse, P. Pognant-Gros, and A. Sciarretta, "Online implementation of an optimal supervisory control for a parallel hybrid powertrain," *SAE International Journal of Engines*, vol. 2, pp. 1630–1638, 10 2009.

[18] L. Guzzella and A. Sciarretta, *Vehicle Propulsion Systems: Introduction to Modeling and Optimization*. Springer, 2012.

[19] L. Serrao, S. Onori, and G. Rizzoni, "A Comparative Analysis of Energy Management Strategies for Hybrid Electric Vehicles," *Journal of Dynamic Systems, Measurement, and Control*, vol. 133, 03 2011. 031012.

[20] S. Di Cairano, W. Liang, I. V. Kolmanovsky, M. L. Kuang, and A. M. Phillips, "Power smoothing energy management and its application to a series hybrid powertrain," *IEEE Transactions on Control Systems Technology*, vol. 21, no. 6, pp. 2091–2103, 2013.

[21] A. Bemporad, D. Bernardini, R. Long, and J. Verdejo, "Model predictive control of turbocharged gasoline engines for mass production," in *SAE Technical Paper*, SAE International, 04 2018.

[22] K. Yu, M. Mukai, and T. Kawabe, "A battery management system using nonlinear model predictive control for a hybrid electric vehicle," *IFAC Proceedings Volumes*, vol. 46, no. 21, pp. 301 – 306, 2013. 7th IFAC Symposium on Advances in Automotive Control.

[23] S. D. Cairano, D. Bernardini, A. Bemporad, and I. V. Kolmanovsky, "Stochastic mpc with learning for driver-predictive vehicle control and its application to hev energy management," *IEEE Transactions on Control Systems Technology*, vol. 22, no. 3, pp. 1018–1031, 2014.

[24] T. Albin, D. Ritter, N. Liberda, R. Quirynen, and M. Diehl, "In-vehicle realization of nonlinear mpc for gasoline two-stage turbocharging airpath control," *IEEE Transactions on Control Systems Technology*, vol. 26, pp. 1606–1618, Sep. 2018.

[25] M. Huang, H. Nakada, K. Butts, and I. Kolmanovsky, "Nonlinear model predictive control of a diesel engine air path: A comparison of constraint handling and computational strategies," *IFAC-PapersOnLine*, vol. 48, no. 23, pp. 372 – 379, 2015. 5th IFAC Conference on Nonlinear Model Predictive Control NMPC 2015.

[26] M. Kang, M. Alamir, and T. Shen, "Nonlinear constrained torque control for gasoline engines," *IFAC-PapersOnLine*, vol. 49, no. 18, pp. 784 – 789, 2016. 10th IFAC Symposium on Nonlinear Control Systems NOLCOS 2016.

[27] P. Zeman, W. Kemmetmüller, and A. Kugi, "Nonlinear Model Predictive Control of Axial Piston Pumps," *Journal of Dynamic Systems, Measurement, and Control*, vol. 139, 05 2017. 081008.

[28] Y. Sakai, M. Kanai, and M. Yamakita, "Torque demand control by nonlinear mpc for speed control of vehicles with variable valve lift engine," *IFAC Proceedings Volumes*, vol. 43, no. 7, pp. 494 – 499, 2010. 6th IFAC Symposium on Advances in Automotive Control.

[29] M. Sivertsson and L. Eriksson, "Optimal Transient Control Trajectories in Diesel-Electric Systems-Part II: Generator and Energy Storage Effects," *Journal of Engineering for Gas Turbines and Power*, vol. 137, 09 2014.

[30] M. Bidarvatan and M. Shahbakhti, "Analysis and Control of Torque Split in Hybrid Electric Vehicles by Incorporating Powertrain Dynamics," *Journal of Dynamic Systems, Measurement, and Control*, vol. 140, 06 2018. 111009.

[31] Y. Huo and F. Yan, "A Predictive Energy Management Strategy for Hybrid Electric Powertrain With a Turbocharged Diesel Engine," *Journal of Dynamic Systems, Measurement, and Control*, vol. 140, 03 2018. 061017.

[32] T. Nueesch, M. Wang, P. Isenegger, C. H. Onder, R. Steiner, P. Macri-Lassus, and L. Guzzella, "Optimal energy management for a diesel hybrid electric vehicle considering transient pm and quasi-static nox emissions," *Control Engineering Practice*, vol. 29, pp. 266 – 276, 2014.

[33] O. Grondin, L. Thibault, and C. Quérel, "Energy management strategies for diesel hybrid electric vehicle," *Oil & Gas Science and Technology*, vol. 70, 01 2014.

[34] G. S. Sankar, R. C. Shekhar, C. Manzie, T. Sano, and H. Nakada, "Model predictive controller with average emissions constraints for diesel airpath," *Control Engineering Practice*, vol. 90, pp. 182 – 189, 2019.

[35] Y. L. Murphey, J. Park, L. Kiliaris, M. L. Kuang, M. A. Masrur, A. M. Phillips, and Q. Wang, "Intelligent hybrid vehicle power control-part ii: Online intelligent energy management," *IEEE Transactions on Vehicular Technology*, vol. 62, pp. 69–79, Jan 2013.

[36] R. Moriyasu, S. Nojiri, A. Matsunaga, T. Nakamura, and T. Jimbo, "Diesel engine air path control based on neural approximation of nonlinear mpc," *Control Engineering Practice*, vol. 91, p. 104114, 2019.

[37] T. D. Gaikwad, Z. D. Asher, K. Liu, M. Huang, and I. Kolmanovsky, "Vehicle velocity prediction and energy management strategy part 2: Integration of machine learning vehicle velocity prediction with optimal energy management to improve fuel economy," in *SAE Technical Paper*, SAE International, 04 2019.

[38] C. Xiang, F. Ding, W. Wang, and W. He, "Energy management of a dual-mode power-split hybrid electric vehicle based on velocity prediction and nonlinear model predictive control," *Applied Energy*, vol. 189, pp. 640 – 653, 2017.

[39] N. Bennabi, J. F. Charpentier, J. Y. Billard, H. Menana, and N. Nottellet, "Modeling and simulation of a series hybrid propulsion chain for small ships," in *2017 IEEE Vehicle Power and Propulsion Conference (VPPC)*, pp. 1–6, 2017.

[40] C. Bordin and O. Mo, "Including power management strategies and load profiles in the mathematical optimization of energy storage sizing for fuel consumption reduction in maritime vessels," *Journal of Energy Storage*, vol. 23, pp. 425 – 441, 2019.

[41] M. R. Miyazaki, A. J. Sørensen, and B. J. Vartdal, "Reduction of fuel consumption on hybrid marine power plants by strategic loading with energy storage devices," *IEEE Power and Energy Technology Systems Journal*, vol. 3, no. 4, pp. 207–217, 2016.

[42] L. Alfieri, F. Mottola, and M. Pagano, "An energy saving management strategy for battery-aided ship propulsion systems," in *2019 IEEE Milan PowerTech*, pp. 1–6, 2019.

[43] E. Ovrum and T. Bergh, "Modelling lithium-ion battery hybrid ship crane operation," *Applied Energy*, vol. 152, pp. 162 – 172, 2015.

[44] Liza Chua Wan Yuan, T. Tjahjowidodo, Gerald Seet Gim Lee, R. Chan, and A. K. Ådnanes, "Equivalent consumption minimization strategy for hybrid all-electric tugboats to optimize fuel savings," in *2016 American Control Conference (ACC)*, pp. 6803–6808, 2016.

[45] T. L. Vu, A. A. Ayu, J. S. Dhupia, L. Kennedy, and A. K. Adnanes, "Power management for electric tugboats through operating load estimation," *IEEE Transactions on Control Systems Technology*, vol. 23, no. 6, pp. 2375–2382, 2015.

[46] T. Q. Dinh, T. M. Bui, J. Marco, C. Watts, and J. I. Yoon, "Optimal energy management for hybrid electric dynamic positioning vessels," *IFAC-PapersOnLine*, vol. 51, no. 29, pp. 98 – 103, 2018. 11th IFAC Conference on Control Applications in Marine Systems, Robotics, and Vehicles CAMS 2018.

[47] M. Kalikatzarakis, R. Geertsma, E. Boonen, K. Visser, and R. Negenborn, "Ship energy management for hybrid propulsion and power supply with shore charging," *Control Engineering Practice*, vol. 76, pp. 133 – 154, 2018.

[48] G. Diju, X. Wang, T. Wang, Y. Wang, and X. Xu, "An energy optimization strategy for hybrid power ships under load uncertainty based on load power prediction and improved nsga-ii algorithm," *Energies*, vol. 11, p. 1699, 07 2018.

[49] A. R. Dahl, L. Thorat, and R. Skjetne, "Model predictive control of marine vessel power system by use of structure preserving model," *IFAC-PapersOnLine*, vol. 51, no. 29, pp. 335 – 340, 2018. 11th IFAC Conference on Control Applications in Marine Systems, Robotics, and Vehicles CAMS 2018.

[50] T. I. Bo, E. Vaktskjold, E. Pedersen, and O. Mo, "Model predictive control of marine power plants with gas engines and battery," *IEEE Access*, vol. 7, pp. 15706–15721, 2019.

[51] J. Hou, Z. Song, H. Park, H. Hofmann, and J. Sun, "Implementation and evaluation of real-time model predictive control for load fluctuations mitigation in all-electric ship propulsion systems," *Applied Energy*, vol. 230, pp. 62 – 77, 2018.

[52] H. Park, J. Sun, S. Pekarek, P. Stone, D. Opila, R. Meyer, I. Kolmanovsky, and R. DeCarlo, "Real-time model predictive control for shipboard power management using the ipa-sqp approach," *IEEE Transactions on Control Systems Technology*, vol. 23, no. 6, pp. 2129–2143, 2015.

[53] A. Haseltalab, R. R. Negenborn, and G. Lodewijks, "Multi-level predictive control for energy management of hybrid ships in the presence of uncertainty and environmental disturbances," *IFAC-PapersOnLine*, vol. 49, no. 3, pp. 90 – 95, 2016. 14th IFAC Symposium on Control in Transportation SystemsCTS 2016.

[54] A. Haseltalab and R. R. Negenborn, "Model predictive maneuvering control and energy management for all-electric autonomous ships," *Applied Energy*, vol. 251, p. 113308, 2019.

[55] E. Silvas, K. Hereijgers, H. Peng, T. Hofman, and M. Steinbuch, "Synthesis of realistic driving cycles with high accuracy and computational speed, including slope information," *IEEE Transactions on Vehicular Technology*, vol. 65, no. 6, pp. 4118–4128, 2016.

[56] Q. Gong, S. Midlam-Mohler, V. Marano, and G. Rizzoni, "An iterative markov chain approach for generating vehicle driving cycles," *SAE Int. J. Engines*, vol. 4, pp. 1035–1045, 04 2011.

[57] P. Nyberg, E. Frisk, and L. Nielsen, "Using real-world driving databases to generate driving cycles with equivalence properties," *IEEE Transactions on Vehicular Technology*, vol. 65, no. 6, pp. 4095–4105, 2016.

[58] J.-M. Zaccardi and F. L. Berr, "Analysis and choice of representative drive cycles for light duty vehicles – case study for electric vehicles," *Proceedings of the Institution of Mechanical Engineers, Part D: Journal of Automobile Engineering*, vol. 227, no. 4, pp. 605–616, 2013.

[59] H. Nareid, M. Grimes, and J. Verdejo, "A neural network based methodology for virtual sensor development," in *SAE Technical Paper*, SAE International, 04 2005.

[60] J. R. Hagena, Z. Filipi, and D. N. Assanis, "Transient diesel emissions: Analysis of engine operation during a tip-in," in *SAE Technical Paper*, SAE International, 04 2006.

[61] D. Prokhorov, "Neural networks in automotive applications," in *Studies in Computational Intelligence (SCI) 132*, Springer-Verlag Berlin Heidelberg, 2008.

[62] M. D. Cesare and F. Covassin, "Neural network based models for virtual nox sensing of compression ignition engines," in *SAE Technical Paper*, SAE International, 09 2011.

[63] S. Haykin, "Neural networks: A comprehensive foundation," *Prentice Hall*, 1999.

[64] I. Arsie, D. Marra, C. Pianese, and M. Sorrentino, "Real-time estimation of engine nox emissions via recurrent neural networks," *IFAC Proceedings Volumes*, vol. 43, no. 7, pp. 228 – 233, 2010. 6th IFAC Symposium on Advances in Automotive Control.

[65] I. Arsie, A. Cricchio, M. De Cesare, F. Lazzarini, C. Pianese, and M. Sorrentino, "Neural network models for virtual sensing of nox emissions in automotive diesel engines with least square-based adaptation," *Control Engineering Practice*, vol. 61, pp. 11 – 20, 2017.

[66] A. Hughes and B. Drury, *Electric Motors and Drives: Fundamentals, Types and Applications*. Elsevier Science, 2013.

[67] S. International, *Serial Control and Communications Heavy Duty Vehicle Network - Top Level Document*, 8 2018.

[68] L. Re, P. Ortner, and D. Alberer, *Chances and Challenges in Automotive Predictive Control*, vol. 402, pp. 1–22. Springer-Verlag Berlin Heidelberg, 11 2010.

[69] L. Guzzella and C. Onder, *Introduction to Modeling and Control of Internal Combustion Engine Systems*. Springer, 2 ed., 2004.

[70] D. Alberer, H. Hjalmarsson, and L. Re, *Identification for Automotive Systems*. Springer-Verlag Berlin Heidelberg, 01 2012.

[71] G. Papalambrou, S. Samokhin, S. Topaloglou, N. Planakis, N. Kyrtatos, and K. Zenger, "Model predictive control for hybrid diesel-electric marine propulsion," *IFAC-PapersOnLine*, vol. 50, no. 1, pp. 11064–11069, 2017. 20th IFAC World Congress.

[72] M. Hirsch, D. Alberer, and L. del Re, "Grey-box control oriented emissions models," *IFAC Proceedings Volumes*, vol. 41, no. 2, pp. 8514 – 8519, 2008. 17th IFAC World Congress.

[73] M. Hirsch and L. del Re, "Adapted d-optimal experimental design for transient emission models of diesel engines," in *SAE Technical Paper*, SAE International, 04 2009.

[74] M. Sivertsson and L. Eriksson, "Optimal Transient Control Trajectories in Diesel-Electric Systems-Part I: Modeling, Problem Formulation, and Engine Properties," *Journal of Engineering for Gas Turbines and Power*, vol. 137, 09 2014.

[75] A. B. of Shipping, *Use of Lithium Batteries in the Marine and Offshore Industries. American Bureau of Shipping*. ABS, 2018.

[76] H. Mu and R. Xiong, *Modeling, Evaluation, and State Estimation for Batteries*, pp. 1–38. Woodhead Publishing, 2018.

[77] T. Hartley and A. Jannette, "A first principles battery model for the international space station," in *3rd International Energy Conversion Engineering Conference.*

[78] S. Xiang, G. Hu, R. Huang, F. Guo, and P. Zhou, "Lithium-ion battery online rapid state-of-power estimation under multiple constraints," *Energies*, vol. 11, p. 283, 01 2018.

[79] X. Liu, W. Li, and A. Zhou, "Pngv equivalent circuit model and soc estimation algorithm for lithium battery pack adopted in agv vehicle," *IEEE Access*, vol. 6, pp. 23639–23647, 2018.

[80] M. Godjevac, J. Drijver, L. de Vries, and D. Stapersma, "Evaluation of losses in maritime gearboxes," *Proceedings of the Institution of Mechanical Engineers, Part M: Journal of Engineering for the Maritime Environment*, vol. 230, no. 4, pp. 623–638, 2016.

[81] B. Taskar, K. K. Yum, S. Steen, and E. Pedersen, "The effect of waves on engine-propeller dynamics and propulsion performance of ships," *Ocean Engineering*, vol. 122, pp. 262 – 277, 2016.

[82] J. Carlton, *Marine Propellers and Propulsion, 4th Edition.* Butterworth-Heinemann, 2018.

[83] J. Dang, J. Brouwer, R. Bosman, and C. Pouw, "Quasi-steady two-quadrant open water tests for the wageningen propeller c- and d-series," in *29th Symposium on Naval Hydrodynamics (ONR), At Gothenburg, Sweden*, 08 2012.

[84] D. M. Macpherson, V. R. Puleo, and M. Packard, "Estimation of entrained water added mass properties for vibration analysis," in *SNAME, New England*, 2007.

[85] T. Perez, O. Smogeli, T. Fossen, and A. Sorensen, "An overview of the marine systems simulator (mss): A simulink toolbox for marine control systems," *Modeling, Identification and Control*, vol. 27, 10 2006.

[86] J.-S. Park and S.-M. Lee, "Characteristics of resistance performance on tugboat in still water and waves," *Journal of the Korean Society of Marine Environment and Safety*, vol. 18, pp. 597–603, 12 2012.

[87] O. Smogeli, *Control of Marine Propellers: from Normal to Extreme Conditions.* PhD thesis, Norwegian University of Science and Technology, NTNU, 10 2006.

[88] S. Li, J. Yang, W. Chen, and X. Chen, "Generalized extended state observer based control for systems with mismatched uncertainties," *IEEE Transactions on Industrial Electronics*, vol. 59, pp. 4792–4802, Dec 2012.

[89] H. Waschl, J. B. Jorgensen, J. K. Huusom, and L. del Re, "A novel tuning approach for offset-free mpc," in *2015 European Control Conference (ECC)*, pp. 545–550, July 2015.

[90] G. Pannocchia, "Offset-free tracking mpc: A tutorial review and comparison of different formulations," in *2015 European Control Conference (ECC)*, pp. 527–532, July 2015.

[91] B. Y. Liaw and M. Dubarry, "From driving cycle analysis to understanding battery performance in real-life electric hybrid vehicle operation," *Journal of Power Sources*, vol. 174, no. 1, pp. 76–88, 2007. Hybrid Electric Vehicles.

[92] G. Fontaras, G. Karavalakis, M. Kousoulidou, T. Tzamkiozis, L. Ntziachristos, E. Bakeas, S. Stournas, and Z. Samaras, "Effects of biodiesel on passenger car fuel consumption, regulated and non-regulated pollutant emissions over legislated and real-world driving cycles," *Fuel*, vol. 88, no. 9, pp. 1608–1617, 2009.

[93] S. Stockar, V. Marano, M. Canova, G. Rizzoni, and L. Guzzella, "Energy-optimal control of plug-in hybrid electric vehicles for real-world driving cycles," *IEEE Transactions on Vehicular Technology*, vol. 60, no. 7, pp. 2949–2962, 2011.

[94] A. Sciarretta, L. Serrao, P. Dewangan, P. Tona, E. Bergshoeff, C. Bordons, L. Charmpa, P. Elbert, L. Eriksson, T. Hofman, M. Hubacher, P. Isenegger, F. Lacandia, A. Laveau, H. Li, D. Marcos, T. Nueesch, S. Onori, P. Pisu, J. Rios, E. Silvas, M. Sivertsson, L. Tribioli, A.-J. van der Hoeven, and M. Wu, "A control benchmark on the energy management of a plug-in hybrid electric vehicle," *Control Engineering Practice*, vol. 29, pp. 287–298, 2014.

[95] V. Schwarzer and R. Ghorbani, "Drive cycle generation for design optimization of electric vehicles," *IEEE Transactions on Vehicular Technology*, vol. 62, no. 1, pp. 89–97, 2013.

[96] H. Tong, H. Tung, W. Hung, and H. Nguyen, "Development of driving cycles for motorcycles and light-duty vehicles in vietnam," *Atmospheric Environment*, vol. 45, no. 29, pp. 5191 – 5199, 2011.

[97] S. Shahidinejad, E. Bibeau, and S. Filizadeh, "Statistical development of a duty cycle for plug-in vehicles in a north american urban setting using fleet information," *IEEE Transactions on Vehicular Technology*, vol. 59, no. 8, pp. 3710–3719, 2010.

[98] S. Seto, W. Zhang, and Y. Zhou, "Multivariate time series classification using dynamic time warping template selection for human activity recognition," in *2015 IEEE Symposium Series on Computational Intelligence*, pp. 1399–1406, 2015.

[99] M. Toyoda, Y. Sakurai, and Y. Ishikawa, "Pattern discovery in data streams under the time warping distance," *VLDB J.*, vol. 22, no. 3, pp. 295–318, 2013.

[100] J. Paparrizos and L. Gravano, "k-shape: Efficient and accurate clustering of time series," *ACM SIGMOD Record*, vol. 45, pp. 69–76, 06 2016.

[101] S. Aghabozorgi, A. Seyed Shirkhorshidi, and T. Ying Wah, "Time-series clustering - a decade review," *Information Systems*, vol. 53, pp. 16 – 38, 2015.

[102] R. C. de Amorim and C. Hennig, "Recovering the number of clusters in data sets with noise features using feature rescaling factors," *Information Sciences*, vol. 324, pp. 126 – 145, 2015.

[103] F. Murtagh and P. Legendre, "Ward's hierarchical clustering method: Clustering criterion and agglomerative algorithm," *ArXiv*, vol. abs/1111.6285, 2011.

[104] M. Cuturi and M. Blondel, "Soft-dtw: a differentiable loss function for time-series," in *ICML*, 2017.

[105] Y. L. Murphey, J. Park, Z. Chen, M. L. Kuang, M. A. Masrur, and A. M. Phillips, "Intelligent hybrid vehicle power control-part i: Machine learning of optimal vehicle power," *IEEE Transactions on Vehicular Technology*, vol. 61, no. 8, pp. 3519–3530, 2012.

[106] C. Sun, X. Hu, S. J. Moura, and F. Sun, "Velocity predictors for predictive energy management in hybrid electric vehicles," *IEEE Transactions on Control Systems Technology*, vol. 23, no. 3, pp. 1197–1204, 2015.

[107] K. Liu, Z. Asher, X. Gong, M. Huang, and I. Kolmanovsky, "Vehicle velocity prediction and energy management strategy part 1: Deterministic and stochastic vehicle velocity prediction using machine learning," in *SAE Technical Paper*, SAE International, 04 2019.

[108] S. Gros, M. Zanon, R. Quirynen, A. Bemporad, and M. Diehl, "From linear to nonlinear mpc: bridging the gap via the real-time iteration," *International Journal of Control*, vol. 93, no. 1, pp. 62–80, 2016.

[109] M. Diehl, H. G. Bock, P. S. Johannes, R. Findeisen, Z. Nagy, and F. Allgower, "Real-time optimization and nonlinear model predictive control of processes governed by differential-algebraic equations," *Journal of Process Control*, 2002.

[110] B. Houska, H. Ferreau, and M. Diehl, "ACADO Toolkit – An Open Source Framework for Automatic Control and Dynamic Optimization," *Optimal Control Applications and Methods*, vol. 32, no. 3, pp. 298–312, 2011.

[111] B. Houska, H. Ferreau, and M. Diehl, "An Auto-Generated Real-Time Iteration Algorithm for Nonlinear MPC in the Microsecond Range," *Automatica*, vol. 47, no. 10, pp. 2279–2285, 2011.

[112] L. Grune, "Nmpc without terminal constraints," *IFAC Proceedings Volumes*, vol. 45, no. 17, pp. 1 – 13, 2012. 4th IFAC Conference on Nonlinear Model Predictive Control.

[113] M. N. Zeilinger, C. N. Jones, and M. Morari, "Robust stability properties of soft constrained mpc," in *49th IEEE Conference on Decision and Control (CDC)*, pp. 5276–5282, 2010.

[114] M. Diehl, R. Findeisen, F. Allgower, H. G. Bock, and J. P. Schloder, "Nominal stability of real-time iteration scheme for nonlinear model predictive control," *IEE Proceedings - Control Theory and Applications*, vol. 152, no. 3, pp. 296–308, 2005.

[115] D. Liao-McPherson, M. M. Nicotra, and I. Kolmanovsky, "Time-distributed optimization for real-time model predictive control: Stability, robustness, and constraint satisfaction," *Automatica*, vol. 117, p. 108973, 2020.

[116] J. Ferreau, C. Kirches, A. Potschka, H. Bock, and M. Diehl, "qpoases: A parametric active-set algorithm for quadratic programming," *Mathematical Programming Computation*, vol. 6, 12 2014.

[117] O. Sundstrom and L. Guzzella, "A generic dynamic programming matlab function," in *2009 IEEE Control Applications, (CCA) Intelligent Control, (ISIC)*, pp. 1625–1630, 2009.